

Study of Transport of Cs^+ through Modified Ion-exchange Membranes

By

SANHITA CHAUDHURY

CHEM01201004016

Bhabha Atomic Research Centre, Mumbai

A thesis submitted to the

Board of Studies in Chemical Sciences

In partial fulfillment of requirements

for the Degree of

DOCTOR OF PHILOSOPHY

of

HOMI BHABHA NATIONAL INSTITUTE



August, 2014

STATEMENT BY AUTHOR

This dissertation has been submitted in partial fulfillment of requirements for an advanced degree at Homi Bhabha National Institute (HBNI) and is deposited in the Library to be made available to borrowers under rules of the HBNI.

Brief quotations from this dissertation are allowable without special permission, provided that accurate acknowledgement of source is made. Requests for permission for extended quotation from or reproduction of this manuscript in whole or in part may be granted by the Competent Authority of HBNI when in his or her judgment the proposed use of the material is in the interests of scholarship. In all other instances, however, permission must be obtained from the author.

Sanhita Chaudhury

DECLARATION

I, hereby declare that the investigation presented in the thesis has been carried out by me. The work is original and has not been submitted earlier as a whole or in part for a degree / diploma at this or any other Institution / University.

Sanhita Chaudhury

List of Publications

Journal

- 1. Temperature Dependence of Ion and Water Diffusion in Crown Ether Loaded Nafion Matrix.**

S. Chaudhury, A. Bhattacharya, C. Agarwal, A. Goswami,

J. Phys. Chem. B, **2011**, 115, 9395 - 9400.

- 2. Self-diffusion of ions in Nafion-117 membrane having mixed ionic composition.**

S. Chaudhury, C. Agarwal, A. K. Pandey, A. Goswami,

J. Phys. Chem. B, **2012**, 116, 1605 - 1611.

- 3. Electrically-driven facilitated transport of Cs^+ across copperferrocyanide channels in track etched membrane.**

S. Chaudhury, C. Agarwal, C. A. K. Pandey, A. Goswami, P. U. Sastry,

J. Membr. Sci., **2013**, 434, 93 - 98.

- 4. Electrodriven Ion Transport through Crown Ether-Nafion Composite Membrane: Enhanced Selectivity of Cs^+ over Na^+ by Ion Gating at the Surface.**

S. Chaudhury, A. Bhattacharyya, A. Goswami,

Ind. Eng. Chem. Res., **2014**, 53, 8804 –8809.

- 5. Copper Ferrocyanide Loaded Track Etched Membrane: an Effective Cesium adsorbent.**

S. Chaudhury, A. K. Pandey, A. Goswami,

J. Radioanalytical Nuc. Chem, **2015**, 304, 697–703.

- 6. Electrodriven Selective Transport of Cs^+ Using Chlorinated Cobalt Dicarbolide in Polymer Inclusion Membrane: A Novel Approach for Cesium Removal from Simulated Nuclear Waste Solution.**

S. Chaudhury, A. Bhattacharyya, A. Goswami,

Env. Sci. Technol. **2014**, 48, 12994-13000.

Symposia

1. *Ion-transport characteristics in Nafion-117 membrane having mixed cationic composition.*

S. Chaudhury, C. Agarwal, A. K. Pandey and A. Goswami,

2nd international symposium on Application of radiotracers in chemical, biological and environmental field (ARCEBS-2) held in SINP, Kolkata during 7-13th Nov, 2010.

2. *Temperature dependence of counter ion mobility in crown ether loaded Nafion matrix.*

S. Chaudhury, C. Agarwal and A. Goswami,

Nuclear and Radiochemistry Symposium (NUCAR - 2011), held at Visakhapattanam during 22nd to 26th February, 2011, P-182.

3. *Study on Self-diffusion of Monovalent Ions in Bi-ionic form of Nafion-117 Membrane.*

S. Chaudhury, C. Agarwal, A. K. Pandey and A. Goswami,

Nuclear and Radiochemistry Symposium (NUCAR - 2011), held at Visakhapattanam during 22nd to 26th February, 2011, P-633.

4. *Electrically-driven Facilitated Transport of Cs⁺ across Copperferrocyanide Channels in Track-etched Membrane.*

S. Chaudhury, C. Agarwal, A.K. Pandey, A. Goswami,

Emerging trends in separation science and technology (SESTEC-2012), held in Mumbai during 27th February to 1st March, 2012, P- 195.

5. *Effect of Dibenzo-21-Crown-7 loading on the structural and diffusional properties of Nafion-117 membrane.*

S. Chaudhury, A. Bhattacharyya and A. Goswami,

Nuclear and Radiochemistry Symposium (NUCAR - 2013), held at Jabalpur during 19th to 23rd February, 2013, P-369.

6. *Electro-driven Selective Transport of Cs⁺ through Crown Ether Loaded Nafion Membrane.*

S. Chaudhury, A. Bhattacharyya, A. Goswami.

DAE-BRNS symposium MEMSEP-13, held in Mumbai during 16th to 18th September, 2013.

7. *Copper Ferrocyanide Loaded Track Etched Membrane: an Effective Cesium Removal Medium.*

S. Chaudhury, A. Bhattacharyya, A. K. Pandey, A. Goswami,

3rd international symposium on Application of radiotracers and Energetic Beams in Sciences (ARCEBS-3) held in Kolkata during 12th to 18th January, 2014.

8. *Electro-driven separation of Cs⁺ from Na⁺ using a polymer inclusion membrane of chlorinated cobalt dicarbollide.*

S. Chaudhury, A. Bhattacharya, and A. Goswami,

Emerging trends in separation science and technology (SESTEC-2014), held in Mumbai during 25th to 28th February, 2014, P-225.

Sanhita Chaudhury

Dedicated to

My Parents

ACKNOWLEDGEMENTS

I avail this opportunity to express my heart felt gratitude to my guide, **Dr. A. Goswami**, for his valuable guidance, motivation, enthusiasm, scientific discussions and encouragement throughout the course of the work. I could not have imagined having a better guide and mentor for my Ph.D. study. He will be a source of inspiration always.

I am thankful to **Dr. K. L. Ramakumar**, Director, Radiochemistry & Isotope group for permitting me to register for my Ph. D. I would also like to thank the members of my Ph.D. committee: **Dr B. S. Tomar**, **Dr P. A. Hassan** and **Dr. C. N. Patra** for their time, insightful comments and questions.

I am highly indebted to **Dr. A. K. Pandey**, Radiochemistry Division, for his wholehearted encouragement and support, without whom it would have been impossible to carry out the work. My words are inadequate to express my deep sense of gratitude to **Dr. A. Bhattacharyya**, Radiochemistry Division, who has been an integral part of all the works presented in this thesis. In fact, he always has been accommodative to me in spite of his busy schedules and facilitated my work in every aspect.

I express my sincere thanks to **Dr. Chhavi Agarwal**, **Mr. Sabyasachi Patra**, **Mr. Vivek Chavan**, **Mr. Amol Mhatre** and **Ms. Apurva Naik** for their continuous help and support throughout the course of the work. I would like to thank all other colleagues of Radiochemistry Division for their direct and indirect support and contribution in this work.

The goodwill, good wishes, affection and encouragement of **my parents** paved the way to success in my life. I highly appreciate the deep concern, co-operation and light hearted moments provided by my family members, friends and relatives. Finally I applaud the patience and cooperation of my husband **Mr. Arka Chaudhury** during my tough Ph.D. schedules. He has been a wonderful source of inspiration for me.

Last but not least, I would like to thank everyone, whose contributions were important for the successful realization of this thesis, but I could not mention them personally.

Sanhita Chaudhury

CONTENTS

	Page No
Synopsis	i
List of Figures	xv
List of Tables	xxi
Abbreviation	xxv
 Chapter 1	
Introduction	1
1.1. Membranes	2
1.1.1. Ion Exchange Membrane	3
1.1.1.1. Nafion	5
1.1.1.2. Track etched membrane	8
1.1.1.3. Polymer Inclusion Membrane	9
1.1.2. Properties of Ion-Exchange Membrane	10
1.1.2.1. Ion Exchange Capacity	11
1.1.2.2. Swelling/ Solvent Uptake Capacity	11
1.1.2.3. Perm-selectivity	12
1.1.3. Physical Characteristics Important for Membrane based Separation Process	14
1.1.3.1. Diffusion	14
1.1.3.2. Ion Exchange Isotherm	20
1.1.3.3. Selectivity	21
1.1.3.4. Permeability	23
1.1.4. Ion Exchange membrane based Separation processes	24
1.1.4.1. Diffusion Dialysis	24
1.1.4.2. Donnan Dialysis	25
1.1.4.3. Electrodialysis	27
1.2. Nuclear Waste	29
1.2.1. Radio-Cesium	32
1.2.2. Health Hazards of Radio-Cesium	34

	1.2.3. Applications of ^{137}Cs	35
	1.2.4. Separation / recovery methods for ^{137}Cs	36
	1.2.4.1. Precipitation Method	36
	1.2.4.2. Ion Exchange Methods	36
	1.2.4.3. Solvent Extraction Methods	39
	1.3. Scope and Aim of Work	42
Chapter 2	Experimental Methods	45
	2.1. Radiotracer based measurements	46
	2.1.1. Self-diffusion co-efficient	46
	2.1.2. Ion Exchange Capacity	47
	2.1.3. Ion Exchange Isotherm	48
	2.1.4. Radiotracers in membrane characterization	49
	2.1.4.1. Choice of a Radiotracer	50
	2.1.4.2. Production of Radiotracers	51
	2.1.4.3. Safety Considerations	52
	2.1.4.4. Measurement of Radiations	52
	2.2. Other Characterization techniques	58
	2.2.1. Electrochemical impedance spectroscopy	59
	2.2.2. Differential scanning calorimeter	63
	2.2.3. UV-Vis spectroscopy	63
	2.2.4. X – ray diffraction	64
	2.2.5. Energy dispersive X-ray fluorescence	65
	2.2.6. Transmission electron microscopy	65
	2.2.7. Secondary ion mass spectrometry	66
	2.2.8. Small Angle X- ray Scattering	68
	2.3. Membranes and Reagents	69
	2.3.1. Membranes	69
	2.3.2. Chemicals	69

Chapter 3	Cation Diffusion in mixed cationic environment in Nafion	71
	3.1. Introduction	72
	3.2. Experimental	76
	3.2.1. Measurement of SDC and Ion Exchange Isotherm	76
	3.2.2. Impedance Measurement	78
	3.3. Calculation	78
	3.3.1. Ion exchange isotherm and Self diffusion coefficients	78
	3.3.2. Water - exchange site mole ratio	78
	3.3.3. Specific Conductivity	79
	3.4. Results and discussion	81
	3.5. Conclusion	93
Chapter 4	Cs ⁺ diffusion and transport in Crown Ether - Nafion Composite membrane	94
	4.1. General Introduction	95
	4.2. Self-Diffusion Studies	97
	4.2. 1. Experimental Section	98
	4.2.1.1. Incorporation of the crown ether	98
	4.2.1.2. Membrane characterization	99
	4.2.1.3. Differential Scanning Calorimetry	99
	4.2.1.4. Self diffusion measurement of cations	99
	4.2.1.5. Self diffusion measurement of water in Cs-Naf-CR1	100
	4.2.1.6. Membrane water content measurement	101
	4.2.2. Results and Discussion	102
	4.2.2.1. Temperature dependence of self diffusion of cations in Cs/Na-Naf-CR1 and Cs-Naf-CR2	102
	4.2.2. 2. Temperature dependence of self diffusion behavior of water	106

4.3. Selective Transport	110
4.3.1. Experimental Section	111
4.3.1.1. Incorporation and Quantification of the crown ether in Cs-Naf-CR _h	111
4.3.1.2. Preparation and Characterization of Cs-H-Naf-CR	112
4.3.1.3. Self diffusion and ion exchange measurement in Cs-Naf-CR _h	115
4.3.1.4. Transport study	116
4.3.2. Results and Discussion	118
4.3.2.1. Cs-Naf-CR _h	118
4.3.2.2. Ion Gated membrane (Cs-H-Naf-CR)	121
4.4. Conclusion	123
 Chapter 5	
Copper Ferrocyanide Loaded Track Etched Membrane: an Effective Cs⁺ Removal Medium	125
 5.1. Introduction	126
5.2. Synthesis of CFCN loaded PTEM	128
5.2.1. Experimental	128
5.2.2. Results and Discussions	129
 5.3. Selective transport of Cs⁺	131
5.3.1. Experimental	131
5.3.2. Results and Discussions	133
 5.4. Preconcentration of Cs⁺	139
5.4.1. Experimental	139
5.4.1.1. Measurement of Ion Exchange capacity, SDC and uptake kinetics	139
5.4.1.2. Treatment of Simulated Nuclear waste	140
5.4.2. Results and discussions	140

	5.4.2.1. Self diffusion and ion exchange capacity	140
	5.4.2.2. Removal of ^{137}Cs	142
	5.4.2.3. Treatment of Simulated Nuclear waste	144
	5.5. Conclusion	147
Chapter 6	Selective transport of Cs^+ using a Polymer Inclusion Membrane of HCCD	148
	6.1. Introduction	149
	6.2. Experimental	151
	6.2.1. Preparation of membrane	151
	6.2.2. Transport Studies with CTA based PIM	152
	6.2.3. Transport Studies with PVC based PIM	153
	6.3. Results and discussion	155
	6.3.1. CTA based PIM for Cs^+ transport from low acidic/neutral feed solution	155
	6.3.2. PVC based PIM for Cs^+ transport from high level waste solution	161
	6.4. Conclusion	163
Chapter 7	Summary and Conclusion	164
Bibliography		170

Synopsis

In recent years, membrane based separation techniques have grown from simple laboratory research scale up to large scale industrial processes [Strathmann 1990] due to the following advantages i) appreciable energy savings, ii) environmentally benign, iii) clean technology with operational ease, iv) greater flexibility in designing systems V) low ligand requirement. It can replace the conventional processes like filtration, distillation, ion-exchange and chemical treatment systems. The membrane based separation processes can either be pressure driven processes (Microfiltration, Ultrafiltration, Nanofiltration), which are governed by size exclusion principles or charged membranes (ion exchange membrane) based processes, where separation is achieved by the interaction of permeating species (i.e. electrolyte) with the fixed charges of an ion exchange membrane (IEM).

Depending upon the type of the replaceable ion, IEMs can be either cation exchangers or anion exchangers. IEMs are semi-permeable, i.e., they allow only the counter ion to pass through them, excluding the co-ions. For example, a cation exchange membrane like Nafion-117 allows only the counter-ions (cations) and excludes all anionic (co-ions) species. The extent of exclusion depends upon the Donnan potential of the membrane at the solution-membrane interface. Most of the applications of IEM are derived from Donnan exclusion principle. While designing target specific membranes, the parameters that have to be kept under consideration are the interaction of the target species with the functional groups and morphology of the membrane matrix. The interaction between the counterions and the fixed charged functional groups in the membrane are electrostatic in nature. Thus, the mutual separation of cations (Na^+ , Cs^+) having the same charge is difficult using these membranes. In order to achieve significant mutual separation of alkali metal ions using cation exchange membrane, the membrane has to be modified with some ion selective reagents. In the present study, we have used homogeneous cation exchange membrane (Nafion-117, pristine or

modified), inorganic ion exchanger loaded polycarbonate track etched membrane (PTEM) and polymer inclusion membrane (PIM).

Nafion-117 is a poly(perfluorosulfonic) acid ion-exchange membrane having a polytetrafluoroethylene (PTFE) backbone with pendant side chains containing $\text{-SO}_3\text{H}$ groups. The industrial applications of Nafion membranes include their use as separators in chlor-alkali industry [Eisenberg and Yeager 1982], in fuel cells etc. In Nafion-117 membrane, the suffix “117” refers to the equivalent weight of 1100 g/equivalent of sulfonic acid groups in dry H^+ -form of the membrane, and the membrane sheet thickness of 7 mil (1mil = 25 μm). The first and the most important morphological description of Nafion is based on “Cluster-channel network model” proposed by Hsu and Gierke [Hsu and Gierke 1982, Hsu and Gierke 1983]. They have concluded that the water-swollen morphology of Nafion is best described by a model of approximately spherical shaped ionic clusters with an inverted micellar structure. It has also been proposed that the high ionic permselectivity in Nafion membranes is due to the interconnectivity between the ionic clusters by narrow channels, thus providing a percolation pathway for ionic transport. This model has received significant acceptance in the literature [Elliott et al. 2011] and has served as the foundation for numerous studies on morphology-property relationships of Nafion.

Homogeneously distributed nanoporous PTEMs are prepared by irradiation of polycarbonate film with accelerated heavy ions and subsequent chemical etching using NaOH. [Fischer and Spohr 1983, Lueck et al. 1990]. Track-etch membranes offer distinct advantages over conventional membranes due to their precisely determined pore structure. The geometrical parameters (pore size, shape and density) of these membranes can be varied in a controlled manner in different stages of the production process by controlling the ion beam parameters (ions energy, ions density) and physicochemical treatment (sensitization, etching process

parameters). These membranes have various applications in analytical chemistry -specifically in membrane- based bioseparations, in electroanalytical chemistry, and in the development of biosensor.

Among different types of membranes, the liquid membranes (bulk liquid membrane, supported liquid membrane-SLM and polymer inclusion membranes-PIM) have drawn considerable attention because of selective carrier mediated transport of molecules of interest. The problem of solvent leaching from the porous support in SLM can be overcome by incorporating the ligand in the polymer matrix, i.e, PIM, resulting in higher lifetime of the membrane [Nghiem et al. 2006]. PIMs are prepared by casting a solution containing an extractant, a plasticizer and a base polymer such as cellulose triacetate (CTA) or poly(vinyl chloride) (PVC) to form a thin, flexible and stable film. The resulting self-supporting membrane can be used to selectively separate the solutes of interest. These membranes are widely used as ion selective electrodes and sensors.

Ion-exchange membranes show physico-chemical and electrochemical properties very similar to conventional ion-exchangers. The final application of these membranes for various separation and analytical processes hinges on the manifestation of some of the properties like ion exchange capacity, self-diffusion coefficient (SDC), permeability, selectivity. Ion-exchange capacity is defined as the number of equivalents of counterions in a specified amount of the material [Helffferich 1962]. This quantity is a characteristic constant of the material and is independent of the experimental condition. The ion exchange isotherm of an ion exchange membrane shows the distribution of a particular type of ion in between the solution and the membrane at equilibrium. This nature of the isotherm indicates the selectivity for a particular ion over another. The selectivity of IEM towards metal ion

depends on i) valence of the counter-ion, ii) ionic solvation of the counter-ions, iii) nature of the functional group on the polymer backbone.

Self-diffusion is diffusion of a species in a medium having no concentration gradient and the SDC gives the true mobility of any species in a matrix. The entropy of mixing is the driving force for self-diffusion. Permeability of a species through a membrane is a practical quantity that governs the rate of transport of the species across the membrane and depends on the SDC and selectivity coefficient. SDC is characteristic for a particular type of cation in a particular medium and depends on the nature and composition of that particular phase and temperature. Diffusion of ions in a membrane matrix is governed by two important factors, the physical and chemical architecture of the polymer matrix through which the counterions are moving and the nature of interaction of the counterions with the functional group on the polymer backbone.

The IEM based separation processes are either Donnan dialysis or electrode dialysis based. The Donnan dialysis based processes are concentration gradient driven and require counter transport of another cation from receiver phase to feed phase to have cation transport from feed phase to receiver phase. In electrodialysis, the cation transport is electric field driven and the anion in the feed compartment is oxidized at anode forcing the cation to move from feed to receiver phase without any counter transport of ion. The use of electric field, thus, eliminates the need of adding salt or stripping agent in the receiver side. Electric field also helps to enhance the cationic flux in the membrane with subsequent reduction in the transport time. In the present work, separation of Cs^+ has been carried out based on the principle of electrodialysis only. This kind of membrane based analyte preconcentration method under the influence of electric field (called as electro-membrane extraction) is currently receiving attention of the scientific community [Pedersen et al. 2008, See and Hauser 2011].

Motivation of the present work:

Cs is one of the most abundant fission products present in nuclear waste. It is of major environmental concern because of the long half-life (30 y) and high gamma energy (662 keV) of its radioisotope ^{137}Cs . Its removal from nuclear waste greatly simplifies subsequent waste handling and storage problem. Management of radioactive liquid wastes produced from reprocessing of spent nuclear fuel requires knowledge on methods of radionuclide separation. Literature reports on separation of Cs from nuclear waste solutions include the use of number of techniques viz., precipitation with sodium phosphotungstic acid [Singh 1983], ion exchange with silicotitanates [Walker 2000] or phosphomolybdates [Buchwald 1958] and solvent extraction using different macrocyclic ionophores [Shinkai et al. 1981, Strzelbicki et al. 1981] or protonated form of the hexachlorinated derivative of cobalt bis (dicarbollide) (HCCD) [Kyras 1994, Hawthorne and Dunks 1997, Scott et al. 2008, Murali et al. 2012]. Mohapatra et al [Mohapatra et al. 2010] have studied the selective transport of cesium using HCCD in SLM and have reported a decontamination factor (D. F, defined as the ratio of product to impurity in the product divided by that in the feed) of ~ 300 over different transition metal ions. Presence of bulk concentration of Na^+ in the nuclear waste solution is the major challenge in recovery/ removal of Cs^+ . Though some macrocyclic carrier based solvent extraction methods [Zhang et al. 2013, Zhang et al. 2014] have studied selective extraction of Cs^+ over Na^+ , but, neither of the membrane based studies [Raut et al. 2012, Mohapatra et al. 2009, Levitskaia et al. 2002, Mohapatra et al. 2010] have addressed the selective separation of Cs^+ from Na^+ ions from nuclear waste solution. With this in view, the aim of this thesis work is to study the different aspects of Cs^+ diffusion and transport through pristine or modified IEMs. Attempt has been made to understand the effect of membrane ionic composition on the SDC of Cs^+ and to prepare Cs^+ selective IEMs for electrodriven selective transport of Cs^+ over Na^+ with emphasis on Cs^+ removal from simulated nuclear

waste solution. In order to have a clean and novel separation method, in the present study, electric field has been used as a driving force for cation transport. The work described in the thesis is organized into the following seven chapters.

Chapter 1: Introduction

This chapter describes the significance of Cs^+ separation from nuclear waste. The health hazard as well as different applications (food preservation, sterilization) of radio isotopes of Cs has also been given in this chapter. It also gives a short account of the already reported solvent extraction or ion exchange based separation methods of Cs^+ from nuclear waste solutions. The advantages of membrane based separation methods over other commonly used separation methods have also been described in this chapter. A brief introduction to the physical and chemical structures of the ion exchange membranes like Nafion -117, inorganic exchanger loaded PTEMs and PIMs has been given. The chapter also gives a detail description of the different parameters of IEMs which influences the mutual separation of alkali metal ions. The principles of two different types of IEM based separation processes have been described and the advantages of electrodialysis based process over conventional Donnan dialysis process have been emphasized. Scope of the present work has also been discussed at the end of this chapter.

Chapter 2: Experimental procedures

The experimental methods along with a brief account of the theoretical details to determine the physico-chemical and electrochemical properties of ion-exchange membranes by radiotracer techniques have been given in this chapter. Details of some of other available methods for the determination of these parameters are also shown. This chapter also describes the instrumental and the experimental details of different characterization techniques used in

the present work. Radiotracers have been used extensively to determine different parameters of IEMs in the present work. Detail of the different aspects of radiotracer based membrane characterization like production and choice of a radiotracer, the associated safety factors have been given in this chapter. Emphasize has been given on the different methods of radiation measurement like detectors, counting techniques. The detail of all the reagents and chemicals used in the present work has also been given in this chapter.

Chapter 3: Cation Diffusion in mixed cationic environment in Nafion-117

This chapter describes the study of the effect of membrane ionic composition on the SDC of different cations, which is important for understanding the competitive cation transport through IEM. It describes the measurement of SDCs of A and B ions (D_A / D_B) in bi-ionic form of Nafion-117 membrane (A-B system) loaded with different proportions of A and B ions using the corresponding radiotracers. In the present work, Na-Cs, Na-Ba, Cs-Ba and Ag-Ba systems have been studied. It has been observed that for Na-Cs and Cs-Ba systems, the SDCs of the cations are independent of the membrane ionic compositions, but in Na-Ba and Ag-Ba systems, SDC of Ba^{+2} decreases continuously with increasing Na^+ / Ag^+ content in the membrane (Na_m^+ / Ag_m^+), whereas the SDC of Na^+ is independent of the membrane ionic composition. The results indicates that D_{Ba} reduces by 70% for 62% Na_m^+ in Na-Ba system, and by 80% for 75% Ag_m^+ in Ag-Ba system as compared to that ($1.5 \times 10^{-7} \text{ cm}^2\text{s}^{-1}$) in pure Ba^{+2} form of Nafion-117. This has been explained based on the locations of the cations in different region of the membrane and their interactions with the backbone and the fixed ionic sites. The explanation is mostly based on the three phase model of Nafion given by Yeager [Yeager and Steck 1981]. In Na-Cs and Cs-Ba systems, the ions follow a mutually independent path and do not influence the SDCs of each other. In Na-Ba system, though both the ions move through water rich region of the membrane, but Na^+ ion possibly remains

mostly dissociated in the water channels, and its transport is not hindered by the Ba^{+2} ions which, being a divalent one, possibly remain in the proximity of the $-\text{SO}_3^-$ ions [Tandon and Pintauro1997]. On the other hand, diffusion of Ba^{+2} ions may be regarded as a lattice diffusion, and increase in the Na^+ content of the membrane increases the average spacing between two successive Ba^{+2} ions, thus affecting the diffusivity of the Ba^{+2} ions. The same reason can explain the change in D_{Ba} in Ag-Ba system.

The Specific conductivities (κ_{imp}) of the membrane in mixed cationic forms have also been obtained from AC impedance measurement (for Na-Cs and Na-Ba systems) and compared with that (κ_{cal}) calculated from the SDC data. The ionic-composition dependent self diffusion behavior of either cation is ultimately reflected in the specific conductance of the system and thus for Na-Ba system, the increment of κ_{imp} with increase in Na^+ content of membrane has been found to be parabolic, whereas for the Na-Cs system, the increment is linear.

Chapter 4: Cs^+ transport in Crown Ether- Nafion-117 Composite membrane.

The study of Cs^+ self-diffusion and transport in crown ether –Nafion composite membrane has been described in this chapter. Crown ethers are an important class of molecules of both inherent and practical interest. The various ring size crown ethers or other complexing agents like calixerenes are having a very good ability to selectively bind particular metal cation from solution depending upon the cavity size and solvents used. The crown ether-Nafion composite membrane system has been chosen with the presumption that highly selective crown ethers can compensate for the low selectivity of IEM and the fixed charge on the membrane can compensate for the charge of the metal ion-crown ether complex. The first part of this chapter describes the morphological changes associated with the crown ether

loading in the membrane and the second part describes a unique way of enhancing the metal ion selectivity by ion gating at the membrane surface.

Earlier work in our lab [Bhattacharyya et al. 2009] with Nafion-crown ether system indicated that the kinetics of isotopic exchange at room temperature with these membranes are too slow. With this in view, the study of temperature dependence (in the temperature range of 50 °C – 70 °C.) of SDC of Cs^+ / Na^+ has been carried out in di-benzo-18-crown-6 (DB18C6) / di-benzo-21-crown-7 (DB21C7) loaded Nafion-117 membrane. Temperature dependence of water diffusion and equilibrium water uptake in DB18C6 loaded Nafion membrane (Cs-Naf-CR1) has also been studied to understand the mechanism of cation and water transport in the membrane. The activation energy ($\sim 80\text{kJ/mole}$) of diffusion for Cs^+ ion and water in Cs-Naf-CR1 has been found to be much higher than that in pure Cs^+ form of Nafion (Cs-Naf). This high value of activation energy, which is typical of ionic diffusion in ionic crystal lattice [Yeager and Steck 1981], has been attributed to enhancement in binding of the ion with the crown ether in the membrane matrix as well as reduction in water content in the membrane matrix due to loading of the crown ether, destroying water clusters in Cs-Naf. The activation barrier for Cs^+ diffusion in DB21C7 loaded Nafion is higher than that of Cs-Naf-CR1 on account of the higher affinity of DB21C7 for Cs^+ than that of DB18C6 [Moyer et al. 1997].. The DSC data shows disruption of water clusters in the membrane, and the attendant loss of plasticity which lowers the self diffusion coefficient values.

In order to achieve selective transport of Cs^+ over Na^+ , two types of Cs^+ ion selective crown ether-Nafion composite membranes have been prepared. In one case, DB21C7 has been incorporated uniformly in Cs^+ form of Nafion-117 membrane in varying molar ratio with respect to Cs^+ and in the other case, Cs^+ driven loading of DB21C7 has been confined to a very small thickness (25 μm) from one of the surfaces of the Nafion-117 membrane (ion

gating). The surface confinement of Cs^+ in the ion gated membrane has been studied by Energy dispersive X-ray spectroscopy and Secondary ion mass spectrometry. The cation (Cs^+/Na^+) transport properties of the membranes have been studied under application of electric field. In the uniformly crown ether loaded membranes, the decrease in crown ether molar ratio has been found to increase the mobility of Cs^+ through the membrane at the cost of mutual cationic selectivity (Cs^+ over Na^+). On the other hand, enhanced selectivity of Cs^+ over Na^+ with significant cationic transport at room temperature has been obtained with the ion gated membrane. When applied for the simulated nuclear waste solution, selective transport of Cs^+ has also been obtained using this gated membrane even in the presence of very high Na^+ ($\text{Cs}^+:\text{Na}^+ = 1:1428$) concentration in aqueous solution.

Chapter 5: Copper Ferrocyanide Loaded Track Etched Membrane: an Effective Cs^+ Removal Medium

This chapter describes the synthesis of highly Cs^+ selective copper ferrocyanide crystals (KCFCN) within the pores of track etched membrane and the use of this composite membrane for selective preconcentration and transport of Cs^+ . The synthesis of the KCFCN crystals have been done by two compartment permeation method using CuSO_4 and $\text{K}_4\text{Fe}(\text{CN})_6$. Characterization by X-ray Diffraction, Small Angle X-ray Scattering, Energy Dispersive X-ray Fluorescence and Transmission Electron Microscopy techniques confirmed the presence of nanosized ferrocyanide particles (radius ~ 40 nm) within the pores of the PTEM. It has been observed from TEM analysis that the KCFCN crystals are almost uniformly filling the conical shaped pores of the PTEM with the dimension of each conical shaped structure being ~ 300 nm dia at surface and ~ 140 nm dia inside. Under electric field, this composite membrane has been found to selectively transport Cs^+ over Na^+ in presence of

nitric acid. The Cs^+ transport rate has been found to be limited by the ion exchange capacity of the membrane.

This chapter also describes the systematic study carried out for removal of Cs^+ from neutral aqueous solution. The self diffusion measurement of Cs^+ in the membrane indicates very fast absorption of the cation. The ion exchange capacity of the composite membrane has been found to be 1.75 mmol / g of the membrane, which indicates that a small piece of membrane can be used to treat a large amount of radioactivity. The ^{137}Cs removal efficacy of the membrane has been found to be affected by the activity dilution and more equilibration time is required when the activity is distributed in larger volume of solution. Application of this composite membrane for removal of Cs^+ from a simulated nuclear waste has indicated exclusive absorption of ^{137}Cs inspite of presence of other radionuclides, though the absorption rate is affected due to their presence. This composite membrane shows promising properties as a sorbent for Cs^+ removal from nuclear waste solution.

Chapter 6: Selective transport of Cs^+ using a Polymer Inclusion Membrane of HCCD

The study of electro-driven separation of Cs^+ from Na^+ using a PIM of hexachlorinated derivative of cobalt bis (dicarbollide) (HCCD) has been described in this chapter. The choice of the carrier is novel as the anion itself is highly selective for a particular metal ion and does not require any extra negative ion as in the case of crown ether based metal ion separation. Use of HCCD for separation of Cs^+ by solvent extraction in trifluoromethylphenyl sulfone [Scott et al. 2008] or nitrobenzene [Murali et al. 2009] medium and supported liquid membrane [Mohapatra et al. 2010] based transport studies are well reported in literature. It is also to be mentioned that use of highly selective HCCD is limited due to toxicity of the

solvents trifluoromethylphenyl sulfone (FS-13) or nitrobenzene. With this in view, in the present work, for the first time, the possibility of using HCCD as a carrier in CTA/PVC based PIM for selective transport of Cs^+ has been explored. 2-nitrophenyl-octyl-ether (NPOE) have been used as the plasticizer. The chapter describes the optimization of the working potential (3 V) of the transport system. Further increase in potential resulted in increased transport rate at the cost of cationic selectivity. The membranes have been applied for selective removal of ^{137}Cs from simulated acidic nuclear waste solution.

The CTA based membrane has been found to selectively transport Cs^+ from a simulated nuclear waste solution containing 0.1 M NaNO_3 and 3.5×10^{-4} M CsNO_3 in 0.4 M HNO_3 with a decontamination factor of > 400 for Cs^+ over Na^+ . It has also been observed that at the end of the transport process, negligible (2.2 %) H^+ has been transported to the receiver phase.

Separation of Cs^+ from SHLW is important from waste management aspect. The SHLW contains a large number of metal ions (Na, Fe, Cr, K, Mn, La) in a high HNO_3 (3M) concentration, where CTA based PIM can't be used due to the acid hydrolysis of the CTA matrix. PVC based membrane has thus been prepared for Cs^+ transport from SHLW. This membrane selectively transported Cs^+ with a decontamination factor of 80 over Na^+ and >100 over other metal ions present in SHLW. The promising results explore the possibility of using this kind of membrane based methods for Cs^+ removal from nuclear waste solution.

Chapter 7: Conclusion

The last chapter of this thesis includes the main conclusions of this work and they have been summarized as follows.

1. In mixed cationic environment, the SDC of cations in Nafion-117 may be influenced depending upon their transport path within the membrane. This ionic composition dependent

self diffusion behavior of either cation is ultimately reflected in the specific conductivity of the system.

2. In crown ether modified Nafion, the SDC of cation is affected by the interaction of the crown ether and the cation as is indicated by the high activation energy of diffusion. A general problem with the IEM is that the enhanced selectivity of an ion is usually accompanied by reduction in mobility of the ion. In the present work, this problem has been successfully overcome by confinement of the templating (with crown ether) only at the surface ion exchange sites. Under electric field, the ion gated membrane has been found to selectively transport Cs^+ over Na^+ from different feed compositions as well as from a simulated nuclear waste solution.

3. Two compartment permeation method using chemical reagents with comparable fluxes appear to be a very good method for synthesis of different inorganic compounds (like KCFCN) within the pores of PTEM. KCFCNm absorbs ^{137}Cs efficiently with high selectivity. For ^{137}Cs removal from radioactive solutions, this sorbent is a promising alternative to commonly used precipitation method or immobilization of copper ferrocyanide in other suitable solid supports. The membrane has also been found to selectively transport Cs^+ over Na^+ under electric field.

4. PIM containing HCCD can be used for effective Cs^+ separations from simulated acidic (0.4 M/ 3 M) nuclear waste solution under applied electric field with a very high D. F over Na^+ .

The Chapter is concluded by bringing out the future scope of the research work related to the topic of the thesis.

List of Figures

Chapter 1

Figure 1.1: Schematic structure of a cation-exchange membrane.

Figure 1.2: Chemical structure of Nafion membrane.

Figure 1.3: Cluster-network model for the morphology of hydrated Nafion.

Figure 1.4. AFM image of the surface of a track etched membrane.

Figure 1.5. AFM image of CTA based PIM surface containing NPOE as plasticizer.

Figure 1.6: Donnan exclusion in a cation-exchange membrane.

Figure 1.7: The ion exchange isotherm for a A-B system under different preferential conditions in IEM.

Figure 1.8: Schematic representation of counterion concentration profile in steady state isotopic diffusion across an IEM.

Figure 1.9: Schematic representation of the principle of Diffusion dialysis for base recovery using cation exchange membrane and acid recovery using anion exchange membrane.

Figure 1.10: Schematic representation of the principle of Donnan dialysis with NaCl in the stripping and CaCl₂ in the feed solution.

Figure 1.11: Schematic representation of the principle of Electrodialysis.

Figure 1.12: Working principle of electric field driven cation transport through cation exchange membrane.

Figure 1.13: Schematic presentation of nuclear fuel cycle.

Figure 1.14: Typical distribution of ¹³⁷Cs in different waste available for recovery at Trombay.

Figure 1.15: Decay scheme of ¹³⁷Cs.

Figure 1.16: Ion exchange cycle for RFPR.

Figure 1.17: Structure of Chlorinated Cobalt Dicarbolide anion.

Chapter 2

Figure 2.1: Schematic representation of energy band in NaI(Tl) detector.

Figure 2.2: Block Diagram of NaI(Tl) detector system.

Figure 2.3: Block Diagram of HPGe detector system.

Figure 2.4: A representative Nyquist plot for a highly conducting membrane.

Figure 2.5: A representative Nyquist plot for a complex systems.

Figure 2.6: Electrochemical cell used for impedance measurement.

Figure 2.7: Schematic diagram of ToF-SIMS instrument.

Figure 2.8: Schematic representation of a scattering experiment and representation of the scattering vector q in the detector plane.

Chapter 3

Figure. 3.1: Ion exchange isotherms for the (a) Na-Ba system and (b) Na-Cs system in Nafion-117 membrane.

Figure 3.2: Diffusion kinetics of (a) Na^+ and (b) Cs^+ for different ionic composition of the membrane in the Na-Cs system.

Figure 3.3: Diffusion kinetics of (a) Cs^+ and (b) Ba^{+2} for different ionic composition of the membrane in Cs-Ba system.

Figure 3.4: Diffusion kinetics of (a) Na^+ and (b) Ba^{+2} for different ionic composition of the membrane in the Na-Ba system.

Figure 3.5: Ba^{+2} diffusion kinetics for different ionic composition of the membrane in Ag-Ba system.

Figure 3.6: Three region structural model for Nafion: A- fluorocarbon phase, B- interfacial zone, C- Ionic Cluster.

Figure 3.7: Nyquist plot obtained from Impedance measurement for Nafion-117 loaded with different proportion of Na^+ and Ba^{+2} ions.

Figure 3.8: Specific conductivities of Nafion-117 membrane containing different proportions of (a) Na^+ and Ba^{+2} ions. (b) Na^+ and Cs^+ ions.

Chapter 4

Figure 4.1: Self diffusion profile of Cs^+ ion in (a) Cs-Naf-CR1 and (b) Cs-Naf-CR2 at different temperatures.

Figure 4.2: Variation of logarithm of self diffusion coefficient of Cs^+ ($\ln D_{\text{Cs}^+}^m$) in (a) Cs-Naf-CR1 and (b) Cs^+ in Cs-Naf-CR2 as a function of inverse of temperature.

Figure 4.3: Comparison between Cs^+ and Na^+ self diffusion profile at 60°C in Cs-Naf-CR1 and Na-Naf-CR1 respectively.

Figure 4.4: Self diffusion profile of water in Cs-Naf-CR1 at five different temperatures.

Figure 4.5: Variation of logarithm of self diffusion coefficient of water ($\ln D_{\text{H}_2\text{O}}^m$) in Cs-Naf-CR1 as a function of inverse of temperature.

Figure 4.6: DSC thermograms of (a) Cs^+ form and (b) Na^+ form of Nafion membrane with and without DB18C6.

Figure 4.7: (a) UV-visible spectrum acquired for 2.0×10^{-4} M DB21C7 solution in DMF. (b) Calibration plot of absorbance vs concentration of DB21C7.

Figure 4.8: (a) Microscopic image of the cross section of Cs-Naf-CR_h ($N = 0.8$) along which EDS analysis has been carried out. (b) Atom % ratio of Cs to S (as obtained from EDS analysis) in Cs-Naf-CR_h ($N = 0.8$) and Cs-H-Naf-CR.

Figure 4.9: ToFSIMS spectra showing (a) Variation of Cs^+ counts and (b) Overlay of Cs^+ ion (green) distribution over total ion (red) along the thickness of Cs-H-Naf-CR membrane.

Figure 4.10: Experimental arrangement for transport studies under applied electric field.

Figure 4.11: Room temperature (a) $\text{Cs}^+_{\text{sol}} \rightleftharpoons \text{Cs}^+_{\text{mem}}$ isotopic exchange profiles and (b) $\text{Na}^+_{\text{sol}} \rightleftharpoons \text{Cs}^+_{\text{mem}}$ ion exchange profiles in Cs-Naf-CR_h membranes with different N.

Figure 4.12: Cation transport paths in (a) Uniformly crown ether loaded Cs-Naf-CR_h membrane and (b) Ion gated Cs-H-Naf-CR membrane.

Figure 4.13: Cation ($\text{Cs}^+ / \text{Na}^+$) transport profiles under different experimental conditions.

Chapter 5

Figure 5.1: XRD pattern of CFCNm.

Figure 5.2: SAXS profile of CFCNm.

Figure 5.3: Transmission Electron Microscopy images of KCFCN loaded PTEM.

Figure 5.4: Experimental arrangement for transport studies under applied electric field

Figure 5.5: Comparison of cation transport profiles under different experimental conditions with HNO_3 (pH=2) in both compartments and 1:20 Cs^+ to Na^+ ratio in feed compartment initially.

Figure 5.6: Comparison of water transport profiles of blank PTEM and KCFCNm.

Figure 5.7: Effect of varying Cs^+ conc. on the cation transport profiles for Naf-KCFCNm composite at 3 V potential with HNO_3 (pH=2) in both compartment.

Figure 5.8: Self diffusion profile of Cs^+ in KCFCNm.

Fig. 5.9: Comparison of the gamma spectra (obtained using HPGe detector) of 5 ml radioactive waste solution, initial and after 3 h membrane preconcentration (a) Full energy range (b) zoomed view of figure 3a) in the energy range of 615-675 keV.(c) Gamma spectra of KCFCNm after 3 h preconcentration.

Chapter 6

Figure 6.1: Cs^+ transport profiles obtained using CTA based PIM at different applied potential for the same feed composition of 0.0025 M NaCl + 0.0025 M CsCl

Figure 6.2: Cation (Cs^+/Na^+) transport profiles obtained using CTA based PIM at 3 V for different Cs^+ to Na^+ ratio in the neutral feed solution.

Figure 6.3: Current profiles obtained for CTA based PIM at 3 V for different neutral feed compositions.

Figure 6.4: Gamma spectra of the initial (simulated RFPR effluent solution) and final feed solution as well as final receiver (93% Cs transport) solution, showing the selective transport of ^{137}Cs over ^{22}Na through CTA based PIM.

Figure 6.5: Transport profile of HNO_3 and $\text{CsNO}_3/\text{NaNO}_3$ obtained using CTA based PIM at zero applied potential with SRELW in the feed compartment.

Figure 6.6: Relative concentrations of different metal ions in the (a) initial feed solution (b) final feed solution and (c) final receiver solution for the treatment of SHLW using PVC based PIM.

List of Tables

Chapter 1

Table 1.1: Membrane based separation processes.

Table 1.2: Major contributors to the radioactivity in the spent fuel after a cooling period of 50 days.

Chapter 2

Table 2.1: Chemical reagents used in the present studies along with the supplying company name.

Chapter 3

Table 3.1: Compositions of equilibrating solutions, ionic compositions, water-exchange site mole ratio (λ) and SDCs of Na^+ and Ba^{+2} ions along with the calculated (κ_{cal}) and measured (κ_{imp}) specific conductivities in Na-Ba system.

Table 3.2: Compositions of equilibrating solutions, ionic compositions, water-exchange site mole ratio (λ) and SDCs of Na^+ and Cs^+ ions along with the calculated (κ_{cal}) and measured (κ_{imp}) specific conductivities in Na-Cs system.

Table 3.3: Compositions of equilibrating solutions, ionic compositions and SDCs of Cs^+ and Ba^{+2} ions in the Cs-Ba system.

Table 3.4: Compositions of equilibrating solutions, ionic compositions and SDCs of Ba^{+2} ions in the Ag-Ba system.

Table 3.5: Comparison of SDCs of Na^+ obtained from radiotracer measurement and specific conductivities of Na^+ form of Nafion-117 membrane.

Chapter 4

Table 4.1: Structural details of the crown ethers used in the present work.

Table 4.2: Variation of $D_{Cs^+}^m$ in Cs-Naf-CR1 and Cs-Naf-CR2 as a function of different temperatures.

Table 4.3: Activation barrier for Cs^+ ion and water in pure and crown ether modified Cs-Naf.

Table 4.4: Variation of $D_{H_2O}^m$ and water content in Cs-Naf-CR1 as a function of different temperatures.

Table 4.5: The time dependent relative cation transport (% Cs^+ / % Na^+) for different membranes.

Table 4.6: The details of the two compartment transport experiments carried out at 4V along with corresponding enrichment factor of Cs^+ over Na^+ and Permeability coefficient of Cs^+ .

Chapter 5

Table 5.1: Experimental details along with percentage cation transport after ~7 h and corresponding enrichment factor of Cs^+ over Na^+ .

Table 5.2: Comparison of the different adsorption parameters of KCFCNm with other literature reported ferrocyanide sorbents.

Table 5.3: Dilution effect on the activity removal efficacy of a 1 cm X 2 cm KCFCNm piece with logarithm of the corresponding distribution coefficients (K_d).

Table 5.4: Elemental composition and corresponding concentration (C_M) of SNW as obtained from ICP-AES. Errors on all the data points are less than 2 %.

Table 5.5: Count rates of different nuclides as observed in the 5 ml radioactive waste solution acquired using a HPGe detector.

Chapter 6

Table 6.1: Elemental composition of the SHLW feed solution used for the transport study.

Table 6.2: Decontamination factors (DF) of Cs^+ over Na^+ in electrodriven (3V) transport experiments using PIMs.

Table 6.3: Current efficiencies obtained using CTA based PIM at 3 V for different neutral feed compositions.

Abbreviations

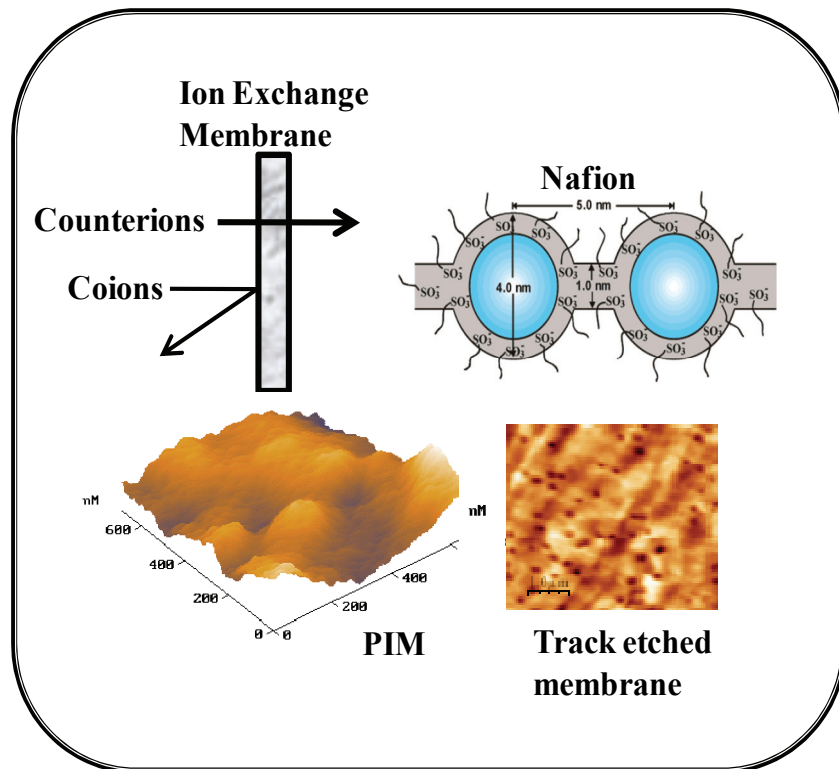
AFM	: Atomic Force Microscopy
AMP	: Ammonium Molybdophosphate
BLM	: Bulk Liquid Membranes
CCD ⁻	: Chlorinated Cobalt Dicarbollide anion
CPE	: Constant Phase Element
Cs/Na-Naf	: Cs ⁺ / Na ⁺ form of Nafion Membrane
Cs-Naf-CR1	: DB18C6 loaded Cs-Naf Membrane
Cs-Naf-CR2	: DB21C7 loaded Cs-Naf Membrane
Cs-Naf-CR _h	: Partial but homogeneously DB21C7 loaded Cs-Naf Membranes
Cs-H-Naf-CR	: Ion gated DB21C7 loaded Membranes
CTA	: Cellulose Tri Acetate
CST	: Crystalline Silicotitanates
DB18C6	: Di-Benzo-18-Crown-6
DB21C7	: Di-Benzo-21-Crown-7
DF	: Decontamination Factor
DSC	: Differential Scanning Calorimetry
EC	: Equivalent Circuit
EDXRF	: Energy Dispersive X-ray Fluorescence
EIS	: Electrochemical Impedance Spectroscopy
EW	: Equivalent Weight
HCCD	: Protonated form of CCD ⁻
HLW	: High Level Waste
HPGe	: High Purity Germanium detector
ICP-AES	: Inductively Coupled Plasma- Atomic Emission Spectroscopy
IEM	: Ion Exchange Membrane

IIX	: Inorganic Ion exchangers
ILW	: Intermediate Level Waste
KCFCN	: Copper Ferrocyanide Crystals
KCFCNm	: KCFCN loaded membrane
LLW	: Low Level Waste
MCA	: Multi Channel Analyser
MF	: Micro Filtration
NF	: Nano Filtration
NMR	: Nuclear Magnetic Resonance
NPOE	: 2-Nitro-Phenyl-Octyl Ether
PAN	: Poly Acrylo Nitrate
PUREX	: Plutonium Uranium Reduced Extraction process
PIM	: Polymer Inclusion Membranes
PTM	: Polycarbonate Track Etched Membranes
PTFE	: Poly Tetra Fluoro Ethylene
PVC	: Poly Vinyl Chloride
RFPR	: Resorcinol Formaldehyde Polycondensate Resin
RO	: Reverse Osmosis
SDC	: Self Diffusion Coefficient
SANS	: Small Angle Neutron Scattering
SAXS	: Small Angle X-ray Scattering
SIMS	: Secondary ion mass spectrometry
SHLW	: Simulated High Level Waste
SNW	: Simulated Nuclear Waste
SRELW	: Simulated Effluent solution of RFPR Resin

SLM	: Supported Liquid Membranes
TEM	: Transmission Electron Microscopy
ToF-SIMS	: Time of Flight SIMS
UF	: Ultra Filtration
WAXS	: Wide angle X Ray Scattering
WAXD	: Wide-angle X-ray diffraction
WDXRF	: Wide-angle X Ray Fluorescence
XRD	: X Ray Diffraction
XRF	: X Ray Fluorescence

Chapter 1

Introduction



1.1. Membranes

A membrane is a discrete, thin interface that moderates the permeation of chemical species in contact with it. This interface may be molecularly homogeneous, that is, completely uniform in composition and structure, or may be chemically or physically heterogeneous, for example, containing holes or pores of definite dimensions or consisting of some form of layered structure. With increasing demand for more effective separations in the chemical, pharmaceutical, environmental and food industries, new materials and technologies have been investigated and developed. Over the years, membrane based separation techniques have grown from simple laboratory research scale up to large scale industrial processes that have considerable, technical and commercial impact [Strathmann 1990] due to the following advantages.

- (a) Appreciable energy savings
- (b) Environmentally benign
- (c) Clean technology with operational ease
- (d) Replaces the conventional processes like filtration, distillation, ion-exchange and chemical treatment systems
- (e) Greater flexibility in designing systems
- (f) Possibility of obtaining high enrichment/ separation factors

The driving force for the transport of a species across membrane can be a difference in concentration, pressure, electrical potential, or temperature [Paul and Peinemann 1996, Cheung and Raj 1996]. Table 1.1 summarizes membrane based separation processes with the type of driving force and separation mechanism.

Table 1.1: Membrane based separation processes

Process	Driving force	Separation mechanism
Diffusion dialysis	ΔC	Diffusion
Microfiltration	ΔP	Sieving
Ultrafiltration	ΔP	Sieving
Nanofiltration	ΔP	Sieving/ Solubility
Reverse Osmosis	ΔP	Sieving/ Solubility
Pervaporation	ΔP	Solubility/ Diffusion
Membrane distillation	ΔP	Solubility/ Diffusion
Gas separation	ΔP	Solubility/ Diffusion
Vapor permeation	ΔP	Solubility/ Diffusion
Electrodialysis	ΔE	Electromigration

* ΔC , ΔP and ΔE stand for differences in concentration, pressure, and electrical potential, respectively.

The separation processes can either be pressure driven processes (RO, NF, UF, MF) which are governed by size exclusion principles or charged membranes (ion exchange membrane) based processes, where separation is achieved by the interaction of permeating species (i.e. electrolyte) with the fixed charges of an ion exchange membrane(IEM). Since the work in this thesis has been carried out using different IEMs, in the rest of this chapter, emphasis is given on this type of membrane based separation process only.

1.1.1. Ion Exchange Membrane

An ion exchange membrane consists of a barrier or thin layer, which contains ionogenic (IEM) groups that restrict the transport of various ionic species. A schematic diagram of a cation exchange membrane is shown in figure 1.1. This membrane consists of a cross linked

polymeric matrix with the fixed negative charges, which attract positively charged mobile ions and rejects negatively charged mobile ions. Ion exchange membranes are, in general, finely micro porous, with the pore walls carrying fixed positive or negative charges [Baker 2004]. An ion-exchange material has fixed positive or negative charges which associate with ions of the opposite charge. These ions are called counterions. Ions that have the same sign as the fixed charges of the ion exchange material are called coions. For example, in figure 1.1, the positively charged mobile ions are counterions and the mobile anions are coions.

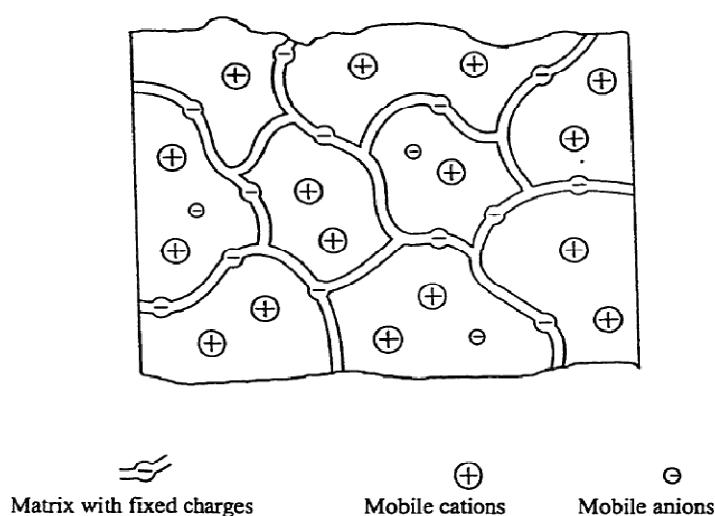


Figure 1.1: Schematic structure of a cation-exchange membrane.

Depending upon the type of replaceable group, IEMs can be either cation exchangers or anion exchangers. IEMs are semi-permeable, i.e., they allow only the counter ion to pass through them, excluding the co-ions. In ion exchange membranes the counterions interact with the fixed charged functional groups in the membrane electrostatically. Separation with charged membranes is achieved mainly by exclusion of the same charge as the fixed groups on the membrane backbone, and to a lesser extent by the pore size. Separation techniques based on IEMs are increasingly gaining importance as relatively clean separations with high separation factors are achievable and also they are cost effective. The key parameters for specific applications of these membranes are: (i) selective partitioning of target species from

solution to membrane phase, (ii) diffusion of the species in the membrane matrix and (iii) release of the target species into the receiver phase. Therefore, the interaction of the target species with the functional groups and, physical and chemical architecture of the membrane matrix play an important role in designing target specific membranes. Depending on the method of preparation, IEMs can be classified as

(a) ***Homogeneous membranes:*** These membranes are prepared by polymerization or condensation of functional monomers or by heating a pre-condensed reaction mixture containing oligomers or mixture of monomers [Helffferich 1962].

(b) ***Graft copolymer membranes:*** These membranes are prepared by incorporating the polyelectrolyte gel within the pores of a robust microporous host membrane and they are having outstanding mechanical and good electrochemical properties.

(c) ***Liquid Membranes (Mobile carrier membranes):*** A liquid membrane utilizes a carrier to selectively transport components such as metal ions at relatively high rate across the membrane interface. The membrane types that are commonly studied are Bulk liquid membranes (BLM), Supported Liquid Membranes (SLM), and Polymer Inclusion Membranes (PIM).

In the present study, we have used either homogeneous cation exchange membrane named as Nafion-117 (modified or as it is) or ion exchanger loaded polycarbonate track etched membranes or polymer inclusion membranes. The details about these different types of membrane are given below.

1.1.1.1. Nafion

Nafion is a cation exchange membrane developed by E.I. DuPont deNemours and Co. Inc. It finds wide applications in separation science and industry. Its chemical structure (figure 1.2)

consists of a polytetrafluoroethylene (PTFE) backbone with pendent side chain containing –SO₃H group. These materials are synthesized by copolymerization of a fluorinated vinyl ether monomer with tetrafluoroethylene [Mauritz & Moore 2004].

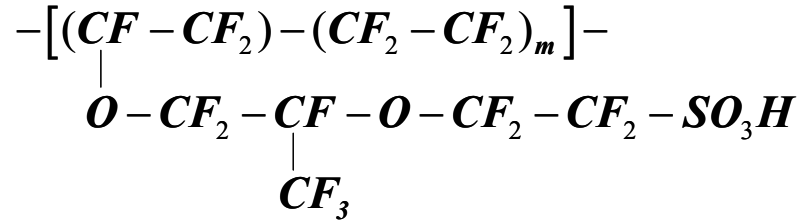


Figure 1.2: Chemical structure of Nafion membrane.

Nafion can be converted into any cationic form by simple ion-exchange process. Membranes having different equivalent weight can be obtained by varying the *m* in the above chemical formula. The equivalent weight (EW) of Nafion is the number of grams of dry Nafion per mole of sulfonic acid groups when the membrane is in acidic form [Mauritz & Moore 2004]. This is an average value obtained from the distribution in the comonomer sequence (value of *m*). The EW is related to *m* as $EW = 100m + 446$. For example, if the value of *m* is 7, then the EW is 1100. In Nafion-117 membrane, the suffix “117” refers to the EW of 1100 g/equivalent of sulfonic acid groups in dry H⁺ -form of the membrane, and the membrane sheet thickness of 7 mil (1mil = 25 μm). Nafion has high degree of disorder in physical organization of its matrix. To obtain information on structural morphology of Nafion under different environment, several experimental techniques like small angle X-ray scattering (SAXS), wide angle X-ray scattering (WAXS), small angle neutron scattering (SANS), atomic force microscopy (AFM), transmission electron microscopy (TEM) and nuclear magnetic resonance (NMR) spectroscopy have been used over the years [Hsu & Gierke 1982, Hsu & Gierke 1983, Xue et al, 1989, Lee et al. 1992, McLean et al 2000, Rollet et al. 2002,]

Based on these studies, different models describing the self-assembling morphology of Nafion under different physico-chemical environments have been proposed [Mauritz & Moore 2004, Kusoglu et al. 2012, Gebel et al. 2000, Schmidt-Rohr et al. 2008, Rubatat et al. 2002, Rollet et al. 2004, Rubatat et al. 2004, Starkweather et al. 1982, Elliott et al. 2011]. The first important morphological description of Nafion is based on “Cluster-channel network model” proposed by Hsu and Gierke [Hsu and Gierke 1982, Hsu and Gierke 1983]. Gierke and co-workers, using SAXS and wide-angle X-ray diffraction (WAXD), have compared the morphological features of Nafion membranes of different equivalent weights. They concluded that the water-swollen morphology of Nafion was best described by a model of approximately spherical shaped ionic clusters with an inverted micellar structure. It was also proposed that the high ionic permselectivity in Nafion membranes is due to the interconnectivity between the ionic clusters by narrow channels, thus providing a percolation pathway for ionic transport. This morphology referred to as the cluster-channel model is shown in figure 1.3. Theoretical calculations based on this model showed that, for a given equivalent weight, the cluster diameter, the exchange sites per cluster, and the number of water molecules per exchange site increased linearly with water content. It was proposed that the growth of clusters with increasing water content is due to a combination of expansion in cluster size and a redistribution of the sulfonate sites to yield fewer clusters in the fully hydrated material. This original, yet phenomenological, cluster-channel model has received significant acceptance in the literature and has served as the foundation for numerous studies of morphology-property relationships of Nafion. In recent times several other models have also been proposed, some of which are described below.

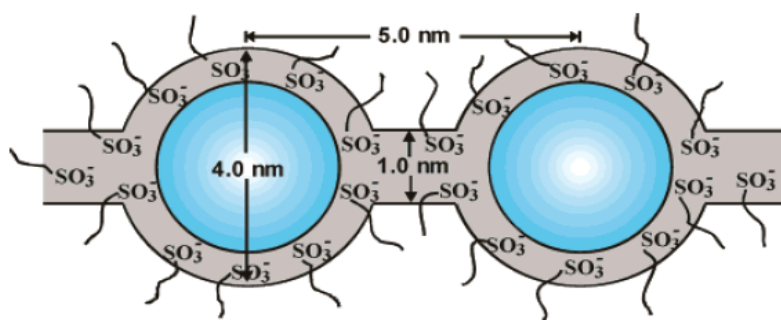


Figure 1.3: Cluster-network model for the morphology of hydrated Nafion.

Rubatat et al. [Rubatat et al. 2002] suggested the “Polymeric bundle model” consisting of fluorocarbon chains surrounded by ionic groups and water. More recently, a unified morphological description of organization of water swollen Nafion has been proposed. This model suggests a bicontinuous network of ionic clusters embedded in a matrix of fluorocarbon chains and accepts the existence of ionic clusters network without need of extended parallel channels. In the present thesis, the observations are discussed based on the cluster channel model of Hsu & Gierke [Hsu and Gierke 1982, Hsu and Gierke 1983]. The other structural and physicochemical properties of Nafion will be discussed in detail in other chapters of this thesis.

1.1.1.2. Track etched membrane

Irradiation of polymer foil (polycarbonate, polyethylene terephthalate) with accelerated heavy ions (that must have enough energy to penetrate) creates latent tracks in the bulk of polymer foil. These on subsequent chemical (using NaOH) etching produces homogeneously distributed track etched membranes [Fischer and Spohr 1983, Bieth et al. 1991, Lueck et al. 1990]. Figure 1.4 shows the atomic force microscopy (AFM) image of the surface of a track etched membrane having $\sim 0.2 \mu\text{m}$ pore size. The use of nuclear tracks for the production of porous membranes was proposed almost immediately after the discovery of particle track etching in thin sheets of materials [Bayley and Martin 2000]. Track-etch membranes offer

distinct advantages over conventional membranes due to their precisely determined structure. The geometrical parameters (pore size, shape and density) of these membranes can be varied in a controlled manner in different stages of the production process by controlling the ion beam parameters (ions energy, ions density) and physicochemical treatment (sensitization, etching process parameters). Track etched membranes because of their homogeneous and nanoporous structures have various applications in analytical chemistry, specifically in membrane based bioseparations, in electroanalytical chemistry and in the development of new approaches to design biosensor. Use of these membranes for the synthesis of different nanostructures is also well established. In the present work, polycarbonate based track etched membrane has been used for the synthesis of nanosized copper ferrocyanide crystals. This inorganic ion exchanger loaded track etched membranes have further been used for the treatment of Cs^+ .

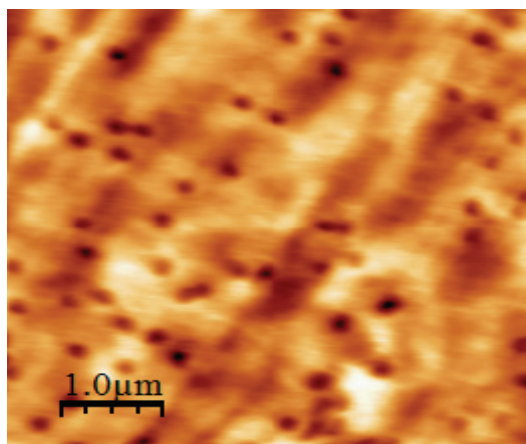


Figure 1.4. AFM image of the surface of a track etched membrane.

1.1.1.3. Polymer Inclusion Membrane

Among different types of membranes, the liquid membranes (bulk liquid membrane, supported liquid membrane-SLM and polymer inclusion membranes-PIM) have drawn considerable attention because of selective carrier mediated transport of molecules of interest. The problem of solvent leaching from the porous support in SLM can be overcome by

incorporating the ligand in the polymer matrix, i.e, PIM, resulting in higher lifetime of the membrane [Nghiem et al. 2006]. These membranes are prepared by physical immobilization of the extractant in a plasticized cellulose tri acetate (CTA) or poly vinyl chloride (PVC) matrix. The surface roughness profiles of a cellulose tri acetate based PIM sample with nitro phenyl octyl ether (NPOE) the plasticizer, as obtained from AFM is shown in figure 1.5 [Sodaye 2007]. The properties of these membranes can be tuned by appropriate selection of the matrix forming polymer, plasticizer and extractant. These membranes have been used as potentiometric sensors as Ion Selective Electrodes and Field Effect Transistors [Bakker et al. 1997, Pretsch et al. 1998, Ngheim et al. 2006].

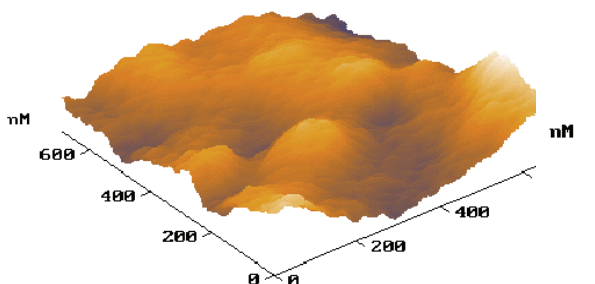


Figure 1.5. AFM image of CTA based PIM surface containing NPOE as plasticizer [Sodaye 2007].

1.1.2. Properties of Ion-Exchange Membrane

Ion-exchange membranes show physico-chemical and electrochemical properties very similar to the conventional ion-exchangers. The final application of these membranes for various separation and analytical processes hinges on the manifestation of some of the following physico-chemical properties, which are briefly described below.

1.1.2.1. Ion Exchange Capacity

IEMs are characterized quantitatively by their ion-exchange capacity, which is defined as the number of equivalents of counterions in a specified amount of the material [Helfferich 1962]. The capacity data, primarily used in the numerical calculations of ion-exchange operations, is a characteristic constant of the material and is independent of the experimental condition. The ion-exchange capacity of these membranes can be determined by pH titration or equilibrating with counterion solutions tagged with radiotracer or using radioanalytical techniques like neutron activation analysis.

1.1.2.2. Swelling/ Solvent Uptake Capacity

IEMs are able to sorb water or polar solvents in which they are placed [Helfferich 1962]. While taking up solvent, the IEMs usually expand or “swell”. This swelling is only up to a limited degree, as swelling does not proceed after equilibrium is attained between the two media. IEMs have ionizable functional groups in their matrix. These groups, as well as the ions they dissociate into, tend to surround themselves with the polar solvent molecules. The swelling equilibrium is a balance of opposing forces. The tendency of the polar and ionic constituents to surround themselves with solvent molecules and thus to stretch the matrix is counterbalanced by an increasing resistance by the matrix. The resistance of the matrix is due to network elasticity arising from the cross-linked polymer chains in the membrane. Equilibrium is attained when the elastic forces of the matrix balance the dissolution or solvation tendency. The extent of swelling depends on:

- (a) Nature of the solvent
- (b) Nature of fixed ionic groups
- (c) Degree of cross-linking (if it is there)

- (d) Nature of counterion
- (e) Concentration of the external solution
- (f) Ion-pair formation and association

1.1.2.3. Perm-selectivity

When an IEM is in contact with electrolyte solutions of low or moderate concentrations, there exist considerable concentration differences between the two phases, the counterion concentration being large in the membrane whereas the solution has a large concentration of the mobile coions [Helfferich 1962]. This process disturbs the electro-neutrality as both the type of ions carry electric charge. The migration of counterions into the solution and of coions into the membrane results in building up of an electric potential difference between the two phases. This potential is called the Donnan Potential and is of opposite sign for cation and anion exchange membranes. This potential repels the coion from the membrane and thus prevents the internal coion concentration from rising beyond an equilibrium value, which is usually much smaller than the concentration of the external solution. The higher is the Donnan potential value, the stronger is the exclusion, i.e., the smaller is the electrolyte uptake by the membrane. Mathematically, Donnan potential (E_{Don}) is written as the difference of potential at the interface and is given by,

$$E_{Don} = \bar{\phi} - \phi = \frac{RT}{z_i F} \ln \frac{a_i}{a_i} \quad (1.1)$$

where Φ is the electric potential, R is the gas constant, T is the absolute temperature, F is the Faraday constant, z_i is the valence and a_i is the activity of the species i . The terms with overbar represent the membrane values. For a given monovalent ionic species at activity ratio ($\frac{a_i}{a_i}$) of 1:10, the Donnan potential is 59 mV. This relation holds for any mobile ionic species

present in the system. When applied to the counterions, it reflects the dependence of the Donnan potential on the concentration (or activity) difference between the two phases and on the counter-ion valence. When applied to the coion, it shows the dependence of coion exclusion on Donnan potential and the coion valence. As the value of the activity of the species in the two phases become equal (at high concentrations in solution), E_{Don} approaches zero, the potential breaks down and there is a free flow of electrolyte through the membrane. This property of exclusion of coions by the IEMs is called Donnan exclusion and is shown in figure 1.6. The membrane is said to be perm-selective or semi-permeable to counterions. The perm-selectivity is reflected not only in differences in permeability but also in the membrane potential. However, when the concentration of the solution is increased, the Donnan exclusion becomes less effective and thus perm-selectivity is reduced.

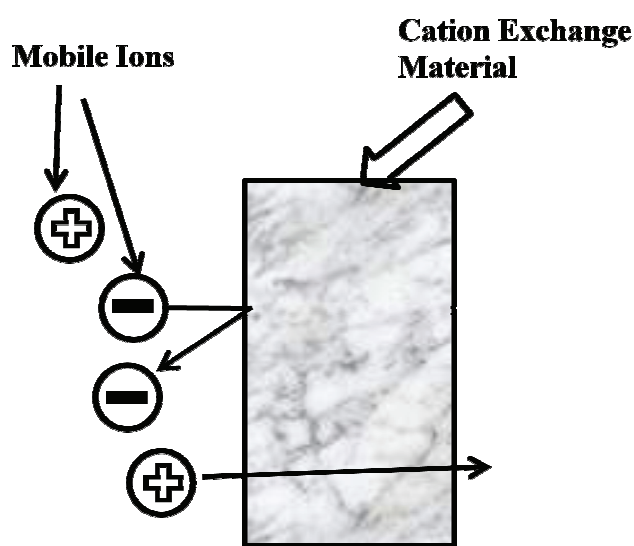


Figure 1.6: Donnan exclusion in a cation-exchange membrane.

1.1.3. Physical properties Important for Membrane based Separation Process

Other than the properties mentioned above, IEMs exhibit many physical properties, which are important in governing the separation processes based on ion-exchange membranes. Some of those properties, that have been studied and are reported in the present thesis, are described below.

1.1.3.1. Diffusion

Diffusion is a process in which matter is transported from one part of the system to another as a result of random molecular motion [Crank 1964]. In the absence of any external force, concentration gradient is the driving force for diffusion. In the context of ion-exchange membranes, diffusion is the process of transport of ionic species across the membrane [Helfferich 1962]. The ionic flux involves a transfer of electric charge. In the absence of electric current, this charge transfer must be balanced by one or more ionic fluxes. The compensation of the fluxes is brought about by the electric potential gradient, called the diffusion potential, built up by the diffusion process. Thus, diffusion of ionic species in membrane is not an independent phenomenon. In certain cases, the overall diffusion rate from bulk solution on one side to bulk solution on the other side may be controlled by diffusion in either the membrane (membrane diffusion control) or the liquid films, which adhere to the membrane surface (film diffusion control). To avoid film diffusion control, the concentrations in the bulk solutions are kept uniform by stirring.

Diffusion process in any isotropic substance, including IEMs, can be expressed mathematically by Fick's laws [Crank 1964]. According to Fick's first law (equation 1.2) of

diffusion, the rate of transfer of diffusing substance through a unit area of a section is proportional to the concentration gradient measured normal to the section

$$J = -D \frac{dC}{dx} \quad (1.2)$$

where, D is the diffusion coefficient of the species (unit cm^2/s) and J is the flux in unit of $\text{moles}/\text{cm}^2/\text{s}$. The negative sign shows that diffusion occurs in the opposite direction to that of increasing concentration. D is a matrix parameter governing the mobility of the ionic species and hence, the transport rate. The change in concentration with time is given by Fick's second law as

$$\frac{\partial C}{\partial t} = D \frac{\partial^2 C}{\partial x^2} \quad (1.3)$$

Self-diffusion is diffusion of a species in a medium or between two media having no concentration gradient. In such a case, the diffusion constant, called the self-diffusion coefficient (SDC), gives the true mobility of any species in the matrix. The entropy of mixing is the driving force for self-diffusion. This is characteristic for a particular type of cation in a particular medium and depends on the nature and composition of that particular phase and on temperature. Self-diffusion of ions in a membrane matrix is governed by two important factors, the physical and chemical architecture of the polymer matrix through which the counterions are moving and the nature of interaction of the counterions with the functional group on the polymer backbone.

It has been generally observed that the SDCs of the ions of same valence in a particular medium decrease with increasing ionic size. Also, the SDCs of monovalent ions are distinctly higher than the divalent ions except for Cs^+ , which has a low SDC. This behavior has been explained on the basis of hydration characteristics of the ions and their electrostatic interactions with the fixed charged groups in the membrane. The distinctly different

behaviors of the mono and divalent ions can be used to identify the valence state of the diffusing ions in the membrane. Radiotracers are extensively used for measuring self-diffusion coefficient of ions in membranes. Other methods like conductivity measurements and pulse field gradient NMR also have been used for the same. The detail of different methods for SDC determination are given below

a) Radiotracer permeation method

This method involves exchange of two isotopic counterions in a system, which is in equilibrium except for isotopic distribution [Helfferich 1962]. In practice, self-diffusion is measured by monitoring the transport of a cation through the membrane from one compartment to another compartment. In one of the compartment, the cation is tagged with an carrier free radiotracer. The two solutions on either side otherwise have the same concentration. The steady state self-diffusion ionic flux is given by [Lopez et al. 1977]

$$J = \frac{-\bar{D} \bar{C}}{d \left(1 + 2 \frac{\bar{D} \bar{C} \delta}{DCd} \right)} \quad (1.4)$$

where, D is the diffusion coefficient, C is the molar concentration, d is the thickness of the membrane and δ is the thickness of the unstirred liquid film at the membrane surface. The over bar terms refers to values in the context of the membrane. The second term in the parenthesis of the denominator is significant only when the diffusion through the unstirred liquid film begins to limit the overall ionic flux. If well-stirred solutions are used, then the equation 1.4 reduces to

$$J = \frac{-\bar{D} \bar{C}}{d} \quad (1.5)$$

Thus \bar{D} can be calculated from measured J and known \bar{C} . This method has been extensively used for determining SDC using radiotracers [Lopez et al. 1977, Yeager and Kipling 1979, Yeager et al. 1980, Yeager & Steck 1981, Yeager 1982 (a), Verbrugge & Hill 1990, Verbrugge et al. 1992, Pourcelly et al. 1996, Rollet et al. 2000].

b) Non-Stationary Radiotracer Method (Transient Method)

This method of measuring self-diffusion coefficient of ions and water in IEMs is essentially based on the analysis of kinetics of isotopic exchange in the membrane using an analytical solution of Fick's second law. This transient method of SDC determination is simple, does not require stringent control over hydrodynamics near the membrane, and is faster because a single measurement can yield the SDCs of the ions [Goswami et al. 2001]. The method is based on the assumptions that (i) it is a membrane controlled diffusion process, (ii) the SDC of any species within the membrane is constant, and (iii) diffusion process is one dimensional. The first assumption is valid only if the concentrations of the radiotracer ions at both the boundaries are same as that in the bulk solution. In the case of radiotracer sorption experiment, the membrane free of radiotracer is kept in contact with an equilibrating salt solution containing radiotracer ions. With the initial conditions $t=0$, $0 < x < L$, $c=0$ and boundary conditions $t>0$, $c=c^*$, $x=0$, and $x=L$, the solution of equation 1.3 is

$$c(x, t) = c^* + \frac{2c^*}{\pi} \sum_{n=1}^{\infty} \frac{(\cos n\pi - 1)}{n} \sin \frac{n\pi x}{L} \exp\left(-D \frac{n^2 \pi^2 t}{L^2}\right) \quad (1.6)$$

where, L is the thickness of the membrane. For a fixed time ($t=t_k$), the amount of radiotracer sorbed by the membrane of area A is given by

$$n(t_k) = A \int_0^L c(x, t) dx \quad (1.7)$$

which on integration gives

$$n(t_k) = n^* \left[1 - \left(\frac{8}{\pi^2} \right) \left\{ \exp \left(-\frac{D \pi^2 t_k}{L^2} \right) + \left(\frac{1}{9} \right) \exp \left(-\frac{9D \pi^2 t_k}{L^2} \right) + \dots \right\} \right] \quad (1.8)$$

where, n^* is the total amount of the radiotracer ions in the membrane at equilibrium ($t=\infty$). In the case of reverse experiment, that is, radiotracer diffusing out of the membrane, n^* represents the total radiotracer ions in the salt solution at equilibrium ($t=\infty$). D is deduced by a non-linear least-squared fit of equation 1.8 with both n^* and D as free parameters.

In the present thesis, SDCs of different ions in different types IEMs have been measured using the non-stationary radiotracer method.

c) Conductivity Measurement

SDC of different ions in the membrane can also be determined by measuring the ionic conductivity [Millet 1990, Gavach et al. 1989, Canas et al. 2001, Bouzek et al. 2003]. The electrochemical mobility (u_i) of an ion is related to the individual diffusion coefficient of the species by Einstein relation

$$u_i = \frac{F}{RT} D_i \quad (1.9)$$

where, F is the Faraday constant, R is the universal gas constant and T is the absolute temperature (K). The diffusion coefficient (D_i) of an univalent cation present inside the membrane, can be evaluated from the membrane conductivity (σ) or resistivity ($\rho = \sigma^{-1}$) measurement as

$$D_i = \frac{kT}{z_i^2 \rho c_i F e} \quad (1.10)$$

where, k is the Boltzmann constant, z_i is the charge of the ionic species i , e is the charge of the electron (1.6×10^{-19} C) and c_i is the mobile ion concentration in the membrane given by

$$c_i = \frac{dC}{1 + dNV_{M,H_2O}C} \quad (1.11)$$

where, d is the density of the dry membrane, N is the molar ratio of water to ion exchange site, V_{M,H_2O} is the partial molar volume of water (18 cm³/mole) and C is the membrane ion exchange capacity.

d) Pulsed Field Gradient Spin-Echo NMR (PFGSE-NMR)

The pulsed-gradient spin-echo sequence permits to measure the diffusion coefficient and is used primarily for studying translational diffusion [Hornak 1998]. In PFGSE-NMR, two gradient pulses are applied. These two gradient pulses are identical in amplitude, G , and width (δ). The two gradient pulses are separated by a time Δ and are placed symmetrically about the 180° pulse. By applying a gradient to the magnetic field, the top of the sample experiences a slightly different magnetic field as compared to the bottom of the sample. Since the magnets precesses at different rates in different fields, after a 90° pulse and a PFG of a few milliseconds, it is possible to have the magnetization vectors along the length of the tube pointing in all directions instead of properly aligned along one axis of the rotating frame. Hence, if the magnetization vectors are pointing in all the directions, there is no net signal. The vectors are said to be dephased. When a PFG of opposite sign is applied for the same time, the magnetization will rephase, a signal is obtained as a measure of the extent of rephasing. So the function of the gradient pulses is to dephase magnetization from spins, which have diffused to a new location in the period Δ . These pulses have no effect on stationary spins. A reference spin is the one, which experiences no gradient pulse. The stationary spin does not diffuse during that time and its signal will be in phase with the reference spin, indicating a positive contribution to the echo. The diffusing spin does not come back into phase with the reference spin so it diminishes the echo height. The

relationship between the signal (S) obtained in the presence of a gradient amplitude G_i in the i direction and the diffusion coefficient (D) in the same direction is given by the following equation

$$S = S_0 \left[-(G\gamma\delta)^2 D(\Delta - \delta/3) \right] \quad (1.12)$$

where S_0 is the signal at zero gradient. The diffusion coefficient is typically calculated from a plot of $\ln(S/S_0)$ versus $(G\gamma\delta)^2 (\Delta - \delta/3)$. Diffusion in the X, Y or Z direction may be measured by applying the gradient respectively in the X, Y or Z direction. This method has been extensively used for measuring ion and water diffusion coefficients in ion exchange membrane [Zawodzinski et al. 1991, Gong et al. 2001, Jayakody et al. 2004, Rollet et al. 2003, Saito et al. 2005, Tsushima et al. 2005].

1.1.3.2. Ion Exchange Isotherm

The ion exchange isotherm of an IEM shows the distribution of a particular type of ion between the solution and the membrane at equilibrium. In this, the equivalent fraction of the counter ion A in the membrane is plotted as a function of the equivalent fraction in the solution. The equivalent ionic fraction is defined as

$$x_A = \frac{z_A m_A}{\sum z_i m_i} \quad (1.13)$$

where the summation is carried out over all counter ion species. Here, m_i is the moles of the i^{th} component. A representative ion exchange isotherm for a bi-ionic system under different preferential conditions is given in figure 1.7.

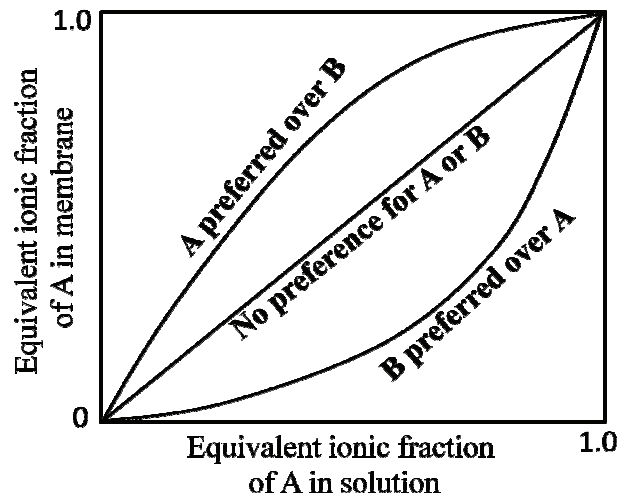


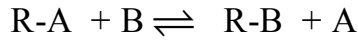
Figure 1.7: The ion exchange isotherm for a A-B system under different preferential conditions in IEM.

If the membrane has no preference for A or B, then the equivalent ionic fractions in the membrane are same as those in the solution, which results in linear plot. On the other hand, if the ion A is preferred in the ion exchange membrane, then, the isotherm is negatively curved and lies above the diagonal, and if B is preferred, the isotherm is positively curved and lies below the diagonal. The nature of the ion exchange isotherm indicates selectivity of a particular ion in mixed ionic system. The equilibrium composition of the IEM at any solution composition can also be read from the isotherm plot.

1.1.3.3. Selectivity

When an IEM is placed in a electrolyte solution containing a counter ion different from that present in the membrane, ion-exchange equilibrium is attained following exchange of ions between the two phases [Helfferich 1962]. The concentration ratio of the two counterions in the IEM is different from that in the solution. The membrane selects one counterion in preference to the other. The ion-exchange equilibrium and the selectivity towards one ion over the other are explained by the selectivity coefficient [Marcus & Kertes 1969]. The

selectivity coefficient (K_A^B) for exchange of monovalent ions (B) with A ions bound to the ion exchanger R- in the membrane samples.



at a given composition of the equilibrating solution is given by:

$$K_A^B = \frac{\overline{x_A x_B}}{x_B x_A} \quad (1.14)$$

where x_i is the ionic fraction of i^{th} type of ion in the equilibrating solution and $\overline{x_i}$ denotes the ionic fraction of the same ion in the membrane phase. The selectivity of polymer systems towards metal ion varies with the experimental conditions and is governed by various physico-chemical parameters. Some of them are

- (a) Valence of the counterion.
- (b) Ionic solvation of the counterions.
- (c) Nature of the functional group on the polymer backbone.
- (d) Swelling characteristics of the matrix.
- (e) Concentration of the equilibrating solution.
- (f) Specific interactions in the ion exchanger like electrostatic interactions, ion-pair formations and ion association.
- (g) Association and complex formation of the counterion in solution, that is, the nature of the coion.
- (h) Dielectric constant and hydrophobicity of the matrix.

1.1.3.4. Permeability

Permeability of a species through a membrane is a practical quantity that governs the rate of transport of the species. The self-diffusion flux of a species across a membrane can be used as a quantitative measure of the permeability of that species [Helfferich 1962]. Frequently, the diffusion across a membrane is described in terms of permeation coefficient. The permeability coefficient P (cm /sec) for any diffusing species is a phenomenological quantity defined by the relation

$$\begin{aligned} J &= P(\Delta C) \\ P &= \frac{DK}{l} \end{aligned} \quad (1.15)$$

where, J is the flux, K is the distribution coefficient or solubility of the species in the membrane phase and the outside solution and ΔC is the difference in concentration of the diffusing species in the two solutions separated by the membrane of thickness l . If C_o^S and C_o^m are the concentration of the species in the solution and the membrane on the feed side (figure 1.8), respectively, and C_l^S and C_l^m are respectively the concentration in the solution and membrane on the receiver/strip side separated by a membrane, then J and K will be given by

$$\begin{aligned} J &= \frac{D}{l}(C_o^m - C_l^m) \\ J &= \frac{DK}{l}(C_o^S - C_l^S) \\ K &= \left(\frac{C_o^m}{C_o^S} \right) = \left(\frac{C_l^m}{C_l^S} \right) \end{aligned} \quad (1.16)$$

The large difference in permeability coefficient of the counter-ion and the co-ion is manifested as the perm-selectivity of the IEMs.

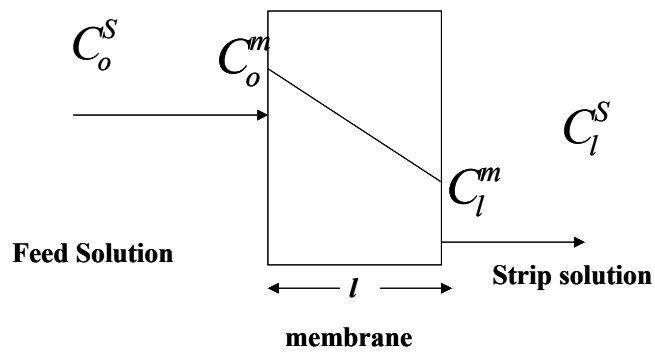


Fig. 1.8: Schematic representation of counterion concentration profile in steady state isotopic diffusion across an IEM.

1.1.4. Ion Exchange membrane based Separation processes

The most important IEM based separation processes are diffusion dialysis, Donnan dialysis and electrodialysis. The first two processes are driven by the concentration gradient, while the last one is driven by the applied electric potential across the membrane. The details of these three different processes are given below.

1.1.4.1. Diffusion Dialysis

This process is mainly used for the recovery of acids and bases from a mixture of salts. The process is based on the permselective property of the IEM. Exceptions are protons and hydroxide ions which can permeate through both cation and anion exchange membranes. The principle of this process is illustrated in figure 1.9. The cation exchange membrane allows only the cations (Na^+) and rejects the anions (other than OH^-). On the other hand, an anion exchange membrane allows only the anions (SO_4^{2-}) and rejects the cations (other than H^+), leading to recovery of acid from a salt-acid mixture.

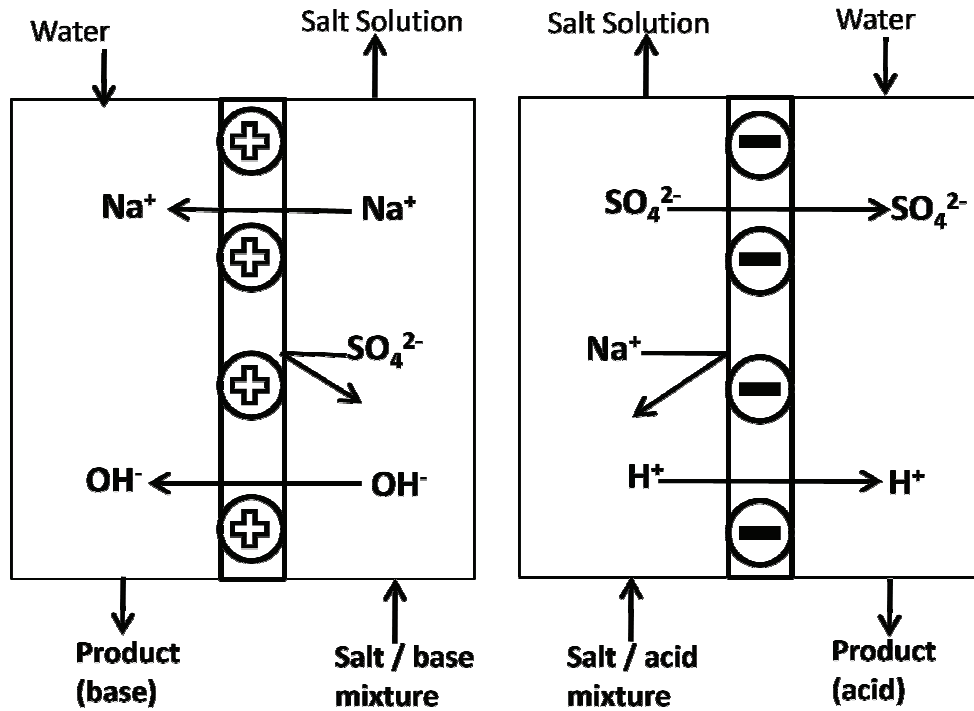


Figure 1.9: Schematic representation of the principle of Diffusion dialysis for base recovery using cation exchange membrane and acid recovery using anion exchange membrane.

1.1.4.2. Donnan Dialysis

In this separation process, ions of the same electrical charge are exchanged between two solutions through an IEM. For the electroneutrality requirement, the fluxes of the ions are coupled, i.e. the flux of a counterion through an IEM, caused by a concentration difference between the two solutions separated by the membrane, leads to a counterion transport in opposite direction. For two different cations A and B, this transport occurs till Donnan equilibrium between the feed and the strip solution is reached. The equilibrium is governed by the following relation.

$$\left(\frac{(C_A)_{feed}}{(C_A)_{strip}} \right)^{1/z_A} = \left(\frac{(C_B)_{feed}}{(C_B)_{strip}} \right)^{1/z_B} \quad (1.17)$$

Where, $(C_i)_{\text{feed} / \text{strip}}$ = Concentration of the i^{th} species either in feed or in strip solution and z_i are the corresponding valencies. The exchange of monovalent and divalent ions through an IEM for water softening is one of the envisioned applications of Donnan dialysis. The principle of this process is illustrated in figure 1.10. In strip solution, the conc. of NaCl is much higher than that of CaCl_2 . The CaCl_2 solution has much lower conc. and is referred as the feed solution. Due to the concentration difference in the two compartments, Na^+ moves from strip to feed solution. In order to maintain electroneutrality, equivalent amount of Ca^{+2} ions moves from feed to strip solution till the electrochemical potential of Na^+ and Ca^{+2} ions are equal in both the solutions. Due to high concentration difference of Na^+ in the two compartments, at Donnan equilibrium, practically all Ca^{+2} is transported to the strip solution. This process can also be used for recovery of valuable ions from a very dilute solution. Sarkar et al. [Sarkar et al. 2010] have reported several interesting separations based on Donnan dialysis, like, separation of alum from water treatment residuals and separation of citric acid and its salts from a fermentation broth.

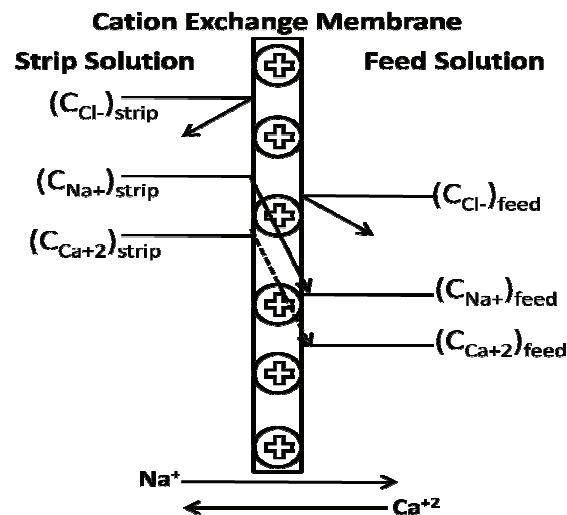


Figure 1.10: Schematic representation of the principle of Donnan dialysis with NaCl in the strip and CaCl_2 in the feed solution

1.1.4.3. Electrodialysis

The principle of this process is illustrated in figure 1.11. It consists of a series of alternating cation and anion exchange membranes. On application of electric potential across the two electrodes, the cations migrate towards the negative cathode and the anions move towards the positive anode. The cations can easily permeate the cation exchange membranes but are retained by the anion exchange membranes, while the opposite is true for the anions. The overall result is an increase in ion concentration in alternating compartments.

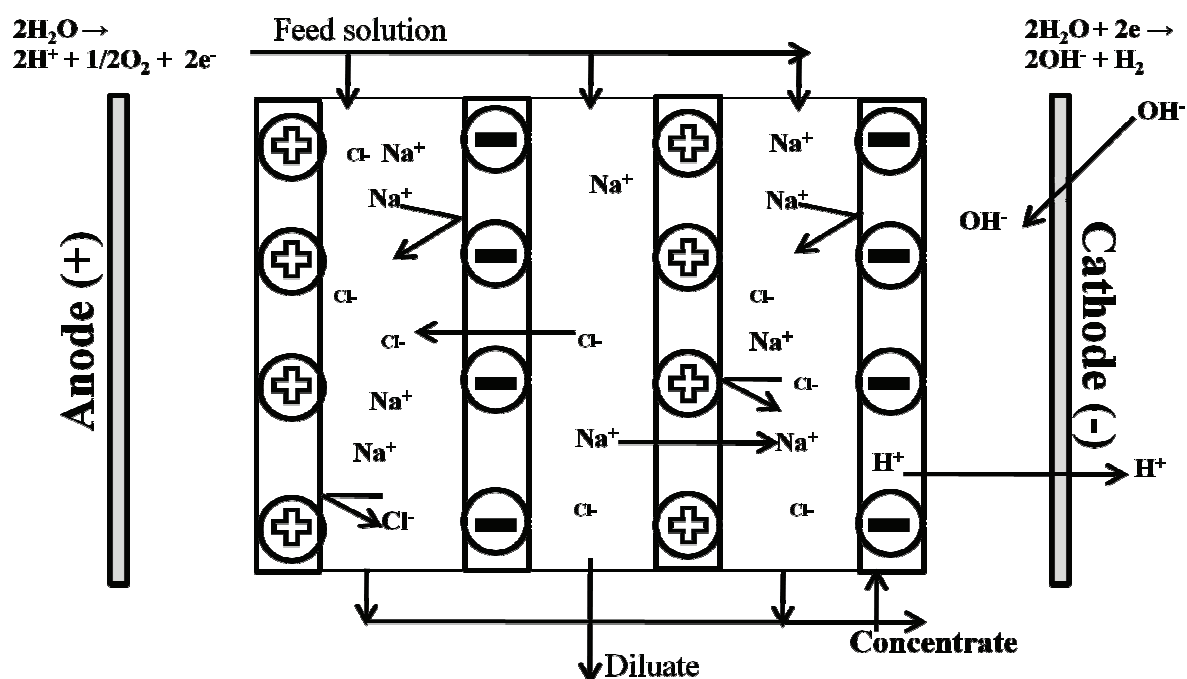


Figure 1.11: Schematic representation of the principle of Electrodialysis

The basic principle of electrodialysis has been applied in some of the experiments described in this thesis. In these works, cation ($\text{Cs}^+ / \text{Na}^+$) transport through different cation exchange membrane has been studied under application of electric field. In Chlor-alkali industry (production of NaOH and Cl_2 from electrolysis of NaCl), this same principle is followed. The working principle of present set of separation experiment is shown in figure 1.12. A mixture

of NaCl and CsCl has been used in the feed compartment and deionized water spiked with NaOH (0.04 mili mole) has been used in the receiver compartment.

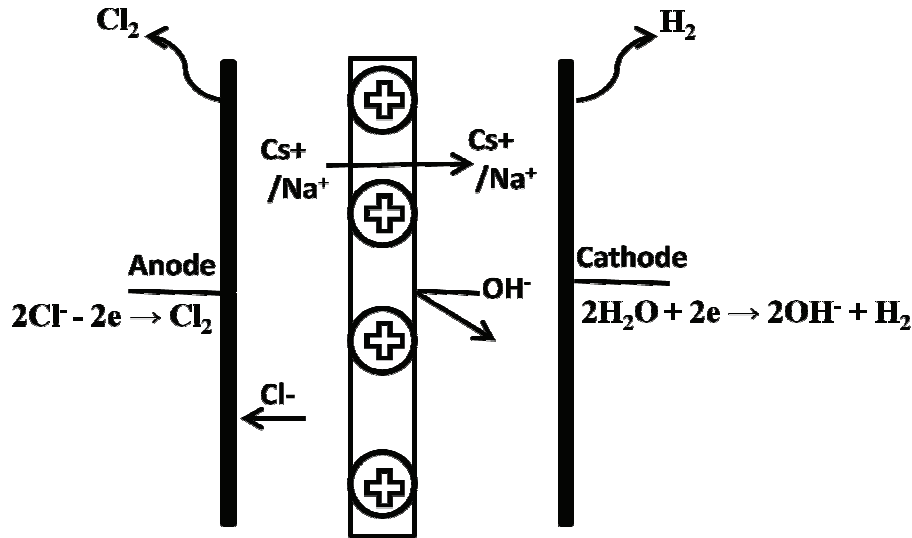


Figure 1.12: Working principle of electric field driven cation transport through cation exchange membrane.

In the present set of experiments, on application of an electric field across the membrane, the anion in the feed compartment is oxidized at the anode, subsequently forcing the cation to move to the receiver phase without requiring any counter transport. The use of electric field, thus, eliminates the need of adding salt or stripping agent in the receiver side. Electric field also helps to enhance the cationic flux in the membrane with subsequent reduction in the transport time. This can be understood from the following relations. Without any applied potential, the flux (J_i) for i^{th} cationic species (valency z_i , concentration C_i and diffusion coefficient D_i) is governed by the concentration gradient of the species and is given by the Fick's 1st law (eq. 1.2)

Under electric field, the enhanced flux of the species is given by the Nernst Planck equation

$$J_i = (J_i)_{\text{diff}} + (J_i)_{\text{el}} = -D_i \left(\frac{\partial C_i}{\partial x} + z_i C_i \frac{F}{RT} \frac{\partial \Phi}{\partial x} \right) \quad (1.18)$$

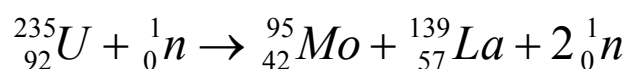
where, Φ = electric potential, F = Faraday constant, R = gas constant and T = absolute temperature. This equation applies whenever an electric field exists. The field may be generated by an external source or by diffusion within the system. Nernst Planck equation does not include the effect of pressure gradient and convection.

This kind of membrane based analyte preconcentration method under the influence of electric field (called as electro-membrane extraction) is currently receiving attention [Pedersen et al. 2008, See and Hauser 2011, Kuban et al. 2010, Morales-cid et al. 2010]. This type of extraction process, being electric field driven, more than 50 % cation transport is expected, which otherwise is not possible in other type of dialysis processes.

In the present work, attempt has been made to understand the effect of membrane ionic composition on the SDC of Cs^+ and to prepare Cs^+ selective IEMs for electrodriven selective transport of Cs^+ over Na^+ with emphasis on Cs^+ removal from simulated nuclear waste solution.

1.2. Nuclear Waste

In India, Nuclear power is the 4th largest source of electricity and there are 21 nuclear power plants (in 2014) in operating condition, generating 5,780 MWe. In nuclear reactor, nuclear fission chain reaction is sustained in a controlled manner and the thermal energy released during the burning of fissile material is utilized for the generation of electricity. This involves the disintegration of the fissile material such as ^{235}U into two fragments and evolution of large amount of energy. A typical fission reaction is presented as:



In India, a closed nuclear fuel cycle is followed, where, U and Pu are recovered from spent nuclear fuel solutions using hydrometallurgical processes. The raffinate of these processes contain several long lived fission products like ^{99}Tc , ^{129}I , ^{135}Cs and ^{97}Zr along with relatively shorter half life fission products such as ^{137}Cs , ^{90}Sr and trans-uranium elements. Because of health hazards associated with the nuclear radiations, nuclear waste disposal needs to be given special attention compared to any other types of industrial wastes. Radioactive wastes are generated at every stage of nuclear cycle and their disposal depends upon the nature of the waste.

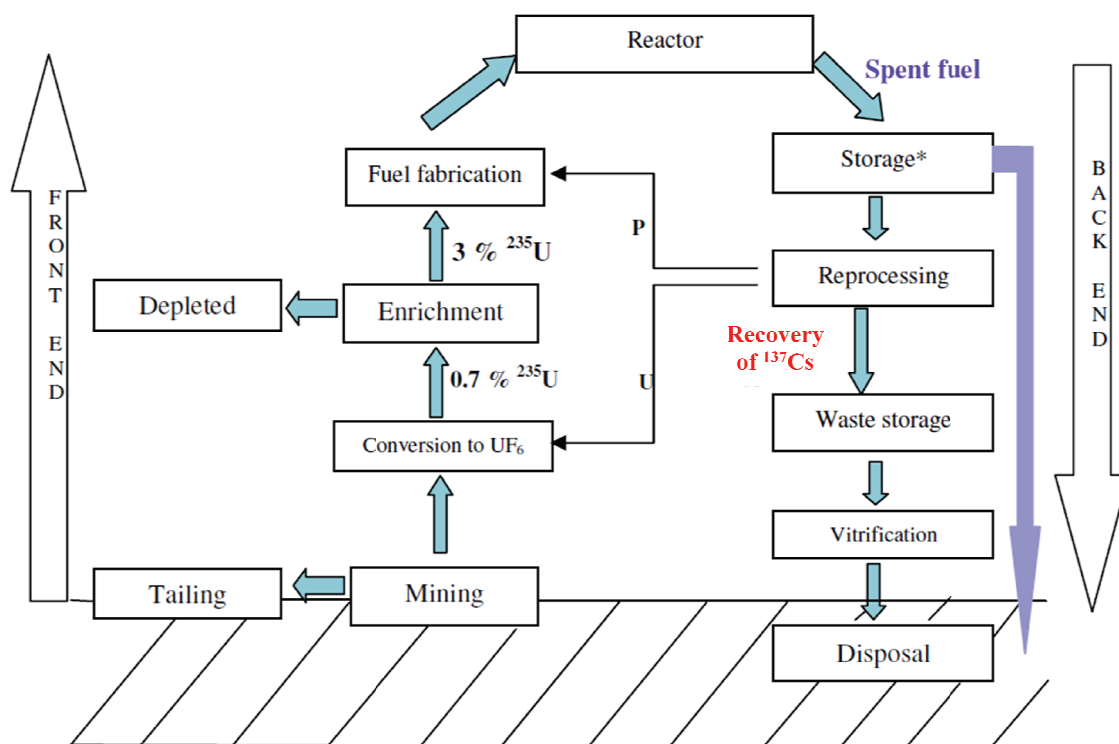


Fig.1.13: Schematic presentation of nuclear fuel cycle. In open fuel cycle storage is followed by disposal (indicated by violet color path) while in closed fuel cycle it follows the steps indicated prior to disposal.

The Nuclear fuel cycle, as shown in Fig. 1.13, begins with mining of uranium and ends with disposal of the wastes generated. The front end of the cycle includes mining, milling, extraction, purification, fuel fabrication and use of uranium in the reactor, while the back end covers the removal of used fuel from the reactor core, its subsequent reprocessing to recover valuables radionuclides, and finally the disposal of the wastes. In closed fuel cycle strategy, the spent nuclear fuel rods, after sufficient cooling period, are dissolved in nitric acid medium (PUREX- Plutonium Uranium Reduced Extraction process) for the recovery of Pu and depleted uranium for their subsequent use as fuels. The raffinate of PUREX process contains a large number of fission products, which are the main contributors for the heat output and are the major source of radiation. Table 1.2 shows the major radioactive nuclides (fission / activation products) that are present in the spent fuel after a cooling period of 50 days [Holder 1978].

Table 1.2: Major contributors to the radioactivity in the spent fuel after a cooling period of 50 days.

Nuclides	Half life	Nuclides	Half life	Nuclides	Half life
^3H	12.3 y	^{95}Nb	35 d	^{140}La	40.2 d
^{85}Kr	10.8 y	^{103}Ru	39.6 d	^{141}Ce	32.4 d
^{89}Sr	50.6 d	^{106}Ru	367 d	^{143}Pr	13.6 d
^{90}Sr	28.5 y	$^{129\text{m}}\text{Te}$	34 d	^{144}Ce	285 d
^{90}Y	64.1 h	^{131}I	8.05d	^{144}Pr	17.3 min
^{91}Y	58.8 d	^{137}Cs	30.07 y	^{147}Nb	11.1 d
^{95}Zr	65 d	^{140}Ba	12.8 d	^{147}Pm	2.62 yr

Depending upon the radioactivity concentration, the radioactive waste can be classified as low level, intermediate level and high level. In low level waste (LLW), the radioactivity concentration is less than mCi/l . It is generated from the hospitals, laboratories and industry as well as from various stages in the nuclear fuel cycle. Usually, it is buried in shallow landfill sites. Before disposal, its volume reduction is done by either compaction or incineration (in closed containers). When the radioactivity concentration in the waste ranges from mCi-ci/l , it is referred to as intermediate level waste (ILW). The ILW typically comprises of the resins, chemical sludge and reactor components. It may be solidified in concrete or bitumen for disposal. The activity concentration in the high level waste (HLW) is greater than Ci/l . It is conceptualized as the waste consisting of the spent fuel and the liquid effluent arising from the reprocessing of the spent fuel. As indicated, the HLW contains the long lived fission products, minor actinides and unrecovered U and Pu along with the structural materials and process chemicals. This type of waste requires proper cooling as well as special shielding during handling and transport. Major challenge in the final disposal of HLW is due to the radio toxicity and health hazards of the long lived minor actinides and the two heat emitting radionuclides viz.; ^{137}Cs and ^{90}Sr . Before disposal, this type of waste requires special treatment to remove certain nuclides and the prescribed treatment depends on the nature of radionuclide, particularly the half life, which range from fractions of second to millions of years.

1.2.1. Sources of Radio-Cesium

Cesium (Cs), being one of the major fission product of U and Pu, is of major environmental concern due to its radiotoxicity and has four major isotopes present in the radioactive waste, ^{133}Cs (stable), ^{134}Cs , ^{135}Cs and ^{137}Cs . ^{135}Cs has a half life in the range of few million years while that of the other cesium isotopes are much lower. Due to very high fission yield (6% from thermal neutron fission of ^{235}U) and high gamma output (at 662 keV), even after 30

years (half life = 30.2 yr), a major portion of the heat and the gamma radiation in HLW is contributed by ^{137}Cs . In terms of weight, it is estimated that about 240 g of ^{137}Cs is produced from 1 tonne of fuel irradiated in Pressurized Heavy Water Reactor at the rate of 6,700 MWD/tonne. Separation and recovery of this radionuclide from nuclear waste will not only solve the problem of personnel exposure, but also will facilitate waste management and make this isotope available for further beneficial use.

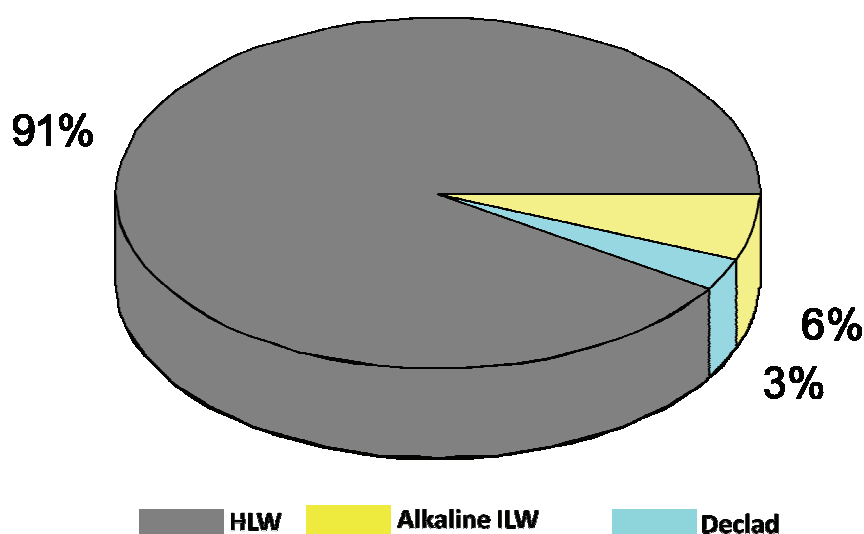


Figure 1.14: Typical distribution of ^{137}Cs in different waste available for recovery at Trombay.

Among the different types of wastes generated, three waste streams are important with respect to Cs recovery point of view. These waste streams are (i) Acidic HLW (ii) Alkaline ILW and (iii) Alkaline declad waste. The acidic HLW generated from reprocessing plants in India have gross β activity in the range of 10-30 Ci/L which is due to the presence of major radionuclides ^{137}Cs (3-10 Ci/L), ^{90}Sr (3-10 Ci/L), fission products and several actinides [Kaushik et al. 2000]. The ILW generated at the back end of nuclear fuel cycle is alkaline in nature and has high salt loads. The waste has gross β activity in the range of 4-50 mCi/L with ^{137}Cs as the major radionuclide and traces of ^{90}Sr , ^{106}Ru etc. The declad waste, generated

from the chemical dissolution of aluminium clad natural uranium fuel irradiated in research reactors, is characterized by much higher concentration of NaOH, Al and Na-salts. However, with respect to activity content, it is similar to that of ILW. It is worth mentioning here that, although ^{137}Cs concentration in both the alkaline streams are quite low, total inventory of ^{137}Cs in these waste streams are quite significant because of high waste volumes. A typical distribution scheme of this radioisotope in the waste streams is shown in figure 1.14. It can be seen that the acidic HLW generated from reprocessing plants is the main source for ^{137}Cs .

1.2.2. Health Hazards of Radio-Cesium

Radio cesium if released in to the atmosphere, gets sorbed by the moisture and return to the earth's crust as a consequence of radioactive fallout. Once, it enters ground water, it is deposited on sediment surfaces and removed from the landscape primarily by the transport processes. The accident at the Chernobyl nuclear power plant resulted in the release of an estimated $5.4 \times 10^5 \text{ Ci}$ ($2.0 \times 10^{16} \text{ Bq}$) of ^{134}Cs and $1.1 \times 10^6 \text{ Ci}$ ($4.0 \times 10^{16} \text{ Bq}$) of ^{137}Cs into the atmosphere over Europe. Once released, the radioactive cesium isotopes persist in the environment, with the potential to cause adverse health effects. Radiation exposure can be external or internal through ingestion of radioactive cesium-contaminated food. The hazards of external exposure to ^{134}Cs and ^{137}Cs are similar to those of other beta- gamma emitting radionuclides. Workers can get exposed to cesium through oral, dermal, and inhalation routes. Energy released by radioactive isotopes can result in significant damage to the living cells. Signs and symptoms of acute toxicity from external and internal exposure to high levels of radiation from ^{134}Cs or ^{137}Cs are typical of those observed in cases of high exposure to ionizing radiation [Sokolov 2001].

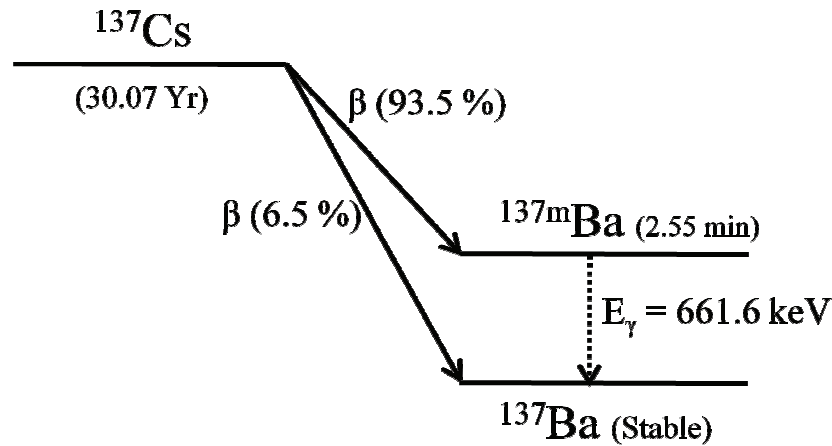


Figure 1.15: Decay scheme of ^{137}Cs .

1.2.3. Applications of ^{137}Cs

The decay scheme of ^{137}Cs is shown in figure 1.15. Due to the reasonably high gamma energy (661.6 KeV) and long half-life, ^{137}Cs has potential application as a radiation source in gamma irradiators in place of ^{60}Co for a variety of purposes as listed below. The use of ^{137}Cs in place of ^{60}Co ($t_{1/2} = 5.2$ years, 1173 KeV, and 1332 KeV) will also reduce shielding requirements and frequency of source replenishment. Various uses of ^{137}Cs based gamma irradiator are listed below [Sadat 1994].

- Food preservation: Irradiation of food samples kills the harmful microorganisms and bacteria resulting in increased shelf life of the food without affecting the taste and flavour.
- Sewage sludge treatment: Disinfection of sewage sludge by gamma radiation is done in order to render it suitable as a fertilizer or soil conditioner in the urban environment. The gamma irradiation of sewage sludge does not cause any coagulation in the waste.
- Sterilization of medical accessories: Different medical products and accessories can be sterilized by the use of gamma irradiation.
- ^{137}Cs irradiators are also used in brachytherapy which is an effective treatment for cancer.

f. ^{137}Cs is widely used throughout the construction industry for level, moisture, and thickness gauging applications. Cesium is also commonly used in medical research & treatment and oil well drilling.

1.2.4. Separation/recovery methods for ^{137}Cs

The scientific principles that govern the separation of Cs from waste solutions are similar to those of other metal ions and are based on chemical reactions, equilibrium kinetics, fluid mechanics and mass transfer from one phase to another. A number of methods have been developed for the recovery of this radionuclide from acidic and alkaline waste solutions. However, few of them have been tested at plant scale [Orth et al. 1994, Schulz 1987]. Literature reports on separation of Cs from acidic waste solutions include the use of number of techniques viz., precipitation, ion exchange and solvent extraction. A brief discussion of these techniques is given below.

1.2.4.1. Precipitation Method

Sodium phosphotungstic acid $\{\text{Na}_3[\text{P}(\text{W}_3\text{O}_{10})]\cdot 4\text{H}_2\text{O}\}$ used for Cs recovery from the acidic waste. Phosphotungstate anion, reacts with Cs(I) ion in acidic (0.5 to 5M HNO_3) medium to form insoluble precipitate. Further, it can be dissolved in NaOH solution to recover Cs. Similar chemistry has been used for recovery of Cs from the PUREX waste at Hanford site, U.S.A. [Singh 1983].

1.2.4.2. Ion Exchange Methods

Ion exchange methods have been widely used for the Cs recovery from the waste solutions. The use of inorganic ion exchangers (IIX) offers many advantages over the use of regenerable organic ion exchangers. The IIX are much more resistant to chemical, thermal and radiation degradation. Three groups of exchangers have potential use in the removal of

cesium from acid wastes: ferrocyanides, phosphates and oxides. Cu-ferrocyanide (CuFC , $\text{K}_2\text{-xCu}_{\text{x}/2} [\text{CuFe}(\text{CN})_6] \cdot \text{nH}_2\text{O}$, $\text{x}=1.22$), heteropolyacids (Ammonium molybdophosphate (AMP), Ammonium tungstophosphate ($(\text{NH}_4)_3\text{PW}_{12}\text{O}_{40} \cdot 3\text{H}_2\text{O}$ (AWP)) and zeolites (modernite, clinoptilolite) were used for the uptake of the Cs [Mimura et al. 2002]. Use of metal ferrocyanides for Cs removal has been discussed in details in the later part of the thesis.

(a) Titanates

Crystalline silicotitanates, (CSTs) are a class of ion exchangers that were jointly invented by researchers at Sandia National Laboratories and Texas A & M University [Miller et al. 1997, Walker 2000]. In alkaline media, cesium is strongly sorbed by CST's. Cesium cannot be easily removed from CST and, therefore, the exchanger becomes part of the final waste form. Major drawbacks such as inefficient elution of the loaded cesium and long term stability are issues which need to be addressed.

(b) Ammonium Molybdophosphate (AMP)

Ammonium molybdophosphate $[(\text{NH}_4)_3\text{Mo}_{12}\text{O}_{40}] \cdot 3\text{H}_2\text{O}$ is a dark yellow crystalline inorganic compound that has been shown to have the requisite selectivity for Cs and stability. Due to its microcrystalline nature it has been always a challenge to the researchers to load it on to a support material. Poly acrylo nitrate (PAN) is commonly used support material for AMP. The performance of the AMP coated PAN has been extensively studied [Sebesta et al. 1996]. The Cs loading in all cases has been found to be related directly to the AMP content of the material and no adverse effect on Cs loading due to support material was reported. However, the elution of the loaded Cs from AMP is not easy task and cesium cannot be quantitatively eluted from this material. The study on radiation stability of AMP [Rao et al. 1995] revealed no effect on the uptake capacity even upto 1 MGy dose. In general, the advantages of AMP are,

- High distribution coefficient in acidic media
- High loading capacity
- High selectivity for Cs ion in complex mixture
- Rapid uptake
- Soluble in alkaline solution

While the disadvantages include,

- Difficulty of elution of the absorbed Cs
- Microcrystalline nature making it unfavorable for column use
- The high loading in the AMP results in high radiation doses in and hot spots on column, requiring cooling solution
- Heat generation can affect the support material.

(c) Resorcinol Formaldehyde Polycondensate Resin (RFPR)

The resin is an alkali catalyzed polycondensation product of resorcinol and formaldehyde, in which the phenolic OH group of resorcinol ionizes under alkaline conditions and functions as cation exchanger. It is noteworthy that the RFPR has extensively been used for the separation of ^{137}Cs from low and medium active alkaline waste solutions [Samanta et al. 1995, Hassan et al. 2004, Fiskum et al. 2008]. The main reasons behind the selection of the ion exchanger are (i) high selectivity for Cs (ii) high ion exchange capacity (iii) high radiation stability and (iii) ease of availability. Further, the weakly acidic nature of the functional groups facilitates the recovery of Cs^+ ions from loaded resin by elution in small volumes of dilute acid. The ion exchange cycle for the separation of ^{137}Cs by RFPR can be represented as follows (figure 1.16). As the resin can only process alkaline solution, it is considered that the acidic eluate will be neutralized prior to Cs separation.

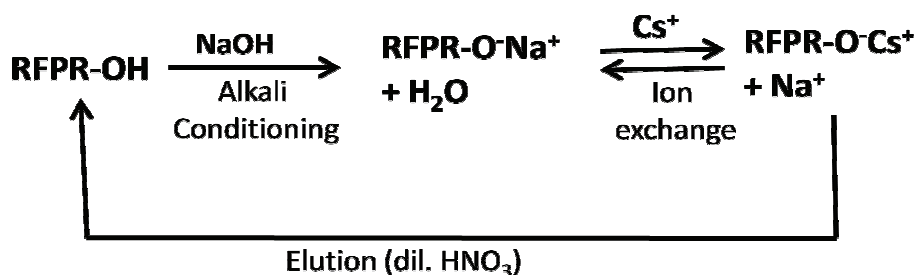


Figure 1.16: Ion exchange cycle for RFPR.

1.2.4.3. Solvent Extraction Methods

Solvent extraction technique is attractive due to large throughput, continuous nature and ease of operations. A number of methods were developed using various reagents so far to recover Cs from the waste solution. These methods primarily dwell on the use of chlorinated cobalt dicarbollide (CCD⁻) and macrocyclic ionophores as the extractants.

(a) Dicarbollides

Cobalt Dicarbollide is an organometallic complex of cobalt with two boron cluster compound. The structure of CCD⁻ is shown in figure 1.17. The protonated form of CCD⁻ (HCCD) has first been prepared by Hawthorne in 1965 and then extensively studied by Czech scientists [Kyrs 1994, Hawthorne 1997]. The process, based on the use of CCD⁻ in polar diluent (metanitrobenzotrifluoride-FS13), has been developed at the Nuclear Research Institute in Czechoslovakia and successfully adopted in the commercial separation plant at Mayak PA in Russia [Ramonovsky 2003]. The loaded Cs on CCD⁻ can be stripped using 5-6 M HNO₃. Poorly hydrated dicarbollide anions associate with the cations to form neutral compounds. Though dicarbollides display good stability towards radiation [Kyrs 1994], main drawback is the large scale use of nitrobenzene as the diluent. Also the halides present in the chlorinated cobalt dicarbollide can get released in the solution, which may lead to corrosion.

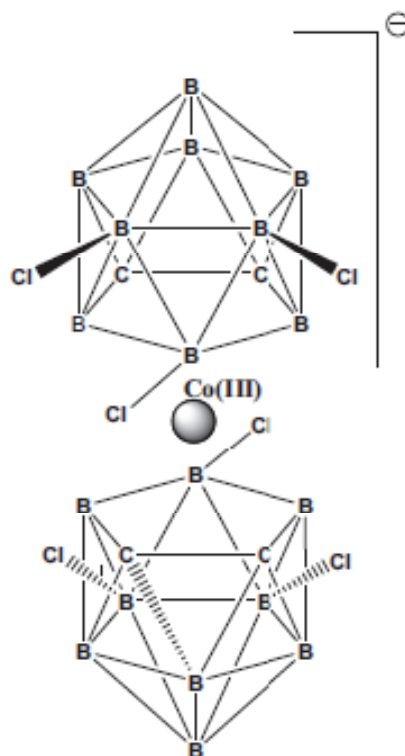


Figure 1.17: Structure of Chlorinated Cobalt Dicarbollide anion.

(b) Macrocyclic Ionophores

Macrocyclic ionophores are relatively large cyclic compounds containing donor atoms to bind metal ions. These compounds, in general have hydrophilic interior and hydrophobic exterior which enable them to extract metal ions efficiently. Macrocyclic ionophores such as crown ethers and calix crowns have also been proposed for selective extraction of cesium.

(i) Crown Ethers

Depending upon the similarities between the cavity size of the ionophores and the ionic size, different crown ethers are known to be selective for different metal ions. Blasius et al. [Blasius et al. 1984-p 173, Blasius et al. 1984-p 207] used DB21C7, out of several crown ethers, to extract cesium from two medium active wastes mainly containing sodium nitrate and nitric acid. Only DB21C7, used in high dielectric constant diluents such as nitromethane and nitrobenzene, showed reasonably good extraction of cesium. However, the distribution

coefficients are too low for practical applications. A way to increase cesium extraction is the addition of voluminous and polarizable anions such as molybdophosphate, tetra phenyl borate, hexachloro antimonite etc. Gerow et al. [Gerow et al. 1979, Gerow et al 1981] developed extraction method for cesium from high active acidic liquid waste using substituted crown ethers. Cesium can be stripped from the aqueous phase by 1M nitric acid. Dietz [Dietz et al. 1996] evaluated several crown ethers, viz.; dicyclohexano-18-crown-6, di-*tert*-butyl-benzo-18-crown-6, di-*tert*-butyl-benzo-21-crown-7 and di-*tert*-butyl-benzo-24-crown-8 for cesium extraction from 4 M HNO₃. However, none of the tested compounds provided the ideal combination of extraction efficiency, selectivity, stability and solubility and thus were employed for actual plant scale use.

(ii) Calixerens

Different types of Calixarenes are found to be selective for different metal ion due to favorable conformations. For example, the cone conformation was found to be highly effective in selective extraction. Arnaud et al. [Arnaud-Neu et al. 1991] reported that calix[4]arenes bearing ester or ketone groups displayed higher affinity for alkali cations, especially for sodium. The introduction of the *p-tert*butyl groups on the calix[6]arenes strongly increases the complexation of the Cs(I). Izatt et al. [Izatt et al. 1985] reported selective transport of Cs⁺ by using calixarene in a mixture of dichloromethane and CCl₄. The selectivity was found to increase as the size of the calixarenes decreased. The major advantages of calixarenes are,

- Negligible carrier loss due to low water solubility.
- Irradiation stability.
- High selectivity

that due to low water solubility, carrier loss is negligible besides its selective nature and irradiation stability.

(iii) Calix crowns

In search of better extractants than crown ethers and calixarenes, efforts were made to include crown ether moieties into the calixarene framework. This led to the synthesis of compounds known as the calixcrown. It has been found that in spite of the presence of two cavities, the stoichiometry of the metal-ligand complex was 1:1 with calix-bis-crown-6 [Haverlock et al. 2000]. The selectivity of this calixcrown-6 is very high for Cs in the presence of Na (29000 in nitro phenyl hexyl ether), which has been attributed to the stabilization of the Cs-calix-crown complexes by the four benzene units. The presence of the 'benzo' or 'naptho' group enhances the organophilicity and selectivity. Even the presence of second benzene group on the crown moiety has shown high distribution coefficient for the Cs(I) at higher acidity (~ 4 M). Wipff and Lauterbach [Wipff and Lauterbach 1995] concluded that this selectivity for cesium is related to solvation effects rather than to interactions with the *pi* electrons of benzene units. Though several solvents have been developed world wide for cesium recovery, calix-crown based reagents are amongst the most promising for the selective recovery of Cs from acidic waste solutions. However, high cost of reagents necessitates the need for development of methods with low ligand inventory.

1.3. Scope and Aim of Work

The aim of this thesis work is to study the different aspects of Cs^+ diffusion and transport through different IEMs. Attempt has been made to understand the effect of membrane ionic composition on the SDC of Cs^+ and to prepare Cs^+ selective IEMs for electrodriven selective transport of Cs^+ over Na^+ with emphasis on Cs^+ removal from simulated nuclear waste solution. In order to have a clean separation of Cs^+ , a novel method of electromembrane extraction has been attempted. The work presented in the thesis can be broadly summarized as follows

1. In order to understand the transport behavior of Cs^+ in Nafion membrane, the self-diffusion coefficient (SDC) of cations (Na^+ / Cs^+ / Ba^{+2}) have been measured in mixed cationic compositions of the membrane.

2. In general, separating (with high degree of selectivity) ions of similar charge using IEM alone is difficult. The selectivity can be imparted by incorporating some macrocyclic ionophores within the membrane matrix. However, high degree of selectivity is achieved only at the cost of cationic mobility within the membrane. In this work, attempt has been taken to enhance the transport selectivity of Cs^+ , by templating Nafion membrane with Cs^+ selective crown ether. This composite membrane system has been chosen because the crown ether can impart the selectivity for the desired metal ion and the polymeric backbone of the membrane can compensate for the charge requirement of the metal ion-crown ether complex. In order to explore the possibilities of tuning the metal ion selectivity at higher temperature, the temperature dependence of the SDCs of cation (Cs^+ / Na^+) and water diffusion within this composite membrane matrix has been studied. In an attempt to achieve selective transport of Cs^+ over Na^+ at room temperature, two types of Cs^+ ion selective crown ether-Nafion composite membranes have been prepared. In one case, DB21C7 has been incorporated uniformly in Cs^+ form of Nafion-117 membrane in varying molar ratio with respect to Cs^+ and in the other case, Cs^+ driven loading of DB21C7 has been confined to a very small thickness (25 μm) from one of the surfaces of the Nafion-117 membrane (ion gating). Electrodriven (4 V) transport experiments using these membranes have been carried out to study the transport selectivity of Cs^+ over Na^+ . The suitability of the gated membrane for selective removal of ^{137}Cs from a simulated nuclear waste solution has also been studied.

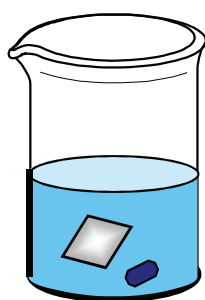
3. In another attempt to prepare Cs^+ selective membrane, copper ferrocyanide crystals (KCFCN) have been synthesized within the pores of track etched membrane. The synthesis of the KCFCN crystals have been done by two compartment permeation method using CuSO_4

and $\text{K}_4\text{Fe}(\text{CN})_6$. The composite membrane (KCFCNm) has been characterized using different techniques like X-ray Diffraction (XRD), Small Angle X-ray Scattering (SAXS), Energy Dispersive X-ray Fluorescence (EDXRF) and Transmission Electron Microscopy (TEM). The transport selectivity of this composite membrane for Cs^+ over Na^+ has also been studied under electric field. Attempt has been taken to systematically study the properties of the KCFCNm for removal of Cs^+ from neutral aqueous solution. The composite membrane has also been used to remove Cs^+ from a 1 L simulated nuclear waste solution.

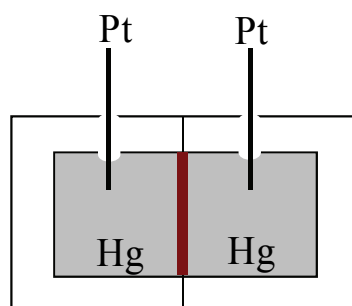
4. A highly Cs^+ selective IEM has been prepared by using HCCD as a carrier in CTA/PVC based PIM. Attempt has been taken to study electrodriven selective transport of Cs^+ over Na^+ using these membranes. Experiments have been carried out to optimize the working potential of the transport system involving CTA based membrane. In view of the different possible compositions of the nuclear waste solutions, experiments have also been carried out for different feed compositions. The suitability of this membrane for selective removal of ^{137}Cs from a simulated nuclear waste solution has been studied. Transport selectivity of Cs^+ from a simulated high level nuclear waste (SHLW) solution using HCCD as carrier in PVC based PIM has also been studied.

Chapter 2

Experimental Methods



SDC Measurement



Impedance measurement



NaI(Tl) detector set up

2.1. Radiotracer based measurements

2.1.1. Self-diffusion co-efficient (SDC)

In the present thesis, self-diffusion coefficients of different ions in different types of ion-exchange membranes measured using the non-stationary radiotracer method. A general description for the measurement of SDC (say, of A^+) in the present work is given below. For the experiments involving diffusion of radiotracer ions from equilibrating solution into the membrane (absorption), a conditioned membrane sample (2 cm X 2 cm) in appropriate ionic form (A^+) was placed in 25 mL of salt solution (say ACl) containing relevant radiotracer ions (A^*) at room temperature. The equilibrium absorption of the radiotracer ion into the membrane is governed by the ratio of the amount of A^+ in the membrane to that in the external solution. If the concentration of the external salt solution is kept high, only a small fraction of radiotracer ions will thus enter into the membrane from the external solution, thereby reducing the sensitivity of radioactivity measurement and requiring a larger quantity of radiotracer to be used. For absorption experiments, the concentration of salt in equilibrating solution was thus kept at 0.02 M to maximize the absorption of radiotracer ions into the membrane. The equilibrating salt solution containing membrane sample was stirred vigorously (~500 rpm) to ensure the boundary conditions. To monitor diffusion of radiotracer ions into the membrane as a function of time, the membrane sample was taken out at regular time intervals, washed thoroughly with deionized water to remove the traces of equilibrating solution clinging to its surface, and counted for radioactivity. The membrane sample was replaced again in the equilibrating solution after counting. The actual residence time of the membrane in the equilibrating solution was used as the time of cation absorption. For γ emitting radio isotopes, the counting of the membrane was done in a fixed geometry using a well type NaI(Tl)

detector connected to a 4k channel analyzer, whereas, for β emitting isotopes, the counting was done using liquid scintillation counting.

The reproducibility of the self diffusion profile of A^+ in an ion exchange membrane by radiotracer absorption method is verified by radiotracer desorption method. For desorption experiments, the membrane samples were loaded with radioactive tracers by equilibrating the membrane sample with relevant radiotracer (A^*) salt solution. Subsequently, the membrane sample was placed in 25 mL of 0.5 M equilibrating ACl salt solution (without radioactive tracer ions) at room temperature. The 0.5 M salt solution was used to maximize desorption of radiotracer ions from the membrane. The other experimental conditions were same as those used in the absorption experiments.

The concentration profile of a radiotracer diffusing in or out of the membrane is a function of time and space and is governed by Fick's second law given by equation 1.3. The SDC of cation in the membrane is obtained from a fit of the experimental data with the equation obtained from the analytical solution of eq 1.8. In the present work, this technique has been used to measure the SDCs of different cations ($Na^+ / Cs^+ / Ba^{+2}$) in membranes like Nafion-117 with mixed ionic compositions, crown ether modified Nafion-117 and copper ferrocyanide loaded track etched membrane.

2.1.2. Ion Exchange Capacity

The experimental procedure of measurement of ion exchange capacity using radiotracer method is described as follows. The membrane was equilibrated in 30 mL well-stirred salt solution (0.1 M) containing known amount of carrier-free radiotracer (of the cation) for 2 h. Filter paper standard was prepared by taking pieces of Whatman-41 filter paper of the same dimensions (2 x 2 cm) as the membrane samples, and drying known volume (100 μ L) of the

radiolabeled 0.1 M stock salt solution on these substrates. The stock salt solution used for preparing standard samples contained same radioactive to natural isotopic ratio of the cations in the solution used for equilibrating the sorbent samples. The standards were prepared in duplicate. The soaked filter papers were dried at room temperature. The membrane samples and filter paper standard were counted in a well type NaI(Tl) detector in a fixed counting geometry. The amount of cation in the membrane sample was obtained by comparing the γ -activity of cation in the samples with filter paper standards as given below:

$$\text{Cation-Exchange Capacity} = \frac{A_{(\text{mem})}}{A_{(\text{std})}} \times M_{(\text{std})} \dots\dots\dots(2.1)$$

where $A_{(\text{mem})}$ and $A_{(\text{std})}$ are γ -radioactivity (counts/min) in sample and standard, respectively. $M_{(\text{std})}$ is moles of the cation in the solution. In the present work, this method has been used to measure the Cs^+ exchange capacity of copper ferrocyanide loaded track etched membrane.

2.1.3. Ion Exchange Isotherm

The ion-exchange isotherms in different binary systems (say, A-B system containing A^+ and B^+ cations) in different IEMs were measured using radiotracers. In this method, a number of (depending upon the experiment) equilibrating solutions containing 0.1 N ACl and 0.1 N BCl in different proportions are used, keeping the total ionic concentration fixed at 0.1 N. For each experiment, the membrane sample (in H^+ form) was kept in well-stirred equilibrating solution (30 ml) at 27°C for ~ 2 h. After equilibration, the membrane was taken out and required radiotracers ($^*\text{A}^+$ / $^*\text{B}^+$) are added to the solution. Filter paper standards from the stock solutions were prepared as described in section 2.1.2 for measuring the ion-exchange capacities. The membrane sample was put into the radiolabeled solution and kept for 3 hr with continuous stirring. When equilibrium is reached, the membrane sample was counted for its uptake of radiotracer. The radioactivity of $^*\text{A} / ^*\text{B}$ (gross) in the membrane samples and

the filter paper standards were counted under fixed counting geometry in the detector. The moles of A^+ or B^+ ions occupying the ion-exchange sites of the membrane samples was calculated as follows

$$A_{mem}^{meq} = \frac{W_{A0} A_{mem}}{A_{mem} + A_{sol}} \quad (2.2)$$

$$B_{mem}^{meq} = \frac{W_{B0} B_{mem}}{B_{mem} + B_{sol}} \quad (2.3)$$

Where, A_{mem}^{meq} or B_{mem}^{meq} = milliequivalence (meq) of the cation in membrane, A_{sol}^{meq} or B_{sol}^{meq} = meq of the cation in solution, W_{A0} or W_{B0} = meq of the cation in solution, A_{mem} or B_{mem} = activity of the cation in membrane after equilibration, A_{sol} or B_{sol} = activity of the cation left in equilibrium solution. In the present work, the ion exchange isotherms of Na-Ba and Na-Cs systems in Nafion-117 membrane have been found by this method.

2.1.4. Radiotracers in membrane characterization

Tracers are materials that are used as markers to follow the course of a chemical reaction or physical process or to show the location of a substance [Ehmann& Vance 1991]. Radiotracers are chemical species that contain a radionuclide, and it is the activity of the radioisotope that is monitored to follow the process under investigation. Radiotracers can be used either qualitatively, as simple markers of a process, or quantitatively, to determine the amount of non-radioactive species. The extensive applications of radioisotopes stem from the fact that isotopes of an element behave chemically in a similar way and hence remain essentially invariant through the course of physical, chemical and biological processes. In the present

work, ^{137}Cs , ^{22}Na , ^{133}Ba and ^3H have been used as radiotracers for Cs, Na, Ba and H_2O respectively.

The most important assumption made in the use of radiotracers is that the radioactive material blends perfectly with the system under study. This implies that the radioactivity emitted by the tracer does not adversely affect any component of the system, and that the tracer behaves in a way that is indistinguishable from the non-radioactive isotopes, except for the emitted radiation. Radiotracers are ideal markers because their radioactive characteristics are not affected by their physico-chemical nature.

In radiotracer technique, radioisotopes are used in very small amounts (10^{-16} to 10^{-6} g) either as such or in large excess of their stable isotopes. This high sensitivity is of great importance in many studies. Interference from other species does not pose a serious problem in radioanalytical technique as compared to conventional methods of analysis. Therefore, sample manipulation is minimum in the measurements of radiotracers. A good account of the application of radiotracers is included in standard textbooks on radiochemistry [Arnikar 1989, Choppin et al. 1995, Ehmann and Vance 1991]. Some of the fields in chemical research, where radiotracers find applications are listed below:

- (a) Analytical chemistry
- (b) Reaction mechanisms
- (c) Equilibrium constant measurements
- (d) Kinetics of exchange reactions
- (e) Self diffusion studies

2.1.4.1. Choice of a Radiotracer

There are several factors that should be considered while choosing a proper radiotracer for study. Some of them are;

- (a) The tracer should be chemically and physically compatible with the system to be studied under real experimental conditions.
- (b) Should have high specific activity (radioactivity per unit mass of the radioactive material), so that the quantity required to trace any chemical or biological process is very small.
- (c) The half-life of the tracer must be long enough to have sufficient activity during the course of experiment for detection and good counting statistics. But it should not be excessively long as that may result in poor specific activity, problem of disposal, storage and also high radiation dose in the case of in vitro studies.
- (d) The type of radiation emitted by the radiotracer must be considered, mainly with respect to penetrating power, ease of measurement and potential for damage to the sample.
- (e) Availability and cost of the radiotracer.
- (f) Easy accessibility of the appropriate detector systems for the measurement of radiation emitted and laboratory equipped with radioactivity handling accessories.

2.1.4.2. Production of Radiotracers

A few radiotracers, such as ^3H , ^{14}C , and products of natural decay chain of U and Th decay, are naturally occurring. However, most radiotracers used in laboratory studies are produced artificially. Radioisotopes are produced by nuclear reactions using neutrons from nuclear reactors and charged particles from various kinds of accelerators. Generally, three common production schemes are employed for the production of primary radiotracers. These are: (i) (n, γ) , (n, p) or (n, α) reactions in a nuclear reactor, (ii) charged particle induced reactions involving the use of an accelerator, and (iii) fission products from chemical separation of neutron-irradiated fissionable targets e.g. ^{235}U , ^{239}Pu . The charged particle induced reactions provide proton-rich radiotracers while other two routes, viz. (i) and (iii) provide neutron-rich

radiotracers. Majority of the radionuclides used in various applications are produced by reactions with slow neutrons in nuclear reactors. The product of (n, γ) reaction is however isotopic with the target element and cannot be used in applications involving carrier free tracers (radiotracer free of stable isotope of that element). Carrier free radiotracers are commonly produced in charged particle induced reactions or in nuclear fission. It should be noted that reference radiotracer standards are required for quantitative analysis of radiotracers in many applications. This is not a problem if carrier-free radiotracer is used. Otherwise, known amount of target should be irradiated to produce radiotracer with known amount of carrier. The unit of radioactivity is “Curie”(Ci) which corresponds to 3.7×10^{10} disintegrations per second. The SI unit is “Becquerel” which corresponds to unit disintegration per second.

2.1.4.3. Safety Considerations

Appropriate safety considerations must be followed during the handling of radiotracers. All radioactive materials can be hazardous if they are not handled properly. For conducting experiments using radiotracers one has to have a fairly good idea about the activity (disintegrations/sec) of the sample. In general micro Curies (μ Ci) to milli Curie (mCi) level of activity is used in radiotracer experiments and the γ -dose does not exceed a few mR/hour (milli Roentgens per hour) at about 1 ft distance from the source. Physical handling of low-level radioactive material is carried out using disposable latex gloves in a fume hood connected to an exhaust system.

2.1.4.4. Measurement of Radiations

In principle, all the modes of radioactive decay viz. alpha (α), beta (β) and gamma (γ) can be used for the analysis of radiotracers [L’Annunziata 2003]. If it is a liquid sample, then liquid scintillation counting is ideal for the measurement of α and β radiations. For solid samples, α

radiations can be measured either by a silicon surface barrier detector or by a flow proportional counter. In this case one has to take care that the sample is thin enough so that α particles are not stopped in the sample itself. Solid samples emitting β particles can be counted either by a Geiger counter or by a proportional counter. However, γ -emitting radiotracers are preferred for studying chemical processes. The choice of γ -emitting radiotracers is related to the fact that no special sample preparation method is required for γ -rays detection. If it is a single radionuclide, NaI(Tl) scintillation detector is ideal for γ -ray counting. Use of short-lived radiotracers has an advantage that they can decay at the conclusion of experiment and leave an essentially “non-radioactive” mixed system for further use. Thus radioactive waste disposal problem can be minimized by the use of short-lived radiotracers. However, measurement of short-lived radiotracer requires appropriate decay corrections. Also, radiotracer should not be too short-lived to decay during experiment itself. This becomes important in the experiments that do not involve rapid equilibrium. In the work presented in this thesis, three types of detectors, namely, HPGe, NaI(Tl) and liquid scintillation counter were used for measuring different types of radioactivity. A brief description of the two detector systems is given below:

(a) NaI(Tl) Detector System

Most commonly used inorganic scintillation detectors are the alkali halide crystals (e.g. NaI, CsI). These crystals can function as radiation detectors because of the electron transitions that take place between the energy levels in the crystal due to the passage of radiation [Ehmann and Vance 1991]. Pure NaI is a crystalline solid with a large band gap (~ 5 eV) between the valence and conduction band [Knoll 1989]. The incoming radiation can excite an electron from valence band to conduction band. This excited electron returns to the valence band, thereby resulting in emission of photon, that is, light scintillation. In pure NaI crystal, the

transition of electron back to the valence band with emission of a photon is an inefficient process. Furthermore, typical gap widths are such that the energy of the emitted photon would be too high to lie in the visible region. These high-energy photons (energy in the UV region) are not compatible with the photo multiplier tubes used for amplification. To overcome this problem, an activator is added to the crystal, which modifies the band structure by creating new levels (activator levels) within the band gap (figure 2.1). In NaI scintillation crystals, thallium (Tl) is the activator used. The electron transitions from the conduction band to these new levels are more probable and the emitted light is in the visible region of the electromagnetic spectrum.

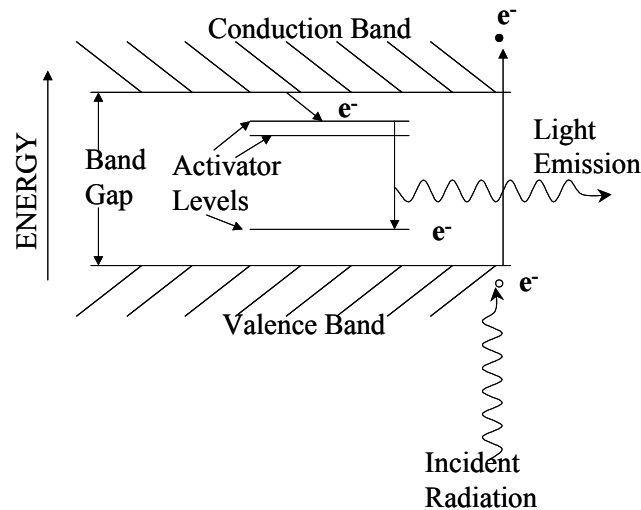


Figure 2.1: Schematic representation of energy band in NaI(Tl) detector.

A 3" x 3" well type detector coupled to a PC based multi-channel analyzer (MCA) were used for all the γ -ray measurements reported in this thesis. The block diagram of the detector setup is shown in figure 2.2. The light scintillations escape the crystal and impinge on the photocathode of the PMT resulting in the release of photoelectrons in the tube. Each of the photoelectron is then multiplied over a million-fold within the tube. This multiplication

process results in the production of a measurable electrical signal, which can be processed.

Some important properties of NaI(Tl) detectors are as follows:

- (a) Best suited for γ -rays, x-rays and sometimes high-energy electrons
- (b) Good efficiency (High density, high Z-element {Iodine} and large crystals available)
- (c) High light output
- (d) Linear energy response

The biggest disadvantage of NaI(Tl) detector is poor energy resolution. Also the crystal is hygroscopic and needs to be sealed in metal containers. But it is an ideal detector when a single radioisotope or two, with well-separated gamma-lines, are to be counted.

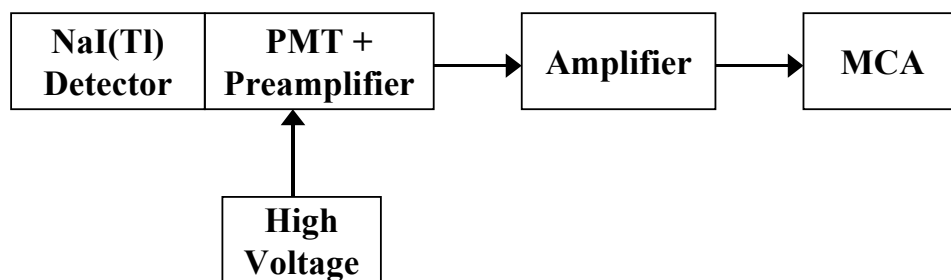


Figure 2.2:Block Diagram of NaI(Tl) detector system.

(b) HPGe Detector System

The most commonly used semiconductor radiation detector is high purity germanium (HPGe) detector with a typical conduction band to valence band gap of 0.67 eV at 300 K. In this type of detector, the photon deposits its energy in the crystal and generates electron-hole pairs, which are collected at the respective electrodes by applying a bias to the semiconductor. The block diagram of different components of a HPGe detector system is given in figure 2.3. These detectors provide good energy resolution (~ 2 keV at 1332 keV), and are preferred for

the assay of radionuclides with complex gamma ray spectra. However, room temperature operation of HPGe detector is not possible due to low band gap in Ge, resulting in high leakage current. Thus, to guarantee an optimum semiconductor performance, the germanium crystal has to be maintained at very low temperatures, typically using liquid nitrogen (77 K) or electro mechanical systems.

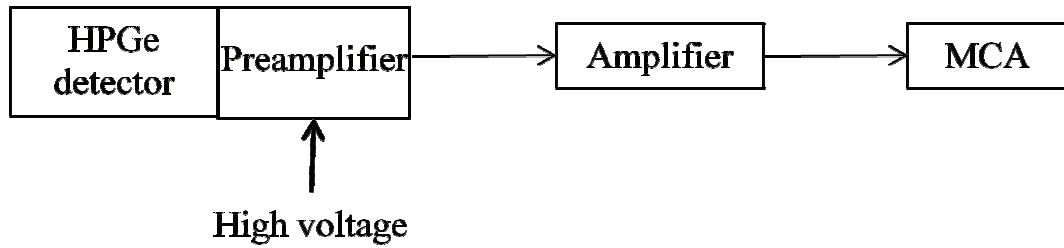


Figure 2.3: Block Diagram of HPGe detector system.

The absolute detection efficiency in HPGe detector can be defined as

$$\varepsilon_{abs} = \frac{\text{number of pulses recorded}}{\text{number of radiation quanta emitted by source}} \quad (2.4)$$

ε_{abs} is dependent on the detector properties and counting geometry, i. e, source to detector distance and source dimensions. The absolute activity of any radioactive source can be determined by the following method. A multi energetic standard source is counted under identical geometrical condition as that of the source to obtain the efficiency at gamma ray energy (ε_i) for that counting geometry using the following equation.

$$\varepsilon_i = \frac{cps_i}{dps_{std} X a_i} \quad (2.5)$$

Where, ε_i = Efficiency at a particular energy, cps_i = count rate at that energy, a_i = individual gamma ray abundance at that energy, dps_{std} = absolute activity of the standard. The

efficiencies at different energies of the standard are fitted to get the efficiency at the source energy. Using this efficiency, the absolute activity of the sample is determined from the experimentally obtained count rate by the following eq.

$$dps_{\gamma} = \frac{cps_{\gamma}}{\epsilon_{\gamma} \times a_{\gamma}} \quad (2.6)$$

Where, ϵ_{γ} = Efficiency at a particular energy, cps_{γ} = count rate at that energy, a_{γ} = individual gamma ray abundance at that energy, dps = absolute activity of the sample. It has been observed that at a large source to detector distance (> 5 cm), the point source efficiencies are comparable to that of an extended source such as disc or cylinder. Thus, at large distance, in absence of a standard source, the point source efficiencies can be used to calculate activity of an extended source.

(c) Liquid Scintillation Counting (LSC)

Liquid scintillation counting is used to measure radiations having very small range such as α , β and low energy γ -rays. In liquid scintillation technique, organic scintillators are dissolved in appropriate solvent along with the radioactive sample. When a radioactive atom undergoes α or β decay, the energetic α or β particles transfer their energy to the solvent molecules. The solvent molecules then undergo random molecular collisions to transfer the energy to the dissolved solute molecules (mainly organic scintillators), which are excited on receiving this energy from the solvent molecules. These excited solute molecules, then, de-excite by emitting light photons (scintillations) in the UV region. Since the PMT used for amplification has a higher efficiency for scintillations in the visible region, wavelength shifters are used to shift the wavelength of the emitted light to visible region. A wavelength shifter is an organic molecule, which absorbs the UV photons emitted in the primary scintillation process and

undergoes fluorescence in the visible region. The light photons, thus emitted are processed in a similar way as the scintillations from NaI(Tl) detector.

The scintillation solution containing the primary and the secondary scintillators in an appropriate solvent is called the “scintillation cocktail”. For aqueous samples, dioxane is used as a solvent whereas, for organic samples toluene is used. Commonly used primary scintillators are 2,5-diphenyl oxazole(PPO), 2-[4-biphenyl]-5-[4-tert-butyl-phenyl]-1,3,4-oxadiazole (Butyl PBD) and p-terphenyl. Commonly used wavelength shifters are 1,4-bis-2-[4-methyl, 5-phenyloxazolyl] benzene (POPOP) and 1,4-bis[2-methylstyryl] benzene (MSB). Some extractants like bis(2-ethylhexyl)phosphoric acid (HDEHP) are used to bring the radioactive atoms into the same phase as the cocktail. Trioctylphosphine oxide (TOPO) is used as an antiquencher as it complexes with quenching agents like dissolved oxygen and acids present in the scintillation cocktail. Since the scintillators undergo degradation due to radiation damage, naphthalene is added to the cocktail to increase its shelf life. A large number of scintillation cocktails are available commercially. Since the emitted α or β (low energy) particles are inside the detector (scintillation cocktail) and have small range, these radiations can be counted with almost 100% efficiency using this technique.

2.2. Other Characterization techniques

Different characterization techniques like electrochemical impedance spectroscopy (EIS), differential scanning calorimetry (DSC), transmission electron microscopy were used in the present work. The specific conductance of Nafion-117 in mixed cationic composition was determined using EIS. Differential scanning calorimetry was performed to understand the changes in the membrane morphology on introduction of crown ether in Nafion-117 membrane. In order to quantify the crown ether in the Nafion matrix, UV-visible spectroscopy was used, whereas the confinement of Cs^+ in the gated composite membrane

(Cs-H-Naf-CR) was studied using secondary ion mass spectrometry and energy dispersive x-ray spectroscopy techniques. The characterization of copper ferrocyanide crystals, synthesized within the track etched membrane was done by x-ray diffraction, transmission electron microscopy and small angle x-ray scattering techniques. The details of the individual techniques are discussed below.

2.2.1. Electrochemical impedance spectroscopy

In the present work, membrane conductivities in different ionic forms were determined using EIS. This technique is often used to characterize a wide variety of electrochemical phenomena concerning solid state, porous materials, synthetic and biological membranes, and liquid electrolytes [Coster et al. 1996]. Moreover, it provides valuable information on the functional and structural characteristics of membrane systems [Alcaraz et al. 1998, Park et al. 2005]. This technique is used in the characterization of membrane capacitance [Fortunato et al. 2006, Muslinkina and Pretsch 2004], resistance [He 2009], dielectric constant, and surface homogeneity. Impedance measurements are carried out by applying an alternating voltage, in a wide range of frequencies (1 MHz to 1 Hz), to an electrochemical cell and by measuring the resulting electric current. In case of ion exchange membrane, the potential is applied across the membrane (kept in the middle of a two compartments cell) using two Pt electrodes and the compartments are filled with either mercury or electrolyte of choice. The voltage applied (v) is a sine wave input, varying with time (t), defined as

$$v(t) = V_0 \sin(\omega t) \quad (2.7)$$

where V_0 is the maximum voltage intensity and ω is the angular frequency. The resulting electric current (i) is also a sine wave:

$$i(t) = I_0 \sin(\omega t + \varphi) \quad (2.8)$$

where I_0 is the maximum current intensity and ϕ is the phase angle between the applied voltage and the current intensity. The electrical impedance, $Z(\omega)$, defined as the ratio between the applied voltage and the resulting electric current, $Z(\omega) = v(t)/i(t)$, is expressed as

$$Z(\omega) = Z_{\text{real}} + jZ_{\text{img}} \quad (2.9)$$

where Z_{real} is the real part of the electrical impedance and Z_{img} is the imaginary one. The analysis of the impedance experimental data obtained $Z(\omega)$ can be carried out either by plotting the impedance imaginary part ($-Z_{\text{img}}$) versus the real part (Z_{real}) in a diagram called as Nyquist plot or by plotting the $-Z_{\text{img}}$ versus the frequency ($f = \omega/2\pi$) in a diagram called as Bode plot. Membrane electrical parameters can be determined by analyzing the impedance plot (Z_{real} versus Z_{img}) by considering an equivalent circuit formed by different combinations of R and C. Different types of plots can be obtained depending on the processes taking place in the system.

i) For highly conducting membranes like Nafion-117, the equivalent circuit can be expressed by a simple resistive component only and the impedance spectrum shows a linear behavior. A representative plot for such type of membranes are shown in figure [Chaudhury et al 2011]

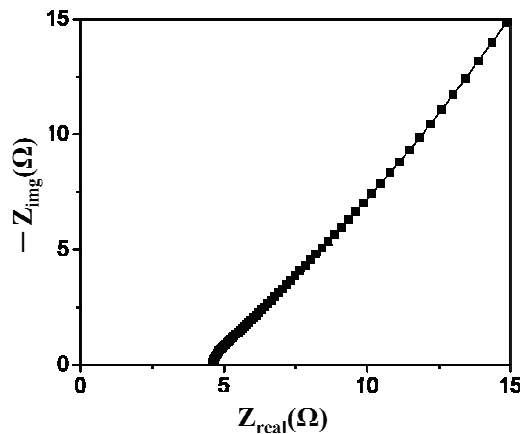


Figure 2.4: A representative Nyquist plot for a highly conducting membrane.

In this case, the resistance of the membrane is directly obtained from the intercept on the real axis in the Nyquist plot.

ii) A parallel R–C circuit gives rise to a semicircle in the Z^* plane, which has intercepts on the Z_{real} axis at R_{∞} ($\omega \rightarrow \infty$) and R_0 ($\omega \rightarrow 0$), ($R_0 - R_{\infty}$) being the resistance of the system. The maximum of the semicircle equals $0.5(R_0 - R_{\infty})$ and it occurs at frequency such that $\omega RC = 1$, RC being the relaxation time [Jonscher 1983].

3) Complex systems may present different relaxation times and the resulting plot is a depressed semicircle. In such cases, a non-ideal capacitor, which is called as constant phase element (CPE), is considered [McDonald 1987]. The impedance for the CPE is expressed by: $Q(\omega) = Y_0(j\omega)^{-n}$, where the admittance $Y_0(\Omega \text{ s}^{-n})$ and n are two empirical parameters ($1 \geq n \geq 0$).

A representative spectrum, along with the equivalent circuit, for such type of system is shown in figure 2.5 [Benavente et al. 2001].

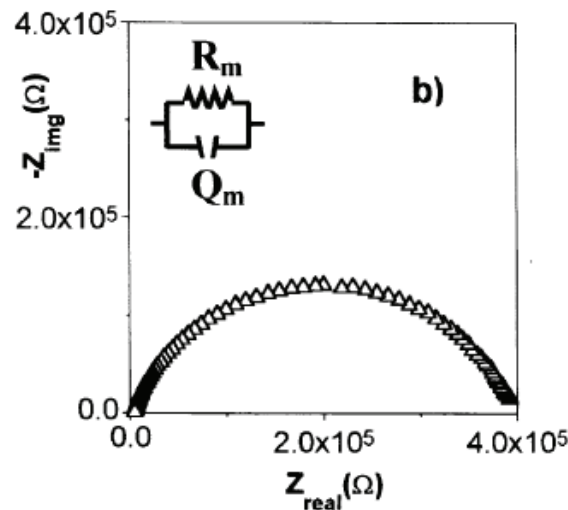


Figure 2.5: A representative Nyquist plot for a complex systems.

When $n=0.5$, the element circuit is called a Warburg impedance, (W), which is associated with a diffusion process according to Fick's first law. For complex systems, equivalent capacitance (C^{eq}) can be determined by the following relation [Jonscher 1983].

$$C^{eq} = \frac{(RY_0)^{1/n}}{R} \quad (2.10)$$

If the system is complex and involves two subsystems with different dielectric properties, two different relaxation processes may appear in the Nyquist plot, and the entire system is a series association of two RC elements, one for each subsystems [Buck 1976, Suarez et al. 1996].

In the present case, the EIS studies were carried out within the frequency range of 1 MHz to 100 Hz, using Autolab PGSTAT 302 voltammetric Analyser in conjunction with the 663 VA stand multimode electrode. The FRA 2 software (developed by Eco-Chemie B. V., The Netherlands) controlled the functions of Autolab PGSTAT 302. The membrane sample, in appropriate ionic form was clamped between two-compartments of a cell. Both the compartments were filled with mercury and impedance diagrams were obtained. The experimental arrangement used for the measurements are shown in figure 2.6.

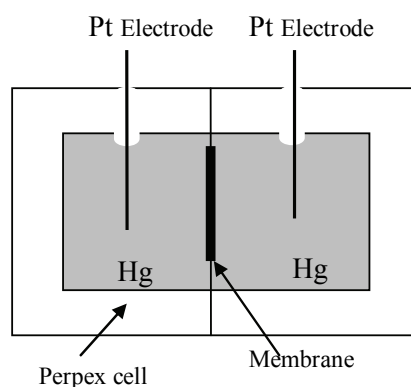


Figure 2.6: Electrochemical cell used for impedance measurement

The area of the membrane was 0.785 cm². The impedance measurements were repeated to check the consistency of the data obtained. The thickness of the membrane before and immediately after the experiment found to be remained same. Thus obtained impedance spectra were analyzed with help of the Frequency Response Analyser software (Eco. Chemie

B.V., Utrecht, Netherlands) to get the membrane resistance (R). Membrane resistivity is obtained from measured membrane thickness (l) and resistance as

$$\rho = \frac{RS}{l} \quad (2.11)$$

where S is the cross sectional area of the membrane in the mercury cell. The relative standard deviation of the specific conductances varied from 2% to 10%.

2.2.2. Differential scanning calorimeter

Differential scanning calorimetry (DSC) is a thermal analysis method designed to determine phase transformations events of a sample with respect to a reference [Brown 2001]. The basic principle of DSC is that, as a sample undergoes a heating cycle, it may undergo exothermic and/or endothermic phase transformations. The DSC can quantify the heat change, which allows one to determine the nature and extent of the physicochemical change taking place. Mettler Toledo DSC 822 was used for measuring DSC profiles of the membrane samples. DSC scans were carried out at heating rate of 10⁰C min⁻¹, under inert atmosphere with an empty aluminum pan as reference. About 7 to 10 mg membrane samples were used to record the scans. Temperature and enthalpy calibration of the instrument was carried out using cyclohexane and indium. The transition enthalpy of the curve was calculated by using the software supplied by Mettler Toledo.

2.2.3. UV-Vis spectroscopy

Measurement of UV-visible absorption spectra has been carried out using the UV-visible spectrophotometer. Modern spectrophotometers employ double beam arrangements whereby the absorbance is measured through two cells, a reference cell and a sample cell [Skoog and

West 1980]. The absorbance (A) at a particular wavelength is related to the concentration (c) by the following Beer-Lambert's relation.

$$A = \varepsilon cl \quad (2.12)$$

Where, 'l' is the path length within the sample and ε is its molar extinction co-efficient.

UV-Vis spectra were recorded using UV Vis Spectrophotometer (V-530, JASCO, Japan).

The absorbance measurements were carried out by taking 1 ml solution in a (1x1x3 cm) quartz cell and placing it in a spectrophotometer to record spectrum with respect to air.

2.2.4. X-ray diffraction (XRD)

X rays are the electromagnetic radiations of wavelength ranging from 0.04 to about 100 Å. X-rays are produced when the high energy charged particles, generally electrons, are accelerated through high potential and allowed to strike a metal target. The incident electrons have sufficient energies to knock out inner orbital electron. Simultaneously an electron from an outer orbital immediately goes to the vacant orbital and the energy released appears as characteristic X – rays. For copper, the most commonly used target, 2p → 1s transition called K_{α} transition has a wavelength of 1.5406 Å. X-ray diffraction has been in use since the early part of this century for the determination of structure of crystalline materials. In 1912, Max von Laue discovered X-ray diffraction from crystalline solids. When X-rays passes through crystalline materials, they get scattered by its constituent atoms. The scattered X-rays interfere with the incident X-ray constructively or destructively depending on the path difference. Condition for the constructive interference can be obtained from the Bragg law. These diffracted X-rays are then detected and counted in a range of 2θ angles. This technique is most extensively used for characterization of solid crystalline materials and determination of their unit cell, lattice parameters and their probable structures [Langford 1996, Jenkins1986]. X-ray diffraction is also used as a method for determining the mean size of

single crystal nanoparticles or crystallites in nanocrystalline bulk materials [Klug 1974]. In the present work, X-ray diffraction (XRD) measurements has been carried out in the range of 2θ (10-70°) on the membrane using monochromatized Cu-K $_{\alpha}$ ($K_{\alpha 1} = 1.5406 \text{ \AA}$ and $K_{\alpha 2} = 1.5444 \text{ \AA}$) radiation by Philips X-ray diffractometer Model PW 1710, Netherlands. Silicon has been used as an external standard for correction due to instrumental broadening.

2.2.5. Energy dispersive X-ray fluorescence

X-ray fluorescence (XRF) is based on the principle of measurement of the energies or wavelengths of the X-ray spectral lines emitted from the sample, which are the characteristic or signature of the elements present in the sample. There are two major modes of analysis in X-ray spectrometer: wavelength dispersive X-Ray fluorescence (WDXRF) and energy dispersive X-ray fluorescence (EDXRF) spectrometry. The difference in these two modes of analysis lies in the detection component. In EDXRF, the detectors directly measure the energy of the X-rays with the help of multichannel analyzer. Whereas in WDXRF, the X-rays emitted from the samples are made to disperse spatially using a dispersion crystal and each wavelength of the emitted X-rays is determined by the detector sequentially. The EDXRF measurements have been carried out using EX 3600-M spectrometer, Jordon valley AR Ltd. (Migdal Haemek, Israel). In energy dispersive mode, the sample is placed at 45° angle to the incident beam as well as the detectors. Hence it's called 45/45 degree geometry.

2.2.6. Transmission electron microscopy

The transmission electron microscope (TEM) operates on the same basic principles as the light microscope but uses electrons instead of light to get enhanced resolution due to the shorter wavelengths of electron beams. The resolution of a microscope is defined as the distance between two details just separable from one another. It can be calculated using the Abb theory of images formation for optic systems and depends upon wave length of light.

In a TEM, the electrons are accelerated at high voltage to a velocity approaching the speed of light. The associated wavelength of the electrons is five orders of magnitude smaller than the light wavelength. Hence, TEM provides enhanced resolution. This resolution enables material imaging and structure determination at the atomic level. First image with a TEM was obtained by Ernst Ruska and Max Knoll in 1932 [Knoll 1932]. The TEM has a similar optical configuration to an optical microscope. By choosing the position of the aperture, either the diffracted beam (dark field) or the unscattered electrons (bright field) can be used to form the image. In the bright field mode of the TEM, image results from a weakening of the direct beam by its interaction with the sample. Therefore, mass-thickness and diffraction contrast contribute to image formation: thick areas, areas in which heavy atoms are enriched, and crystalline areas appear with dark contrast. In dark field mode, the direct beam is blocked by the aperture while one or more diffracted beams are allowed to pass the objective aperture. Since diffracted beams have strongly interacted with the specimen, very useful information is present in dark field images, e.g., about planar defects, stacking faults or particle size [Williams 2009].

For TEM analyses of cross-section of membrane, the membrane samples were sectioned under cryogenic conditions in Leica ultramicrotome to 70 nm thicknesses by using glass and diamond knives. The sections were picked on 200 mesh Cu grids. The grids were examined in an FEI Technai G2 electron microscope in IIT Bombay [Central Facility at SAIF], at 120 KeV without any staining or post-treatment. The sizes of nanoparticles were measured manually using the image analysis software (Image Z, version 1.33 U).

2.2.7. Secondary ion mass spectrometry

Secondary ion mass spectrometry (SIMS) is a technique used in materials science to analyze the composition of solid surfaces and thin films by sputtering the surface of the specimen

with a focused primary ion beam (either +ve beam like Cs/Au or –ve beam like oxygen) and collecting and analyzing ejected secondary ions. The mass/charge ratios of these secondary ions are measured with a mass spectrometer to determine the elemental, isotopic, or molecular composition of the surface to a depth of 1 to 2 nm. Due to the large variation in ionization probabilities among different materials, SIMS is generally considered to be a qualitative technique, although quantitation is possible with the use of standards. SIMS is the most sensitive surface analysis technique, with elemental detection limits ranging from parts per million to parts per billion.

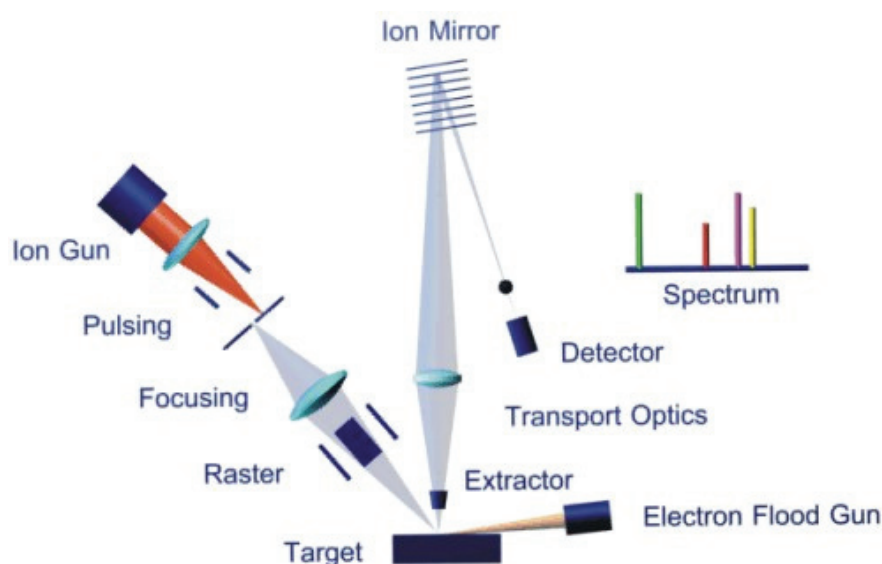


Figure 2.7: Schematic diagram of ToF-SIMS instrument.

The mass analyzer can be either quadrupole, or magnetic sector or time of flight (ToF). In ToF-SIMS method, pulses of secondary ions are accelerated to a given potential (3-8 keV) such that all ions possess the same kinetic energy. They are then allowed to drift through a field-free space before reaching the detector. In a more sophisticated design, the TOF analyser corrects for small differences in initial energy and angle in order to achieve high mass resolution. Major advantages of this approach over quadrupole and magnetic sector type analysers are the extremely high transmission, the parallel detection of all masses and the

unlimited mass range. In this technique, ion images are produced by scanning the primary beam over the sample surface and recording the number of ion as a function of the position.

2.2.8. Small Angle X- ray Scattering

Small Angle X ray Scattering (SAXS) is a material characterization (size range of 1-100 nm) technique in which elastic scattering of X rays (having wavelength 0.01 -0.2 nm) by a sample are detected at low detection angle (0- 10⁰). This method can be used to analyze the size and form of particulate system (Colloids, Globular proteins, etc), correlation length of inhomogeneous structure (Polymer chain, two-phase system etc.), lattice parameters of distorted crystals (para-crystal) and degree of crystallinity, crystal size, crystal distortion of a crystalline polymer. The main principles and equations still in use are exposed by Guinier and Fournet [Guinier 1955] in the very first monograph on SAXS.

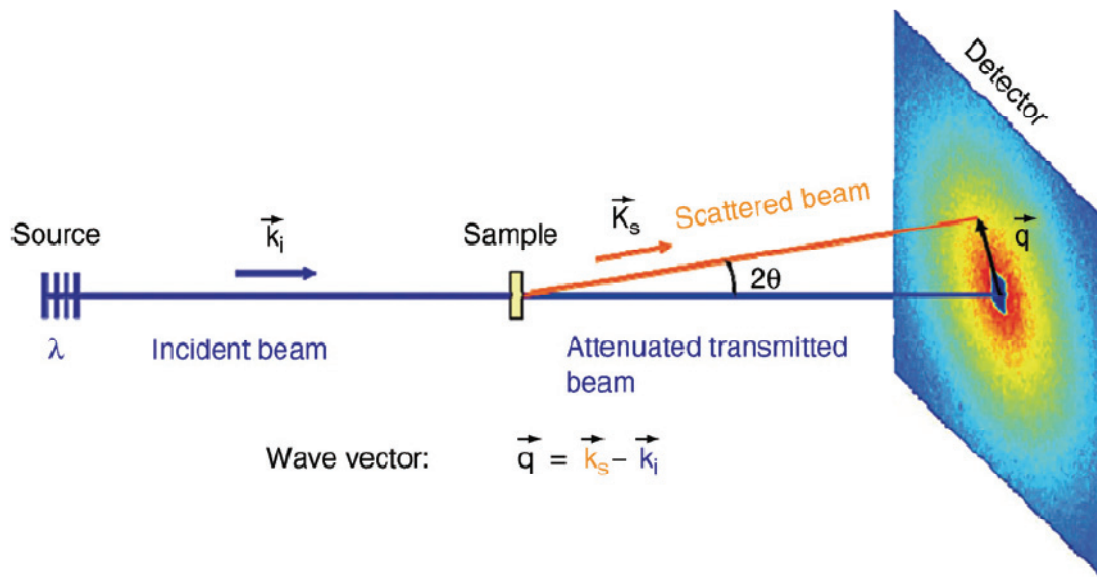


Figure 2.8: Schematic representation of a scattering experiment and representation of the scattering vector \vec{q} in the detector plane.

In general, in SAXS, the structural interpretation is done based on the plot of intensity vs the scattering vector \vec{q} (or wave vector). A schematic representation of a scattering experiment along with the scattering vector is shown in figure. The magnitude of q quantifies the lengths in the reciprocal space and is expressed in \AA^{-1} or nm^{-1} .

2.3. Membranes and Reagents

2.3.1. Membranes

Nafion-117 (178 μm thickness) and Nafion-1135 (88 μm thickness) ion exchange membrane (purchased from Du Pont) with an equivalent weight of 1100 have been used for the present set of experiments. These membrane samples have been preconditioned to remove organic impurities following the method as described elsewhere [Goswami et al 2001]. Precisely, the samples have been refluxed in 5 M HNO_3 for 3 h. These have been then treated with 0.5 M NaOH and 0.5 M HCl separately.

Whatmann grade Nuclepore Track Etched Membrane (0.2 μm pore size and 10 μm thickness) has been used for the present set of experiments. In order to remove the organic impurities, these samples have been preconditioned by methanol and water.

2.3.2. Chemicals

A list of the chemicals used in the present experiments along with their supplier's name, is given in table 2.1. While the metal salts are of ultrapure grade (99.999% purity), the crown ethers and the acids are of analytical reagent grade. The 0.1 N salt solutions have been prepared by dissolving a known amount of the respective salt in 250 mL deionized water. Deionized water with specific resistance of 18 $\text{M}\Omega/\text{cm}$ has been used in the present

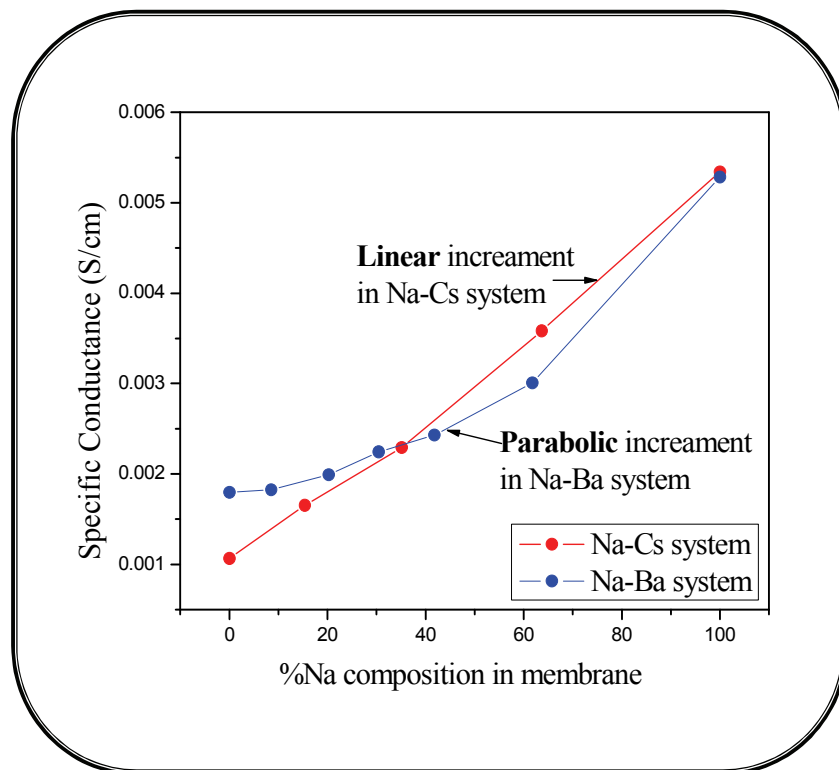
study. Radiotracers (^3H , ^{22}Na , ^{133}Ba and ^{137}Cs) used in the present study have been obtained from Board of Radiation and Isotope Technology, Mumbai, India.

Table 2.1: Chemical reagents used in the present studies along with the supplying company name.

Chemical Reagents	Manufacturing Company
Cesium Chloride (CsCl)	Sisco Research Lab., Mumbai
Cesium Nitrate (CsNO_3)	Apex chemicals, Mumbai
Sodium Chloride (NaCl)	Sisco Research Lab., Mumbai
Sodium Nitrate (NaNO_3)	Sisco Research Lab., Mumbai
Barium Chloride (BaCl_2)	Sisco Research Lab., Mumbai
Barium Nitrate ($\text{Ba}(\text{NO}_3)_2$)	Sisco Research Lab., Mumbai
Silver Nitrate (AgNO_3)	Sisco Research Lab., Mumbai
Copper Sulfate (CuSO_4)	Sisco Research Lab., Mumbai
Potassium ferrocyanide ($\text{K}_4[\text{Fe}(\text{CN})_6]$)	Sisco Research Lab., Mumbai
Nitric acid (HNO_3)	S.D. Fine Chemicals, Mumbai
Hydrochloric Acid (HCl)	S.D. Fine Chemicals, Mumbai
Sodium Hydroxide (NaOH)	S.D. Fine Chemicals, Mumbai
Dibenzo-18-crown-6 (DB18C6)	PCR Research Chemicals, Inc./Gainesville
Dibenzo-21-crown-7 (DB21C7)	Sigma Aldrich, U. S. A
Chlorinated Cobalt Dicarbolide (HCCD)	Katchem, Czech Republic
Dichloromethane (CH_2Cl_2)	Sigma Aldrich, U.S.A.
Dimethyl formamide (DMF)	S.D. Fine Chemicals, Mumbai
Metahnol (CH_3OH)	S.D. Fine Chemicals, Mumbai
Cellulose tri acetate (CTA) Mol. Wt. = 72000–74000	Fluka, Switzerland
Poly Vinyl Chloride (PVC)	Fluka, Switzerland

Chapter 3

Cation Diffusion in Mixed Cationic Environment in Nafion



3.1. Introduction

Ion-exchange membranes (IEM) can act as a separator between two electrolyte solutions due to the Donnan exclusion of the co-ions and permeation of the counter ions. On the ground of their excellent permselective property, the IEMs are widely used in various industrial fields as separators in the chlor-alkali industry [Eisenberg and Yeager 1982, p - 41], battery cells and in pervaporation to dehydrate organic solvents [Maeda et al. 2001]. The permselectivity is also utilized in the ion-exchange based separation processes such as in Donnan dialysis and electrodialysis [Sata et al. 2004]. The transport characteristics of a diffusing species across the membrane govern its permeability in the membrane [Yasuda et al. 1971, Crank 1968]. The permeability coefficient of a species depends on its self diffusion coefficient (SDC) in the membrane and partition coefficient between the solution and the membrane phase. The ratio of permeability coefficients of two diffusing species across the membrane determines their separation factor. Understanding the mechanism of diffusion of ions in the IEMs has been the subject of extensive research for designing membranes for specific applications. It has been observed that the transport properties of the ions are dependent not only on the physical and chemical structures of the membrane but also on the nature of interactions of the ions with the membrane [Yeager 1982 (b)]. Since there is no external gradient involved in the measurement of SDC of the ions, the study of SDCs of different valence counterions is useful in modeling of the cumulative effects of counterions and membrane structural parameters on the diffusional ion-transport process.

Nafion is an extensively studied membrane having polytetrafluoroethylene (PTFE) backbone with pendant side chains containing $-\text{SO}_3\text{H}$ groups. The high electrical conductivity, remarkable permselectivity, and excellent thermal and chemical stability of Nafion membranes compensate for their high cost. It is extensively used in chlor-alkali industries, solid polymer electrolyte fuel cells, and Donnan dialysis based applications [Ng et

al. 1983, Scherer et al. 1990, Doston et al. 1982]. In general, Nafion-117 membrane is known to have different microstructure and water content depending upon the counterions and pretreatment conditions [Heitner-Wirgin 1996, Mauritz and Moore 2004]. Yeager [Yeager 1982 (b)] has found the uptake selectivity order for different cations in Nafion membrane to be $\text{Cs}^+ > \text{Rb}^+ > \text{Ba}^{+2} > \text{K}^+ > \text{Mg}^{+2} > \text{Na}^+ > \text{H}^+ > \text{Li}^+$. The SDCs of water and variety of counterions have been measured in this membrane. Most of the SDC measurements of the counterions have been carried out involving either isotopic-exchange or counterions exchange [Suresh et al. 2004]. The SDCs thus obtained represent diffusion mobility of the single counterion or exchanging counterions [Sodaye et al. 2009].

These membranes provide an unusual degree of permeability selectivity in favor of cations over anions. This selectivity is in addition to the well understood Donnan permselectivity which is based on the differences in the equilibrium sorption of counter ions and coions in an ion exchanging medium. This “superselectivity” [Reiss et al. 1982, Selvey et al. 1985] has been related to the microphase separated morphology of the perfluorinated ionomers. The separation of ions into a separate microphase in Nafion was first indicated by SAXS and later confirmed by neutron scattering experiments. According to the cluster-channel model of Hsu and Gierke [Hsu and Gierke 1982, Hsu and Gierke 1983], the ions and water in the membrane form spherical clusters (figure 1. 3) connected by narrow channels and the ions move through these water channels. This model is reasonably successful in predicting current efficiencies in chlor-alkali cells. However, the exact details of this interconnectivity and its underlying cause are still a subject of study [Robertson 1994]. The relationships among the ionic diffusion coefficients of small cations in these polymers were found to be different from those seen for standard cross-linked ion exchange resins [Bonner and Smith 1957]. For ions of the same charge but of different size such as sodium and cesium ions, the larger, more hydrophobic ion has a significantly smaller diffusion coefficient. This is in contrast to the

relative diffusion behaviors both in ion exchange resins and in water. Interestingly, the activation energies of diffusion for these ions in the membranes are all similar and close to those seen for these ions in water. Yasuda et al. [Yasuda et al.1968] showed from the free-volume theory of Cohen and Turnbull [Cohen and Turnbull 1959] that the tortuosity effect on diffusion coefficient, D , could be related to the polymer volume fraction of the matrix using the expression

$$D = D_0 \exp[-b(V_p/(1-V_p))] \quad (3.1)$$

where, D_0 is the aqueous diffusion coefficient of the species, V_p is the volume fraction of polymer in the water-swollen membrane, and b is an empirical parameter, obtained from a fit of the experimental data using eq. 3.1. This equation provides excellent correlation between the diffusion coefficients of the ions and the degree of cross-linking and/or water contents in the polystyrenesulfonate ion-exchange resin. The pre-exponential factor however is found to deviate from the diffusion coefficient of the ions in pure water, reflecting electrostatic interactions of the counterions to the fixed charge sites in the ion-exchange resin. According to this free-volume approach to diffusion [Yasuda et al. 1968], a change in the water content has a significant effect on diffusion coefficient of the ion in the polymer matrix. This is because of the fact that the displacements of the mobile counterions occur through a region containing water and are obstructed by the polymer chains. Hence, the tortuosity effect which represents the lengthening of the path of moving ions is fundamentally related to the polymer volume fraction (V_p) in the polymer matrix. This equation has been used by Yeager [Yeager 1982 (b)] to explain the variation of D (self-diffusion coefficient) with the water content in Nafion membrane for individual cations (Na^+ and Cs^+). The study of Samec et al. [Samec et al. 1994, Samec et al. 1997] showed that the diffusion coefficient data of several monovalent cations in the Nafion-117 membrane can be represented by the single exponential constant b in eq 3.1. Yeager and Steck [Yeager and Steck 1981], suggested that the diffusional properties

of Nafion cannot be explained based only on this free volume theory, as there are distinct regions in which cations may exist depending upon its charged density and ionic size. Robertson et al [Robertson and Yeager 1996] showed using fluorescence probe that Cs^+ is located on an aqueous side of the interfacial region that separates the fluorocarbon phase from the ion and water rich phase, while other hydrated alkali metal ions prefer the water rich phase of the membrane. The lower diffusion coefficient and higher selectivity of Cs^+ over other alkali metal cations for Nafion-117 has been attributed to this difference in the average location and the transport pathways. The work of Bontha and Pintauro [Bontha and Pintauro 1994] revealed that the concentration of large-radius counterions near the wall charges is high due to the dominant effect of electrostatic attraction forces, whereas unfavorable (repulsive) hydration forces confine the small monovalent cations to the central region of the pore. Pintauro and co-workers [Pintauro et al. 1995, Tandon and Pintauro 1997] studied the divalent/monovalent cation uptake selectivity in Nafion-117 and concluded that a fraction of the divalent cations exist as ion-pair with the fixed charges of the membrane backbone and this fraction varies with the extent of monovalent cation present.

Goswami and co-workers showed that [Goswami et al. 2001] the SDCs of the divalent and monovalent cations varied linearly with free volume fraction with different slopes, indicating higher interaction of the divalent cation with the fixed charges of the backbone. It can be concluded from these studies that hydrated monovalent cations like H^+ , Li^+ , Na^+ would prefer to transport through the central region of the water channels, while for divalent ions, a significant fraction may remain as a contact ion-pair. For Cs^+ , on the other hand, there is a third region of transport. Thus the SDCs of cations may be modified by the ionic composition of the membrane due to their different location and strength of interaction in the membrane.

It is not clearly known how the self diffusion mobility of the counterion would be modified in the presence of other counterions. Okada et al. [Okada et al. 2002] determined ionic mobility

in Nafion-117 in mixed ionic composition of H^+ ion and alkali metal cations. They did not observe any significant dependence of counterion mobilities on the ionic composition of the membrane. Pourcelly et al.[Pourcelly et al. 1996] observed from radiotracer studies that SDC of Na^+ and Ca^{+2} were independent of ionic composition of the membrane. Karavanova and Yaroslavtsev[Karavanova and Yaroslavtsev 2010] studied the diffusion parameters of mixed monovalent cation membranes and evaluated diffusion coefficient from ionic conductance. They reported a parabolic variation of ionic conductance with mole fraction of KCl in the membrane MK-40.

In this chapter, the measurement of SDCs of X and Y ions (D_X / D_Y) in bi-ionic form of Nafion-117 membrane (X-Y system) loaded with different proportions of X and Y ions, are reported. The systems studied are Na-Cs, Na-Ba, Cs-Ba and Ag-Ba. The proportions of the cations in the membrane samples have been varied by equilibrating the membrane with solutions containing different proportions of the corresponding salt solution. The ion exchange isotherms for the Na-Ba and Na-Cs systems in Nafion-117 membrane have also been generated. Further, AC impedance measurement studies using frequency response analyzer system have been carried out with Nafion-117 having different mixed cationic compositions for Na-Cs and Na-Ba systems. The specific conductances obtained from the impedance measurement have been compared with those calculated from the corresponding SDCs.

3.2. Experimental

3.2.1. Measurement of SDC and Ion Exchange Isotherm

For the Na-Ba system, five different equilibrating solutions containing different proportions (as shown in table 3.1) of 0.1 N NaCl and 0.1 N $BaCl_2$ have been prepared keeping the total

ionic concentration fixed at 0.1N. For each equilibrating solution, two set of experiments have been carried out, one for the Na^+ ion and another for the Ba^{+2} ions. In each experiment, the conditioned membrane sample (2 cm X 2 cm) in proton form is kept in well-stirred equilibrating solution (30 mL) at 27 °C for ~3 h. After equilibration, the membrane sample is taken out and the required (^{22}Na or ^{133}Ba) radiotracer is added to the respective solution. In order to ensure that there is no change in the ionic composition of the membrane and the external solution, the self-diffusion measurement of the respective ions ($\text{Na}^+ / \text{Ba}^{+2}$) in the membrane sample has been carried out with this radiolabeled equilibrating solution. The further steps involved in the measurement of SDC is same as described in section 2.1.1. Experiments with ^{22}Na and ^{133}Ba radiotracer have been done separately since the 511 keV γ -ray of ^{22}Na can cause significant increase in the background in the low energy γ -rays of ^{133}Ba . For the measurement of ion exchange isotherms, the total amount of radioactivity added into the equilibrating solution and the equilibrium uptake of radiotracer in the membrane are required. The amount of radiotracer in the equilibrating solution has been accounted by preparing filter paper standards following the method described in section 2.1.2. Same procedure has been followed for equilibrating solutions of different ionic compositions.

For the other ionic systems (Na-Cs, Cs-Ba and Ag-Ba), same experimental procedure has been followed to obtain the SDCs of the individual cation. It is to be mentioned that, for Ag-Ba system, 0.1 N AgNO_3 and 0.1 N $\text{Ba}(\text{NO}_3)_2$ solutions have been used to avoid precipitation of AgCl . In this system, the self diffusion profile of only Ba^{+2} ion has been monitored. The compositions of the equilibrating solutions used for these three ionic systems are given in table 3.2, 3.3 and 3.4 respectively.

3.2.2. Impedance Measurement

The specific conductances of the membrane samples in different mixed cationic composition have been obtained from electrochemical impedance measurements for the Na-Ba and Na-Cs systems as per the experimental details given in section 2.2.1. The conditioned Nafion-117 samples (2 cm X 2 cm) in H⁺ form have been kept for ~3 h in different equilibrating solutions containing different proportions of NaCl and CsCl/BaCl₂ as given in the table 3.1 & 3.2. After attainment of equilibrium, the membrane samples have been kept in deionized water to ensure that there are no sorbed electrolytes in the membranes. Different membrane samples have been used for different cationic compositions.

3.3. Calculation

3.3.1. Ion exchange isotherm and Self diffusion coefficients

The ion exchange isotherms for the mixed ionic systems (Na-Cs / Na-Ba) were calculated from the equilibrium uptake of radiotracer in the membrane and the amount of total radioactivity added to the equilibrating solution following the method described in section 2.1.3. The SDCs of each cation for different compositions of the membrane were obtained from the experimental radiotracer exchange data by the method described in section 2.1.1.

3.3.2. Water - exchange site mole ratio ($\lambda = n_{H_2O}/n_{SO_3^-}$)

The water-exchange site mole ratio (λ) is calculated from the percentage water uptake of the membrane (in a particular ionic form) using the following relation

$$\lambda = \frac{\text{percentage water uptake} \times \text{mol.wt. of Nafion}}{\text{mol.wt. of water}} \quad (3.2)$$

The percentage water uptake of the membrane is obtained from the weight of the membrane in fully dried and fully hydrated condition. In order to obtain the weight of the membrane in

fully dried condition, the membrane sample is dried in vacuum at 70⁰C for 4-5 h. The weight of the membrane in fully hydrated condition is obtained after equilibrating the sample in water for 2 h.

3.3.3. Specific Conductance(κ)

The obtained impedance spectra were analyzed with help of the Frequency Response Analyser software and the resistance (R) of the membrane samples were obtained from the intercept of the Nyquist plot with the real axis [Robinson and Stokes 1965, Subrahmanian and Lakshminarayanaiah 1968, Pourcelly et al. 1990, Pourcelly et al. 1996, Millet 1990, Gavach et al. 1989]. The specific conductances (κ_{imp} Scm⁻¹) of the membrane samples were calculated from the total resistance (R) using the following expression.

$$\kappa_{imp} = \frac{L}{RA} \dots\dots (3.3)$$

Where, L is the membrane thickness in fully hydrated condition and A is the membrane contact area (0.785 cm²) during the impedance measurement.

In the present work, an attempt was made to calculate the specific conductances (κ_{cal}) of the membrane samples from the SDCs of the cations in the pure monocationic form of Nafion-117 using the equations described by Nwal [Nwal et al. 2003]. Precisely, the Nernst-Planck equation for two counter ions (1 and 2) can be written as

$$J_1 = \frac{z_1 D_1 c_1 KF}{RT} \frac{dE}{dx} + u_c c_1 \quad (3.4)$$

$$J_2 = \frac{z_2 D_2 c_2 KF}{RT} \frac{dE}{dx} + u_c c_2 \quad (3.5)$$

where, Z_1 and Z_2 are the valences of the cations present in the membrane. F and R are Faraday constant ($C \text{ eq}^{-1}$) and ideal gas constant ($J \text{ mol}^{-1} \text{ K}^{-1}$) respectively. C_i (mole cc^{-1}) is the concentration of i^{th} species in the membrane. D_i is the diffusion coefficient in the membrane (cm^2/s), E is the electrical potential, (V), F is the Faraday constant (coulomb/mole); J_i is the molar flux ($\text{mol}/\text{cm}^2/\text{s}$), T is the absolute temperature (K), u_c is the convective flow rate (cm/s), x is the geometrical coordinate (cm) in the direction of flow.

Conditions of electroneutrality and no current requires

$C_4 = C_1 + C_2$ and $z_1 J_1 + z_2 J_2 = 0$, where C_4 is the fixed ionic group concentration in the membrane.

It can be considered that the classical Nernst-/Einstein relation is valid in the aqueous phase of the membrane $D_i = \mu_i RT$, where u_i is the absolute mobility of i^{th} species.

The electrical conductivity κ_{cal} can be related to the current as follows

$$\kappa = \frac{i}{\frac{dE}{dx}} = F \frac{z_1 J_1 + z_2 J_2}{\frac{dE}{dx}} \quad (3.6)$$

Neglecting the convective term of electrical conductivity for ion exchange membrane [Schaetzel and Auclair 1993, Schaetzel et al.1997], the final expression for electrical conductivity for a monovalent-monovalent system (Na-Cs) can be written as follows.

$$\kappa_{cal} = \frac{F^2 C_4}{RT} [y_1 (D_{Na} - D_{Cs}) + D_{Cs}] \quad (3.7)$$

Where, $y_1 = C_1/C_4$ and $C_4 = Z_1 C_1 + Z_2 C_2$

For Na-Ba system, the expression for specific conductances were calculated using the equation

$$\kappa_{cal} = \frac{F^2 c_4}{RT} [y_1 (D_{Na} - 2D_{Ba}) + 2D_{Ba}] \quad (3.8)$$

3.4. Results and discussion

The isotherm for Na-Ba system, as shown in figure 3.1 (a), indicates higher selectivity of Nafion-117 membrane for Ba^{+2} compared to Na^{+} counterion. This is also evident from the data given in table 3.1. For example, 40% of the ion exchange sites in Nafion-117 membrane is occupied by Ba^{+2} when equilibrated with solution containing 97% Na^{+} and 3% Ba^{+2} .

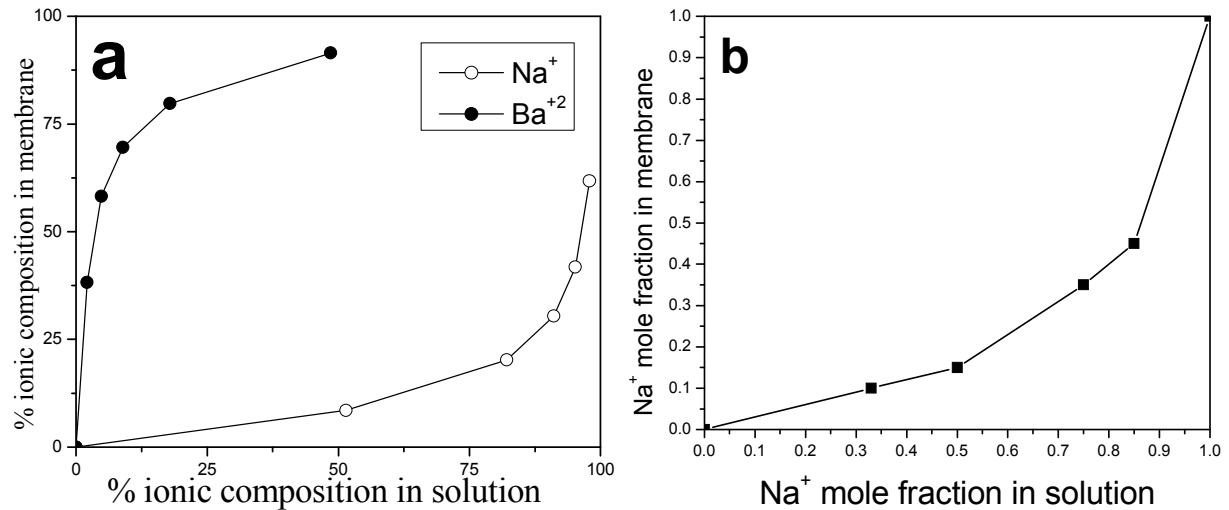


Figure 3.1: Ion exchange isotherms for the (a) Na-Ba system and (b) Na-Cs system [Sodaye et al 2008] in Nafion-117 membrane.

For Na-Cs system, the isotherm is in good agreement with that (as shown in figure 3.1 (b)) reported in the literature [Sodaye et al. 2008]. Here also, the membrane is more selective for Cs^{+} than Na^{+} and 85 % sites are occupied by Cs^{+} ions when equilibrated with solution containing 50% Na^{+} and 50% Cs^{+} . The higher selectivity of Ba^{+2} as compared to Na^{+} can be

explained on the basis of stronger electrostatic interaction of the former ion with the fixed ionic sites in the membrane backbone. Cs^+ being less hydrated than Na^+ , are more electrostatically bound to the ionic sites in the membrane, resulting in higher selectivity of the former as compared to the later.

Table 3.1: Compositions of equilibrating solutions, ionic compositions, water-exchange site mole ratio (λ) and SDCs of Na^+ and Ba^{+2} ions along with the calculated (κ_{cal}) and measured (κ_{imp}) specific conductances in Na-Ba system.

$\text{Na}^+ : \text{Ba}^{+2}$ in equilibrating solution	λ ($n_{\text{H}_2\text{O}}/n_{\text{SO}_3^-}$)	Ionic composition in membrane (%)		SDC ($\times 10^6 \text{ cm}^2 \text{ s}^{-1}$)		Specific Conductance($\times 10^3 \text{ Scm}^{-1}$)	
		Na^+	Ba^{+2}	Na^+	Ba^{+2}	κ_{cal}	κ_{imp}
0:1	9.47	-	100	-	0.15	1.5	4.3
1:1	9.67	8.6	91.4	0.94	0.125	1.9	4.4
4:1	9.77	20.3	79.7	0.96	0.083	2.3	4.8
8:1	10.02	30.5	69.5	0.93	0.063	2.7	5.4
14:1	10.47	41.8	58.2	0.94	0.057	3.1	5.9
29:1	10.65	61.8	38.2	0.96	0.045	3.8	7.3
1:0	10.51	100	-	1.03	-	5.3	12.8

The kinetics of isotopic exchange of different cations in mixed composition of the Nafion membrane, obtained from radiotracer measurement, are shown in figure 3.2-3.5. It is to be mentioned that the error bars associated with the experimental data points are of the size of

the symbols. The experimental isotopic-exchange rate profiles obtained for Na^+ and Cs^+ ions in the Na-Cs system are shown in figure 3.2.a and 3.2.b respectively.

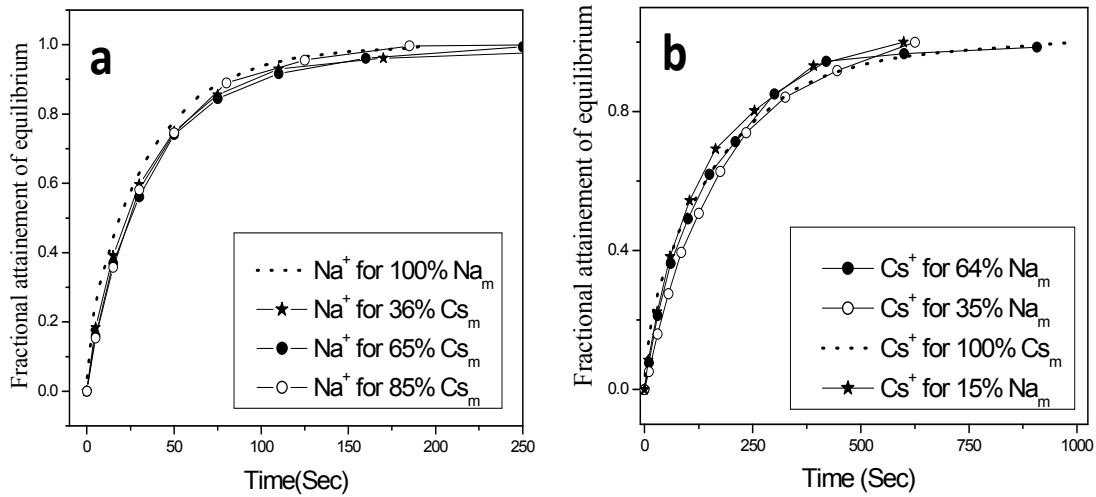


Figure 3.2:Self-diffusion kinetics of (a) Na^+ and (b) Cs^+ for different ionic composition of the membrane in the Na-Cs system.

The figures indicate that there is no significant change in $\text{Na}^+ / \text{Cs}^+$ isotopic-exchange rates for membrane samples having different ionic compositions. The D_{Na} and D_{Cs} values, obtained for different ionic compositions along with the corresponding water - exchange site mole ratios ($\lambda = n_{\text{H}_2\text{O}}/n_{\text{SO}_3^-}$) are given in table 3.2.

The isotopic exchange profiles obtained for Cs^+ and Ba^{+2} ions in Cs-Ba system in the Nafion membrane with different ionic compositions are shown in figure 3.3.a and 3.3.b respectively and the corresponding SDCs obtained are given in table 3.3. The data indicates that the results are similar to what has been observed in the Na-Cs system. It can be seen that for the Cs-Ba system, though there is $\sim 10\%$ increment in D_{Cs} but D_{Ba} is independent of the membrane cationic composition.

Table 3.2: Compositions of equilibrating solutions, ionic compositions, water-exchange site mole ratio (λ) and SDCs of Na^+ and Cs^+ ions along with the calculated (κ_{cal}) and measured (κ_{imp}) specific conductances in Na-Cs system

$\text{Na}^+ : \text{Cs}^+$ in equilibrating solution	λ ($n_{\text{H}_2\text{O}}/n_{\text{SO}_3^-}$)	Ionic composition in membrane (%)		SDC ($\times 10^6 \text{ cm}^2 \text{ s}^{-1}$)		Specific Conductance($\times 10^3 \text{ Scm}^{-1}$)	
		Na^+	Cs^+	Na^+	Cs^+	κ_{cal}	κ_{imp}
0:1	5.01	-	100	-	0.19	1.1	2.5
1:1	5.37	15.4	84.6	0.93	0.192	1.8	4.0
3:1	7.54	35.1	64.9	0.90	0.188	2.5	5.5
14:1	9.18	63.7	36.3	0.92	0.184	3.9	8.7
1:0	10.51	100	-	1.03	-	5.3	12.8

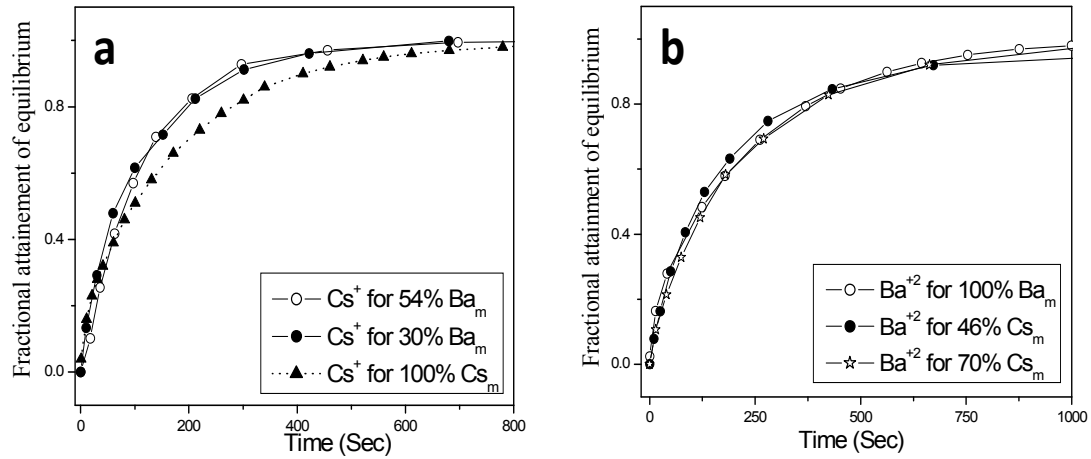


Figure 3.3: Self-diffusion kinetics of (a) Cs^+ and (b) Ba^{+2} for different ionic composition of the membrane in Cs-Ba system.

Table 3.3: Compositions of equilibrating solutions, ionic compositions and SDCs of Cs^+ and Ba^{+2} ions in the Cs-Ba system

$\text{Cs}^+ : \text{Ba}^{+2}$ in equilibrating solution	Ionic composition in membrane (%)		SDC ($\times 10^6 \text{ cm}^2 \text{ s}^{-1}$)	
	Cs^+	Ba^{+2}	Cs^+	Ba^{+2}
0:1	-	100	-	0.15
1:1	46.2	53.8	0.21	0.16
4:1	70.1	29.9	0.21	0.14
1:0	100	-	0.19	-

For Na-Ba system, the self diffusion profiles of Na^+ and Ba^{+2} ions are shown in figure 3.4.a and 3.4.b respectively. It is seen from the figures that the rate of isotopic exchange for Na^+ ion does not change with change in ionic composition of the membrane while that of Ba^{+2} ion decreases significantly with increase in Na^+ content (Na_m^+) in the membrane. The data given in table 3.1 indicates that D_{Na} is reduced by $\sim 7\%$ compared to the value of $1.03 \times 10^{-6} \text{ cm}^2 \text{ s}^{-1}$ for pure Na^+ form of Nafion-117 and it is independent of the membrane composition. On the contrary, D_{Ba} gradually decreases as Na^+ content in the membrane increases. At 61.8% Na_m^+ , the D_{Ba} is reduced by $\sim 70\%$ compared to that ($1.5 \times 10^{-7} \text{ cm}^2 \text{ s}^{-1}$) at pure Ba^{+2} form of Nafion-117. The water - exchange site mole ratios (λ) obtained for different ionic compositions in Na-Ba system is also included in table 3.1.

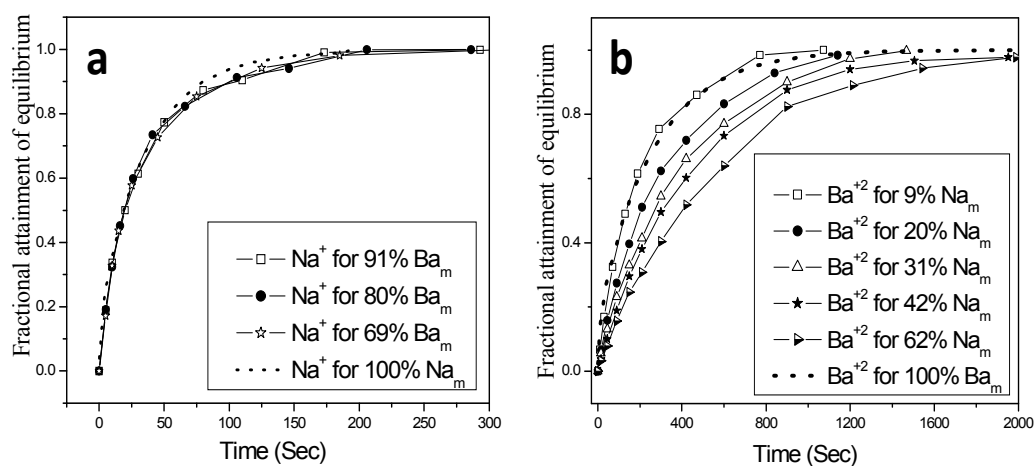


Figure 3.4: Self-diffusion kinetics of (a) Na⁺ and (b) Ba²⁺ for different ionic composition of the membrane in the Na-Ba system.

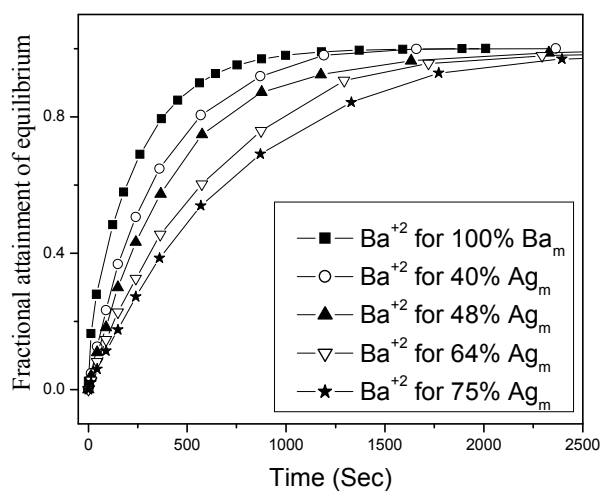


Figure 3.5: Ba²⁺ self-diffusion kinetics for different ionic composition of the membrane in Ag-Ba system..

For Ag-Ba system, the self diffusion profiles of Ba^{+2} ion with different ionic compositions are shown in figure 3.5 and the change in the D_{Ba} with change in membrane composition for Ag-Ba system is shown in table 3.4. It can be seen that, as in the case of Na-Ba system, here also D_{Ba} decreases continuously as the amount of Ag^+ (Ag_m^+) increases in the membrane. The data indicates that there is 80% reduction in D_{Ba} for 75% Ag_m^+ than that in pure Ba^{+2} form of the membrane.

Table 3.4: Compositions of equilibrating solutions, ionic compositions and SDCs of Ba^{+2} ions in the Ag-Ba system

$\text{Ag}^+ : \text{Ba}^{+2}$ proportion in equilibrating solution	% of Ag^+ in the membrane	SDC of Ba^{+2} ($\times 10^6 \text{ cm}^2 \text{ s}^{-1}$)
0:1	0	0.154
4:1	35	0.077
8:1	41	0.059
14:1	60	0.040
29:1	71	0.029

The observed dependence of the SDCs of the different cations on the membrane cationic composition can be qualitatively explained based on the locations of the cations in different region of the membrane and their interactions with the backbone and the fixed ionic sites. Based on the investigation of spectroscopic and diffusional properties, Yeager and Steck [Yeager and Steck 1981] have shown a diagrammatic representation (figure 3.6.) of Nafion structure. It consists of three regions, A, B and C.

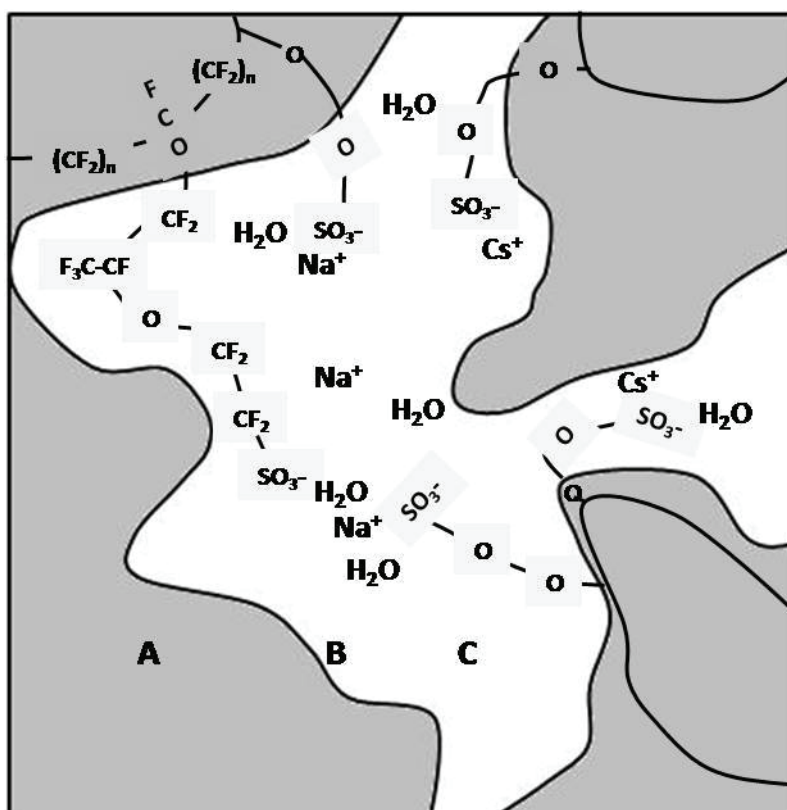


Figure 3.6: Three region structural model for Nafion: A- fluorocarbon phase, B- interfacial zone, C- Ionic Cluster.

Region A consists of fluorocarbon phase, region C consists of ionic clusters i.e. sulfonate exchange sites, while region B is viewed as one of relatively large fractional void volume, containing pendant side chain material, a smaller amount of sorbed water, some sulfonate exchange sites which have not been incorporated into clusters, and a fraction of the counterions. The relative proportions of counterions in regions B and C would depend upon the size, charge density, and hydration energy of the cation. Thus Cs^+ with low charge density follows a transport pathway through the aqueous side of the interfacial region, while Na^+ moves mainly through the water rich [Yeager and Steck 1981, Robertson and Yeager 1996] micro phase of the membrane. Hence the ions follow a mutually independent path and do not influence the SDCs of each other. The slight decrease ($\sim 10\%$) in D_{Na} with increase in Cs^+ content in the membrane is due to reduction in the net water content of the membrane.

These observations agree with that of Yeager and Steck [Yeager and Steck1981]. The observations obtained for Cs-Ba system can also be explained due to the different locations of the ions in the membrane.

The variation of SDCs in Na-Ba system can be explained based on the observations of Pintauro and co-workers [Bontha and Pintauro 1994, Pintauro et al. 1995, Tandon and Pintauro1997]. They have reported that, due to dominant electrostatic attraction forces, the large-radius divalent counterions are mostly concentrated near the wall charges and a fraction of them may exist as ion-pair with the fixed charges of the membrane backbone. In Na-Ba system, both the ions move through water rich region of the membrane, but Na^+ ion possibly remains mostly dissociated in the water channels, and its transport is not hindered by the Ba^{+2} ions which, being a divalent one, possibly remain in the proximity of the $-\text{SO}_3^-$ ions[Tandon and Pintauro1997]. On the other hand, diffusion of Ba^{+2} ions may be regarded as a lattice diffusion, and increase in the Na^+ content of the membrane increases the average spacing between two successive Ba^{+2} ions. This enhanced hopping distance with increased Na^+ content may strongly affect the diffusivity of the Ba^{+2} ions. The same reason can explain the change in D_{Ba} in Ag-Ba system.

A representative set of Nyquist plot obtained from the AC impedance measurement for Nafion-117 loaded with different proportions of Na^+ and Ba^{+2} ions are shown in figure 3.7. The κ_{imp} values as a function of ionic composition of the membrane for the Na-Ba and Na-Cs systems are shown in table 3.1 and 3.2 respectively. The corresponding κ_{cal} values obtained using eq. 3.8 and 3.7 are also included in the tables.

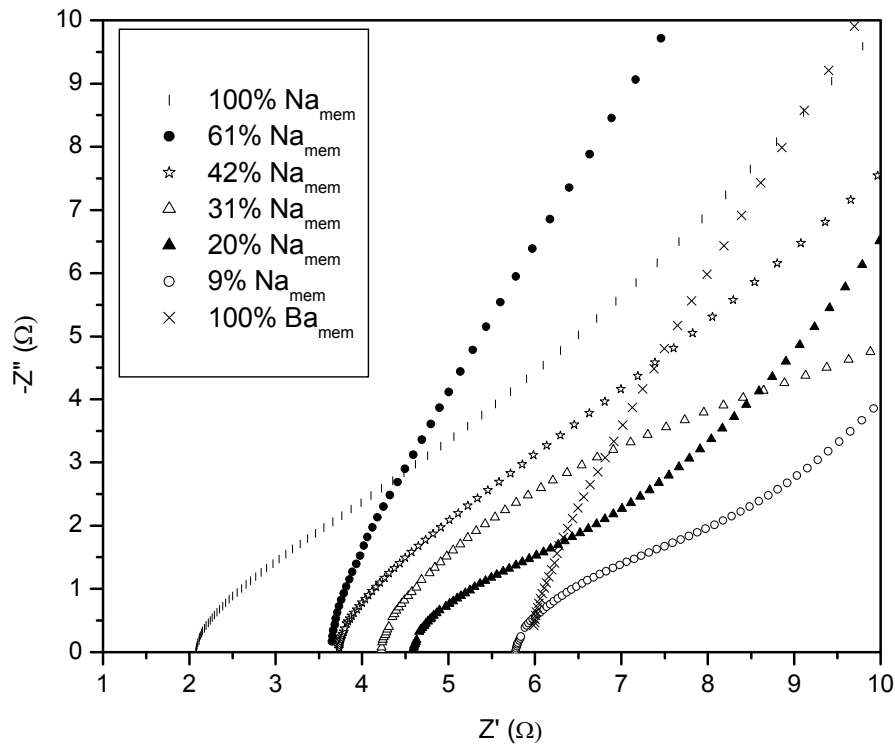


Figure 3.7: Nyquist plot obtained from Impedance measurement for Nafion-117 loaded with different proportion of Na^+ and Ba^{+2} ions. (Z' and Z'' are the real and imaginary components respectively of impedance as a function of frequency).

A list of SDCs of Na^+ obtained from radiotracer measurement and specific conductances of Na^+ form of Nafion-117 membrane in different literatures are shown in table 3.5. It is seen from the table that, though there is a good consistency in the SDCs obtained from radiotracer measurement but the specific conductances obtained from impedance measurement show wide divergence in different literatures. There is not enough literature where measured diffusion coefficient has been correlated to the measured specific conductance of the membrane. Millet [Millet 1990] has shown that D_{Na} , calculated from specific conductances are comparable to that given by Yeager and Steck [Yeager and Steck 1981]. Pourcelly et al [Pourcelly et al. 1996] have also determined D_{Na} from specific conductance data and the

value differed by a factor of 1.8 from the quoted literature [Goswami et al. 2001]. In the present work, the data given in Table 3.1 and 3.2 indicates that there is a ~ 2.5 times difference between the κ_{imp} and κ_{cal} values for pure Na^+ form of the membrane in both Na-Ba and Na-Cs systems.

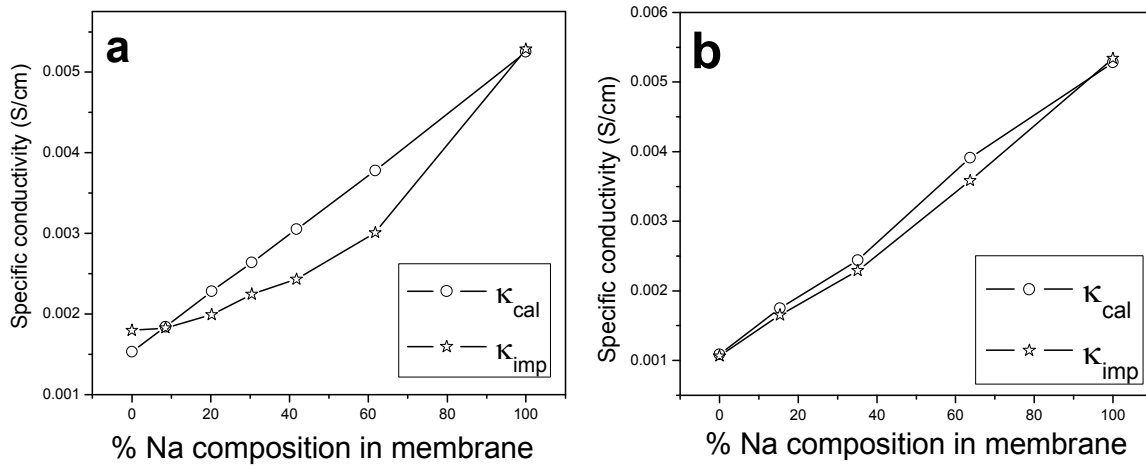


Figure 3.8: Specific conductances of Nafion-117 membrane containing different proportions of (a) Na^+ and Ba^{+2} ions. (b) Na^+ and Cs^+ ions.

The values of κ_{imp} , normalized at calculated specific conductance of pure Na^+ form of Nafion-117, are plotted as a function of Na^+ content in the membrane in figure 3.8a and 3.8b for Na-Ba and Na-Cs system respectively. The corresponding κ_{cal} values using equation 3.8 and 3.7 are also shown in these figures. As expected from equations, there is a linear increase in κ_{cal} with increase in Na^+ content of the membrane for both the type of ionic systems. For Na-Cs system, the increment in κ_{imp} follows the same linear trend as that of corresponding κ_{cal} . This linear trend essentially indicates that there is no mutual interaction of the ions when they move in the membrane. However, for Na-Ba system, κ_{imp} increases in a parabolic fashion [Karavanova and Yaroslavtsev 2010, Okada et al. 1998, Hirofumi et al. 1994]. The deviation from linearity in the Na-Ba system is indicative of interaction between the diffusing

ions in the membrane [Okada et al. 1998]. However in the present case, the self diffusion data shows that diffusion of Na^+ ions is not affected by the Ba^{+2} ions, while, the diffusion of the latter is strongly influenced by the former one. This essentially shows that the observed deviation from linearity as a function of ionic composition need not necessarily result from the change in SDC of both the components in the membrane due to their mutual interaction. Other factors such as different extent of interaction of the cations with the fixed charges of the membrane can also play the role. A clear understanding of the cause of diffusional differences of different types of ions may permit diffusional discriminations to be designed into polymer membranes for specific separations.

Table 3.5: Comparison of SDCs of Na^+ obtained from radiotracer measurement and specific conductances of Na^+ form of Nafion-117 membrane

Serial No.	Diffusion Coefficient ($\times 10^6 \text{ cm}^2 \text{ s}^{-1}$)		Specific Conductance $\kappa_{\text{imp}} (\times 10^2 \text{ Scm}^{-1})$
	Radiotracer measurement	Impedance measurement	
I ^{a,f}	0.94 - 0.98	-	-
II ^b	1.8	1.7	0.8
III ^{c,f}	-	1.1	0.5
IV ^d	-	6.5	3.0
Present Work	1.0 ^e	2.6	1.3

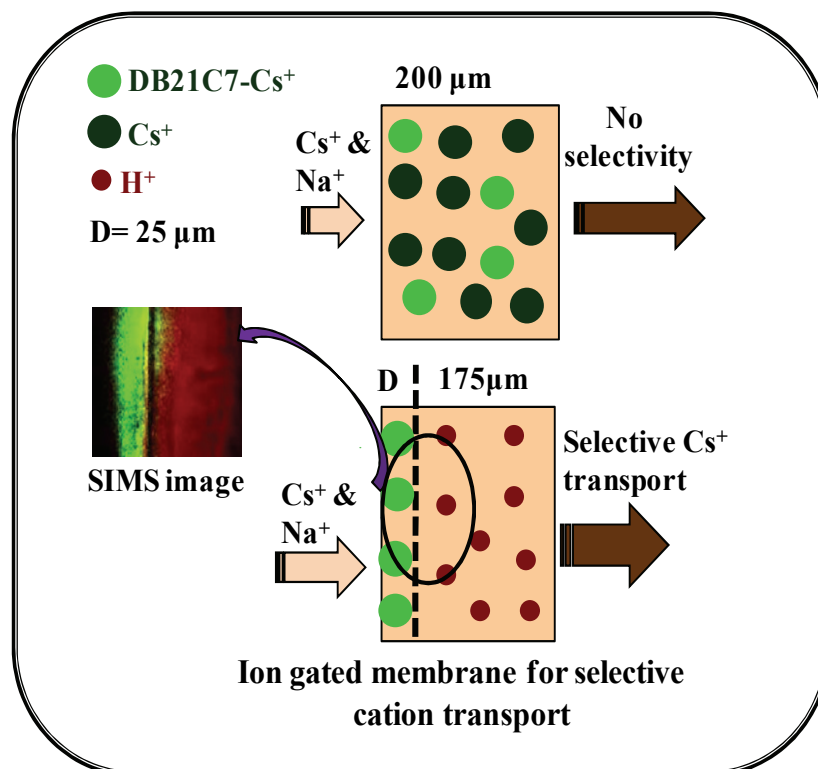
^aYeager 1981; ^bPourcelly 1996; ^cMillet 1990; ^dOkada 1998; ^eGoswami 2001, ^fNafion-120

3.5. Conclusion

Results of the present work show that the SDC of an ion in Nafion-117 membrane may be influenced by the ionic composition of the membrane phase, depending upon the path of transport of the two cations within the membrane. If the two ions are moving through different pathways in a bi-ionic system, then none of the SDCs of the cations are affected, whereas if they are moving through an overlapping path, then depending upon the electrostatic binding of the cation with the fixed charge group of the membrane, the SDCs will be affected. This ionic composition dependent self diffusion behavior of either cation is ultimately reflected in the specific conductance of the system.

Chapter 4

Cs^+ diffusion and transport in Crown Ether - Nafion Composite membrane



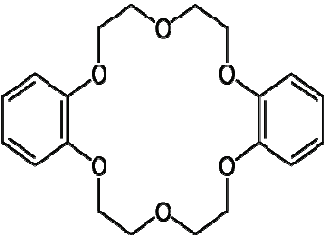
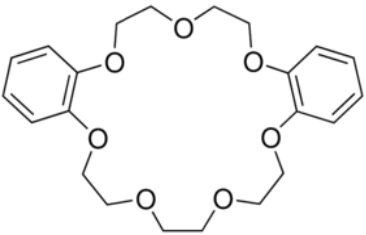
4.1. General Introduction

In spite of the wide application in various fields, the ion exchange membranes (IEM) show very poor selectivity between two different metal ions (of same charge) and thus are rarely used in mutual separations of different metal ions. One way to increase the metal ion selectivity is to incorporate some ligand within the membrane matrix having high selectivity for the metal ion of interest. Alkali metal ion selective crown ethers, calixarenes and cryptands are well known in literature and use of these ligands in membrane for development of various ion selective electrodes has been studied [Buhlmann et al. 1998, Xia et al. 1998]. Crown ethers mimic the ability of biological cation transport systems and of some antibiotics, which also bind metal cations selectively [Dobler 1981]. The major drawback associated with the separation of alkali metal ion using these ligands [Talanova et al. 1999, Gokel et al. 2004, Charewicz et al. 1982, Walkowiak et al. 1990] is that they require an equivalent amount of counter ion and the separation factor depends on the anion also [Hankins et al. 1993]. The charge compensation of the metal ions has been achieved by incorporating anionic functional groups either in the crown ether or in the polymer backbone of the membrane. Cation exchange membranes can provide the negative charge required by the metal ion-crown ether complex, obviating the need of additional counter-anions. Significant effect of the crown ethers on the transport selectivity has been observed in the proton driven cation transport experiments [Kimura et al. 1983]. Increase in hydrophilicity of the membrane matrix resulted in higher transport rate indicating the important role of water in the transport mechanism [Sakamoto et al. 1986]. Nafion-117 is a widely used and well studied IEM which consists of polytetrafluoroethylene backbone with pendant side chains containing $-\text{SO}_3\text{H}$ groups. Different attempts have been made to modify the transport properties of Nafion for its use in fuel cell [Choi et al. 2008, Shim et al. 2005, Sen et al. 2008, Gribov et al. 2009], chemical

sensors and ion selective electrodes [Torma et al. 2008] by incorporating suitable crown ethers in the membrane.

In earlier work with Nafion-crown ether system [Bhattacharyya and Goswami 2009], attempt has been made to prepare an alkali metal ion selective membrane by loading Dibenzo-18-crown-6 (DB18C6) in Nafion-117 cation exchange membrane. The structural details of DB18C6 are given in table 4.1. It has been observed that the transport behaviors of the alkali metal ions in those membranes are strongly dependent on the cationic form of the membrane in which the crown ether is loaded. When the crown ether was loaded in Li^+ form of the membrane, the entire ion exchange sites are available for counter ion exchange and the membrane showed enhanced selectivity for Cs^+ over Li^+ . Complete ion exchange equilibrium could be reached within practical time scale because of favorable ion exchange kinetics. On the other hand, when the crown ether was loaded in Cs^+ form of the membrane, all the ion exchange sites were not available for counter ion exchange due to drastic decrease of the mobility of the alkali metal ions in the membrane. This could be due to strong binding of this crown for Cs^+ , K^+ and Na^+ over Li^+ as observed in the literature [Takeoka et al 1990]. It has also been observed from the infra-red (IR) studies [Bhattacharyya and Goswami 2009], that the Nafion matrix becomes more hydrophobic on introduction of crown ether. As has been described in the cluster channel network model of Gierke [Hsu and Gierke 1982, Hsu and Gierke 1983], water plays an important role in the transport properties of Nafion-117 membrane. Also, the earlier works on temperature dependence of ion and water diffusion in Nafion matrix [Yeager and Steck 1981, Saito et al. 2005] show that activation energy for water diffusion in Nafion is comparable to that in pure water, indicating very little barrier for water transport in the membrane.

Table 4.1: Structural details of the crown ethers used in the present work.

Crown Ether	Dibenzo-18-crown-6 (DB18C6)	Dibenzo-18-crown-6 (DB21C7)
Molecular Formula	$C_{20}H_{24}O_6$	$C_{22}H_{28}O_7$
Structure		
Molecular Weight (g)	360.40	404.45

In the present work, the factors governing the diffusional properties of different cations (Cs^+ , Na^+) in Nafion-crown ether composite membrane have been studied with a view of possible selective transport of Cs^+ through the composite membrane.

4.2. Self-Diffusion Studies

From the earlier work [Bhattacharyya and Goswami 2009] with Nafion-DB18C6 composite system, it is not clear whether the cation driven loading of DB18C6 in the Nafion-117 matrix provides template effect for improving the selectivity for other alkali metal ions, viz. Na^+ or K^+ vis-à-vis Cs^+ because of too slow kinetics of isotopic exchange of these metal ions when DB18C6 has been loaded in those cationic form of Nafion-117. DB18C6 is reported to bind Na^+ more strongly compared to Cs^+ as shown by the higher stability constant [Katsura et al. 2004] in the former case. In the present work, experiments were therefore carried out to see the change in diffusional behavior for Cs^+ and Na^+ when DB18C6 (CR1) is loaded in the respective cationic form of Nafion-117. Since the kinetics of isotopic exchange at room temperature with these membranes (M-Naf-CR1, M = Na/ Cs)) are too slow, self diffusion

experiments have been carried out as a function of temperature to understand the mechanism of transport. In the present work, the effect of temperature on the self diffusion coefficients (SDC) of water in Cs-Naf-CR1 and the corresponding equilibrium water uptakes have also been measured. The activation energy for self diffusion of both Cs^+ and water have been calculated and compared with that in Nafion-117 in absence of DB18C6. DSC measurements have also been carried out to supplement the observations obtained from self diffusion measurements. Di-Benzo-21-Crown-7 (DB21C7 i.e., CR2, structural detail given in table 4.1) is reported [Moyer et al. 1997] to be more Cs^+ selective than DB18C6. In order to study the effect of affinity of the crown ether for a particular metal ion on the activation energy of diffusion, the Cs^+ self diffusion studies in DB21C7 loaded Cs-Naf-CR2 has been carried out at different temperature. From the data, an attempt has been made to explain the membrane transport behavior in terms of hydration state of the membrane as well as the affinity of the crown ether for a particular metal ion.

4.2. 1. Experimental Section

4.2.1.1. Incorporation of the crown ether

Incorporation of the crown ethers (CR1/CR2) in the membrane samples having desired (Cs^+/Na^+) ionic form was done following the method described below. Precisely, the Nafion-117 samples in appropriate cationic form were placed in a saturated solution of either of the crown ether in 200 mL dimethyl formamide for 24 h. The samples were subsequently removed from the solution, and excess solution was wiped out. The samples were washed thoroughly with deionised water and dried under vacuum.

4.2.1.2. Membrane characterization

The weight of dry membrane was obtained by heating the membrane sample in $\text{Cs}^+ / \text{Na}^+$ form for 6–8 h at 60 °C. The extent of loading of crown ether was confirmed from the change in the dry weight of the sample before and after the loading of crown ether. The loading of DB18C6 was found to be in the molar ratio of 1:1 with respect to Na^+ , while it was 0.7:1.0 with respect to Cs^+ . In case of DB21C7, the molar ratio was found to be 0.8:1.0 with respect to Cs^+ . Infrared spectra of the Cs/Na-Naf-CR1 have also been recorded using a Jasco Fourier transform IR spectrometer model JASCO FTIR4100 (Japan). The spectra obtained were found to be similar to that shown in earlier work [Bhattacharyya and Goswami 2009]. The thicknesses of the membranes were measured using a digital micrometer (Mitutoyo, Japan) which is having an accuracy of 0.001 mm.

4.2.1.3. Differential Scanning Calorimetry (DSC)

DSC measurements for the $\text{Cs}^+ / \text{Na}^+$ form of Nafion with and without DB18C6 were done using a Mettler Toledo DSC 822 instrument at a heating rate of 10 °C/min within the temperature range of -10 °C to 300 °C. About 7 - 8.5 mg of membrane samples were used to record the scans. The scans were recorded under inert atmosphere with an empty aluminum pan as the reference. Indium was used as the calibration standard. The DSC traces were analyzed using the software supplied by Mettler Toledo.

4.2.1.4. Self diffusion measurement of cations

The Cs^+ ion self diffusion measurement in Cs-Naf-CR1/ Cs-Naf-CR2, were measured by the method as described in chapter 2. For Cs-Naf-CR1, the measurements were carried out at 4 different temperatures, viz, 50 °C, 55 °C, 60 °C and 65 °C, while for Cs-Naf-CR2, measurements were carried out at 3 different temperatures (60 °C, 65 °C and 70 °C). The temperature of the solution has been maintained using a constant temperature bath. During

the course of the experiment, the temperature was monitored constantly using an external thermometer. The experiments at each temperature were repeated to verify the reproducibility of the measurement. The dry weight of the membrane was taken before and after every experiment. It was observed that the weight of the membrane sample remains constant indicating that crown ether did not come out of the membrane during the course of the experiment.

In case of Na-Naf-CR1, the self diffusion study of Na^+ ion was carried out only at 60 °C since the kinetics was found to be too slow at lower temperatures. Even at 60 °C, it was not possible to reach complete equilibrium after long time period. In order to obtain the fractional attainment of equilibrium as a function of time (t), the amount of radiotracer ions in the membrane at equilibrium ($t = \infty$) is required. This was found out indirectly, assuming that the amount of radiotracer ion in the membrane at infinite time is governed by the ratio of the amount of sodium ion in the membrane to that in the external solution. Total radioactivity added in the external salt solution was obtained by counting 100 μL of the solution in NaI(Tl) detector connected to a 4k channel analyzer. The number of available ion exchange sites (mili equivalent) in the membrane was obtained from the dry weight of the membrane sample before incorporation of the crown ether. The equilibrium radioactivity in the membrane was obtained from the product of the ratio of Na^+ in the membrane to that in the external salt solution and the total activity present in the external salt solution. It is assumed that the uptake of radiotracer in the membrane did not alter the radioactivity concentration in the external salt solution.

4.2.1.5. Self diffusion measurement of water in Cs-Naf-CR1

In order to study the self diffusion behavior of water in Cs-Naf-CR1, the membrane sample (2 cm X 2 cm) was equilibrated in water spiked with ^3H (HTO) at a constant temperature

with stirring for 2 h. After equilibration, the membrane was taken out and gently wiped with a filter paper to remove the water droplets attached to the surface. Then the sample was placed in 25 mL deionised water which is kept at the same temperature at which equilibration of the membrane with HTO has been carried out. The water was continuously stirred (~ 52 rad/s) during the course of the desorption experiment to minimize the film diffusion. The water diffusion rate in the membrane sample was measured by pipetting out 50 μL of the equilibrating solution after regular time intervals. The β activity of ^3H has been measured by mixing the sample in a vial with 5 mL of scintillation cocktail-w (2, 5-diphenyl oxazole (PPO) = 0.7%, 1,4-di-2-(5-phenyloxazolyl benzene (POPOP) = 0.03%, naphthalene = 10%, and tri-n-octyl phosphine oxide (TOPO) = 1% in 1,4-dioxane solvent), and counting the samples with a liquid scintillation analyzer. The water diffusion experiments were carried out at 27 $^{\circ}\text{C}$, 38 $^{\circ}\text{C}$, 45 $^{\circ}\text{C}$, 51 $^{\circ}\text{C}$ and 56 $^{\circ}\text{C}$.

4.2.1.6. Membrane water content measurement

The water content (cm^3) of the membrane was obtained from the uptake of ^3H β activity at equilibrium in the membrane and the radioactivity concentration of the ^3H labeled water (HTO) used for equilibration. Assuming the density of water to be 1 g cm^{-3} in the membrane phase, and using the dry weight of the membrane after incorporation of the crown ether, the membrane water content (water to exchange site mole ratio = $\lambda = n_{\text{H}_2\text{O}} / n_{\text{SO}_3^-}$) was obtained. In Cs-Naf-CR1 the water content has been measured at 27 $^{\circ}\text{C}$, 38 $^{\circ}\text{C}$, 45 $^{\circ}\text{C}$, 51 $^{\circ}\text{C}$ and 56 $^{\circ}\text{C}$ while that for Na-Naf-CR1 has been carried out only at 56 $^{\circ}\text{C}$.

4.2.2. Results and Discussion

4.2.2. 1. Temperature dependence of self diffusion of cations in Cs/Na-Naf-CR1 and Cs-Naf-CR2

The temperature dependences of Cs^+ self diffusion profiles in Cs-Naf-CR1 and Cs-Naf-CR2 are shown in figure 4.1(a) and figure 4.1 (b) respectively. As seen from the figure, there is a steady increase in isotopic exchange rate with increase in temperature, indicative of existence of barrier for diffusion. Along with the experimental points, the fitted lines to these self diffusion profiles in Cs-Naf-CR1 are also shown in the figure 4.1a.

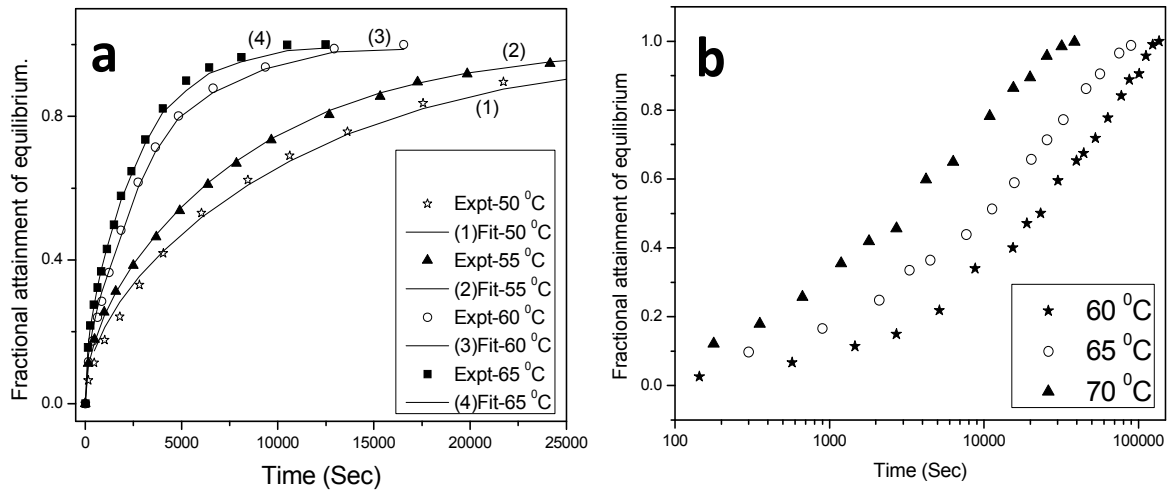


Figure 4.1: Self diffusion profile of Cs^+ ion in (a) Cs-Naf-CR1 and (b) Cs-Naf-CR2 at different temperatures. The symbols are the experimental points and the lines are the fitted line to those experimental points.

The SDCs for Cs^+ ($D_{\text{Cs}^+}^m$) ion in these membranes at each temperature have been obtained from these profiles using eq 1.8 [Goswami et al. 2001] and are listed in table 4.2. The Arrhenius plot of the $D_{\text{Cs}^+}^m$ data in Cs-Naf-CR1 and Cs-Naf-CR2 are shown in figure 4.2a and 4.2b respectively. From the slope of this linear plot, the activation energy for diffusion of Cs^+

has been obtained which is given in table 4.3 along with the literature [Yeager and Steck 1981] reported activation energy for Cs-Naf (Nafion-120). The value of activation energy (E_a) is seen to have increased by a factor of ~ 2.2 in Cs-Naf-CR1 compared to Cs-Naf, accounting for the very slow diffusion rate of Cs^+ ion in Cs-Naf-CR at room temperature, as observed in our earlier work [Bhattacharyya and Goswami 2009].

Table 4.2: Variation of $D_{\text{Cs}^+}^m$ in Cs-Naf-CR1 and Cs-Naf-CR2 at different temperatures

Temperature ($^{\circ}\text{C}$)		50	55	60	65	70
$D_{\text{Cs}^+}^m \times 10^6$ (cm^2/Sec)	Cs-Naf-CR1	3.50E-03	5.13E-03	1.32E-02	1.32E-02	--
	Cs-Naf-CR2	--	--	7.40E-04	2.00E-03	7.02E-03

In Cs-Naf-CR2, E_a for Cs^+ diffusion has been calculated as 213 ± 16 KJ/mole, which is much higher than that in Cs-Naf-CR1. The result clearly shows much higher affinity of Cs^+ for DB21C7 than DB18C6 as expected. Such a large value of activation energy is typical of ionic diffusion in ionic crystal lattice rather than in swollen polymers [Yeager and Steck 1981]. This is indicative of significant change in the morphology and different mechanism of Cs^+ ion diffusion in the crown ether modified Cs-Naf compared to Cs-Naf.

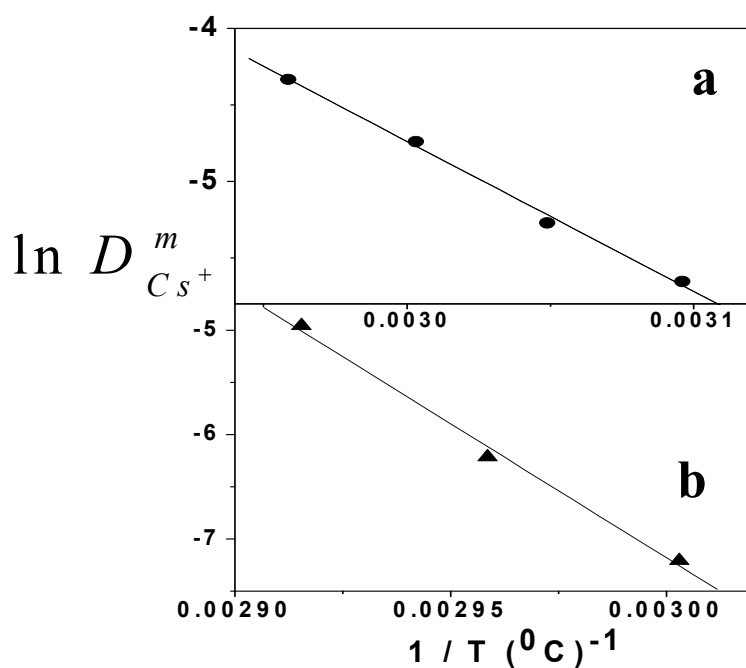


Figure 4.2: Variation of logarithm of SDCs of Cs^+ ($\ln D^m_{\text{Cs}^+}$) in (a) Cs-Naf-CR1 and (b) Cs^+ in Cs-Naf-CR2 as a function of inverse of temperature. The solid points are the experimental points while the lines are the fitted line.

Table 4.3: Activation barrier for Cs^+ ion and water in pure [Yeager and Steck 1981] and crown ether modified Cs-Naf

Membrane	Activation Energy (Cs^+) (kJ/mol)	Activation Energy (H_2O) (kJ/mol)
Cs-Naf	35.9	22.0
Cs-Naf-CR1	80.1 ± 4.0	79.8 ± 5.0
Cs-Naf-CR2	213.0 ± 16.0	--

Attempt to carry out similar self diffusion experiments with Na-Naf-CR has not been possible at lower temperature as the isotopic exchange kinetics was too slow to reach complete equilibrium within reasonable time scale. Figure 4.3 shows the comparison between the isotopic exchange kinetics for Cs^+ and Na^+ with Cs-Naf-CR1 and Na-Naf-CR1 respectively at 60 $^{\circ}\text{C}$.

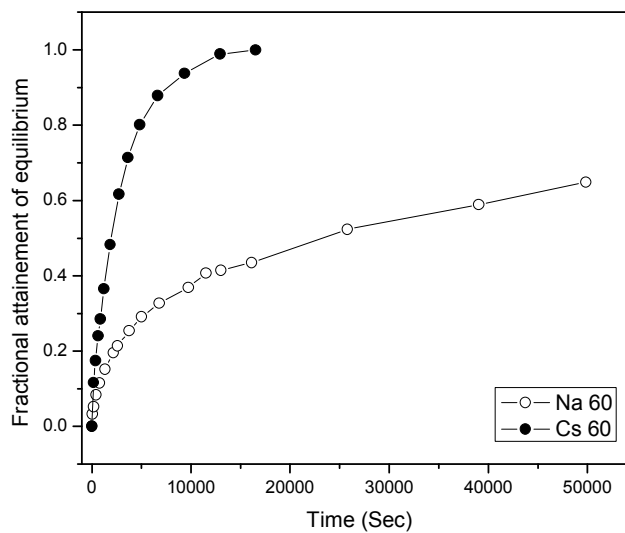


Figure 4.3: Comparison between Cs^+ and Na^+ self diffusion profile at 60 $^{\circ}\text{C}$ in Cs-Naf-CR1 and Na-Naf-CR1 respectively.

As can be seen from this figure, the Cs^+ isotopic exchange is complete within ~ 20000 sec, while the Na^+ isotopic exchange is not complete even at 50000 sec. The lower mobility of Na^+ in Na-Naf-CR1 indicates higher activation energy for diffusion of Na^+ in this membrane. This may reflect the stronger binding of Na^+ with the DB18C6 in membrane matrix, retarding the mobility of the Na^+ ion [Katsura et al. 2004]. There are literature reports [Muraviev et al. 1995, Zagorodni et al. 1997, Cerjan-Stefanovic et al. 1984, Zahran et al. 2010], where selectivity of ion exchange resins and ion selective electrode have been enhanced by carrying out the measurement at elevated temperatures. It will be of interest to see whether the

selectivity of this crown ether loaded membrane could be tuned by carrying out the transport study at higher temperature.

4.2.2. 2. Temperature dependence of self diffusion behavior of water

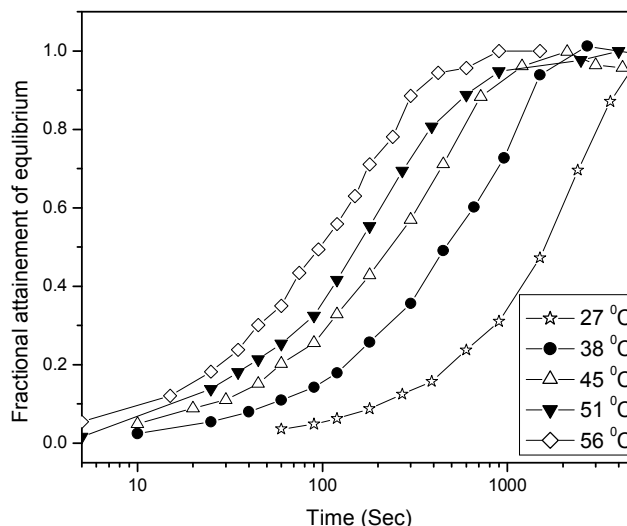


Figure 4.4: Self diffusion profile of water in Cs-Naf-CR1 at five different temperatures.

Figure 4.4 shows the self diffusion behavior of water in Cs-Naf-CR1 studied with tritium labeled water at five different temperatures. Here again, the rate of $\text{HTO}_{(m)} \rightleftharpoons \text{H}_2\text{O}_{(aq)}$ exchange increases with the rise in temperature. The SDCs of water ($D_{\text{H}_2\text{O}}^m$), calculated from a fit of the experimental data with equation 1.8 are given in table 4.4. The $D_{\text{H}_2\text{O}}^m$ values at a given temperature are $\sim 30 - 40$ times higher than the $D_{\text{Cs}^+}^m$. It indicates that, as in the case of Cs-Naf, water diffusion in Cs-Naf-CR1 faces less hindrance than the diffusion of Cs^+ ion. However, all the values are substantially lower than the $D_{\text{H}_2\text{O}}^m$ in Cs-Naf, showing that the mobility of the water in Cs-Naf-CR1 is considerably hindered compared to that in Cs-Naf. The value of the activation energy, obtained from the Arrhenius plot (figure 4.5) is also given

in the table 4.3 along with the activation energy for Cs-Naf [Yeager and Steck 1981]. It is seen that the activation energy increases by a factor of ~ 4 and is comparable to the activation energy for Cs^+ diffusion in Cs-Naf-CR1. Such a high value of activation energy indicates that there is no continuous water channel in the Cs-Naf-CR1.

Equilibrium uptake of water as a function of temperature in Cs-Naf-CR1 has also been measured and the corresponding $n_{\text{H}_2\text{O}} / n_{\text{SO}_3^-}$ values are given in table 4.4. As seen from the data, the water uptake has reduced significantly in Cs-Naf-CR1 over Cs-Naf ($n_{\text{H}_2\text{O}} / n_{\text{SO}_3^-} = 5.01$, at room temperature) showing that dehydration of Cs^+ in Cs-Naf-CR1 has occurred.

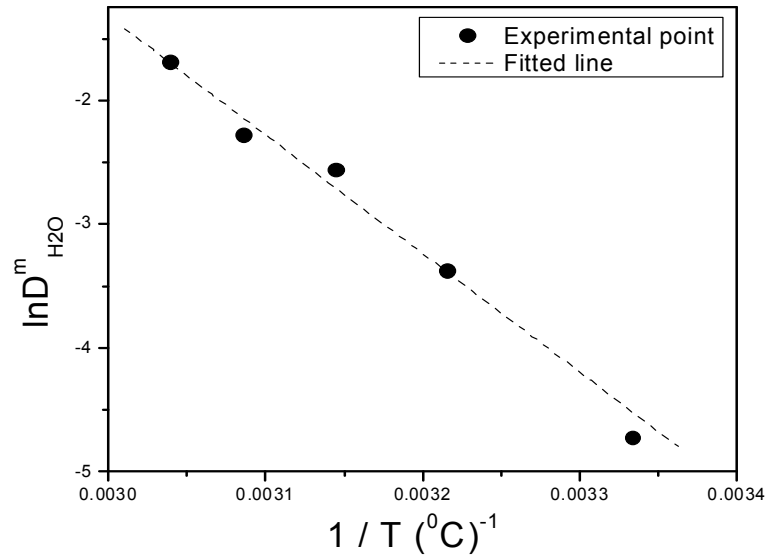


Figure 4.5: Variation of logarithm of self diffusion coefficient of water ($\ln D_{\text{H}_2\text{O}}^m$) in Cs-Naf-CR1 as a function of inverse of temperature. The solid points are the experimental points while the lines are the fitted line.

Table 4.4: Variation of $D_{H_2O}^m$ and water content in Cs-Naf-CR1 as a function of different temperatures

Temperature ($^{\circ}\text{C}$)	27	38	45	51	56
$D_{H_2O}^m \times 10^6 (\text{cm}^2/\text{Sec})$	8.88E-03	3.43E-02	7.74E-02	1.02E-01	1.85E-01
$n_{H_2O} / n_{SO_3^-}$	1.02	1.09	1.12	1.36	1.40

Reduction in water signal as observed from IR data [Bhattacharyya and Goswami 2009] in Cs-Naf-CR1 as compared to Cs-Naf also confirms the increased hydrophobicity of the Nafion sample after incorporation of DB18C6 in the membrane matrix. This shows that complexation of DB18C6 with Cs^+ ion accompanied by the disruption of the water cluster channel network of Nafion-117 has taken place, thereby reducing the $D_{H_2O}^m$ significantly. The effect of water content in Nafion-117 on the self diffusion coefficient of water was extensively studied by Zhao et al. [Zhao et al. 2011] and it has been concluded that the diffusivity changes significantly when $n_{H_2O} / n_{SO_3^-}$ becomes less than 4. At the $n_{H_2O} / n_{SO_3^-}$ values close to that in the present experiment (~ 1), values of diffusion constants reported at different temperature are comparable to the values observed in the present experiments. This shows, apart from the crown ether, water content in the membrane also plays an important role in the cation transport property of the membrane. These results explain why incorporation of hydrophilic species in the membrane increases the cation diffusion rate in the crown ether loaded membrane matrix [Sakamoto et al. 1986].

The cause of enhancement in the activation energy of Cs^+ ion in the crown ether loaded Nafion membrane compared to pure Nafion-117 could be due to enhancement in binding of

the ion with the crown ether in the membrane matrix and also due to the reduction in water content in the membrane matrix due to loading of the crown ether, destroying water clusters in Cs-Naf.

In the case of Na-Naf-CR1, equilibrium uptake of water was measured and the corresponding $n_{H_2O} / n_{SO_3^-}$ value was found to be 1.07. As can be seen from table 4.4, the value is slightly lower than that of Cs-Naf-CR1, indicating higher degree of dehydration of Na^+ in Na-Naf-CR1 as compared to Na-Naf which again reflects that DB18C6 binds more strongly with Na^+ ion in the membrane matrix. Higher $D_{Cs^+}^m$ as observed in our earlier work [Bhattacharyya et al 2009], when DB18C6 was loaded in the Nafion-117 membrane in Li^+ form could be due to at least partial retention of the water channels in Li-Naf-CR1. This is due to the lower binding of DB18C6 with Li^+ , thereby failing to completely dehydrate the Li^+ ion in the membrane matrix unlike Cs-Naf-CR1 and Na-Naf-CR1.

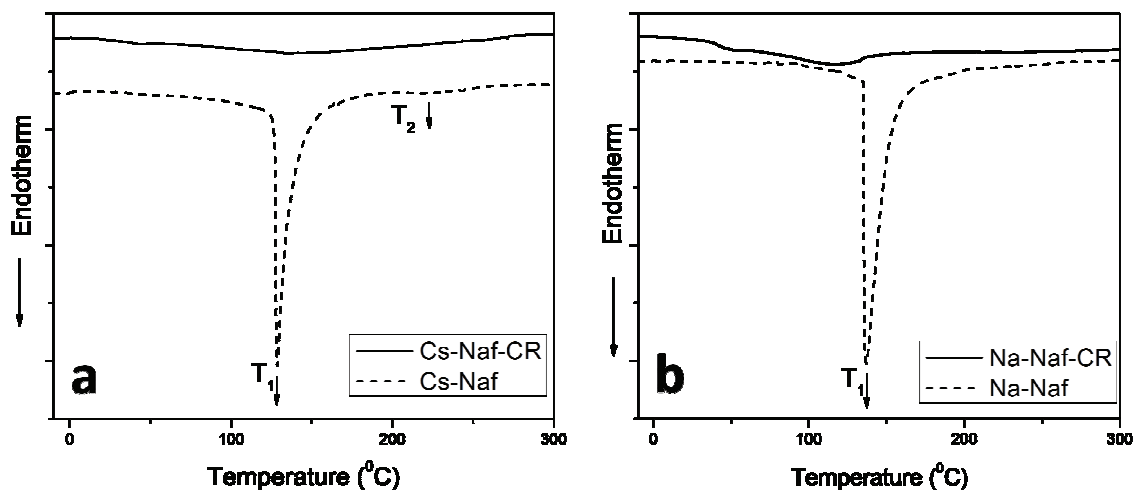


Figure 4.6: DSC thermograms of (a) Cs^+ form and (b) Na^+ form of Nafion membrane with and without DB18C6.

Figure 4.6a and 4.6b depicts the DSC traces of pure and DB18C6 modified Cs^+/Na^+ form of Nafion respectively. In the case of Cs-Naf, one sharp endothermic peak at 128°C and another broad endothermic peak at 242°C have been observed while for Na-Naf only one sharp endothermic peak at 136°C has been observed. This behavior of Cs^+/Na^+ form of Nafion is well explained in the literature [Almeida and Kawano 1999, Stefanithis and Mauritz 1990]. Thus the transition at $\sim 130^\circ\text{C}$ (T_1) has been associated with the transition into the ionic clusters and that at $\sim 245^\circ\text{C}$ (T_2) has been associated with the region of crystallite melting of the ionomers. The comparison of the DSC traces of Cs-Naf and Cs-Naf-CR1 shows that the sharp endothermic peak at 128°C in Cs-Naf has almost disappeared in Cs-Naf-CR1. As can be seen from figure 4.6b, the same is true for Na-Naf-CR1 also. This change in DSC traces could be attributed to the absence of regions of water cluster channels after incorporation of DB18C6 in the Nafion-117 matrix. This corroborates our observations already obtained from equilibrium water uptake measurement and self diffusion measurement of cations and water.

4.3. Selective Transport

A general problem with the IEM is that the enhanced selectivity of an ion is usually accompanied by reduction in mobility of the ion. Enhancement in the permeability retaining the selectivity, therefore, is a challenge for use of IEM in separating ions of similar charge. Possible solutions can be the partial incorporation of the ligand (<1 mole ratio with respect to no. of ion exchange sites), so that the ion exchange sites free of ligand can provide faster transport pathway for the cations while the ligand occupied sites can provide selectivity. Alternatively, the crown ether can be loaded in a membrane where only a thin surface layer is occupied by the desired ion (templating only at the surface layer). Such an ion templated crown ether loaded thin layer may prevent the transport of undesirable ions, allowing the desired cations to selectively pass through a thin surface barrier in shorter time. Also,

permeation of ion from feed to receiver phase through IEM requires counter transport of another ion from receiver to feed phase to maintain electrical neutrality. This however, can be avoided if an electric field is used as a driving force for cation transport.

With this in view, in the present work, a Cs^+ selective Dibenzo-21-crown-7 (DB21C7=CR), has been incorporated uniformly in Cs^+ form of Nafion-117 membrane in varying molar ratio ($N = n_{\text{CR}} / n_{\text{Cs}^+}$) with respect to Cs^+ in the membrane. The $\text{Cs}_{\text{sol}}^+ \rightleftharpoons \text{Cs}_{\text{mem}}^+$ (sol = solution and mem = membrane) isotope exchange kinetics and $\text{Na}_{\text{sol}}^+ \rightleftharpoons \text{Cs}_{\text{mem}}^+$ ion exchange kinetics in these homogeneously crown ether loaded membranes (Cs-Naf-CR_h) have been studied to assess the transport rate of the ions in these membranes. A crown ether-Nafion composite membrane has also been prepared by incorporating DB21C7 in a thin surface layer (few μm) of Nafion-117 membrane (ion gating). The surface confinement of Cs^+ in this ion gated membrane (Cs-H-Naf-CR) has been studied using Energy Dispersive X-ray spectroscopy (EDS) and Time of Flight Secondary Ion Mass Spectrometry (ToFSIMS). A comparative account of these 2 types of membranes (Cs-Naf-CR_h and Cs-H-Naf-CR) for electro-driven selective transport of Cs^+ from Na^+ is also presented. The suitability of this ion gated membrane for selective removal of ^{137}Cs from a simulated nuclear waste solution has also been studied. The results have been discussed in terms of cationic diffusivity and selectivity.

4.3.1. Experimental Section

4.3.1.1. Incorporation and Quantification of the crown ether in Cs-Naf-CR_h

The loading of DB21C7 in Cs-Naf was done by the method mentioned in section 4.2. The extent of loading in the membrane was controlled by varying the dissolved amount of DB21C7 in Dimethyl formamide (DMF), so that the mole ratio of Cs^+ in the membrane and

dissolved DB21C7 in solution varies from 1:1 to 4:1. The quantification of the crown ether in the membrane matrix was done by gravimetric method as well as by UV-visible spectrophotometry, where, the spectra of the left over DB21C7 in DMF solution (after crown ether loading in the membrane) were used for the quantification. A representative UV-visible spectrum for 2.0×10^{-4} M solution of DB21C7 in DMF is shown in figure 4.7a. Using very dilute solution ($\mu\text{M}/\text{L}$) of DB21C7 in DMF, a linear calibration plot of absorbance vs. concentration of DB21C7 (figure 4.7b) is obtained at $\lambda_{\text{max}} = 281$ nm. For solutions of higher concentration, nonlinear behavior is observed. In gravimetric method, the dry weights of the membranes before and after loading of the DB21C7 were used to calculate N. The weight of dry membrane was obtained by heating the membrane sample for 6–8 h at 70°C .

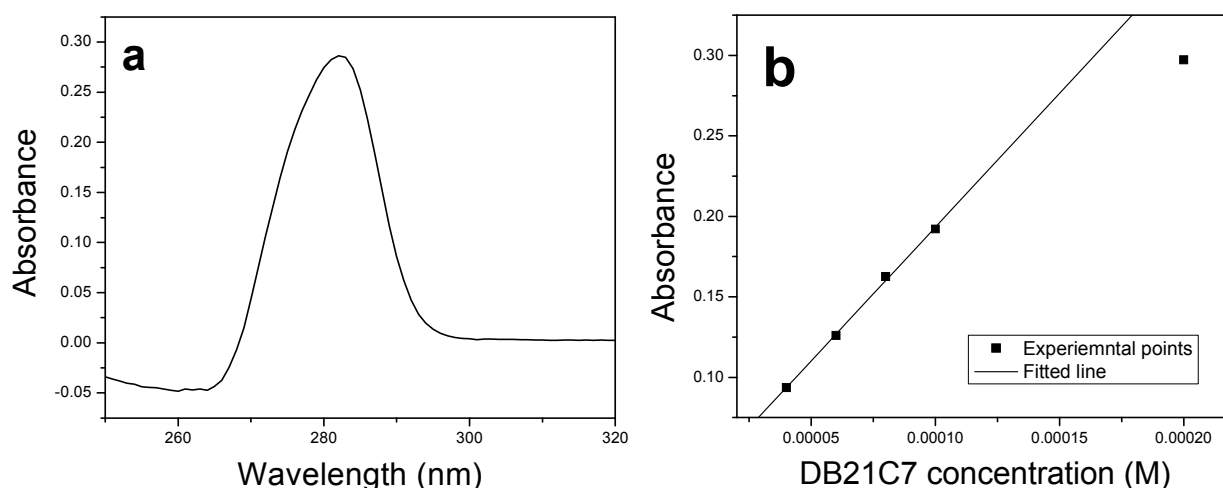


Figure 4.7: (a) UV-visible spectrum acquired for 2.0×10^{-4} M DB21C7 solution in DMF. (b) Calibration plot of absorbance vs concentration of DB21C7.

4.3.1.2. Preparation and Characterization of Cs-H-Naf-CR

The Cs^+ gated membrane (Cs-H-Naf-CR) was prepared by first exposing H-Naf (pure Nafion-117) membrane to 0.1 M CsCl solution from one surface for 15 seconds. The exposure time was decided from the $\text{Cs}^+ - \text{H}^+$ ion exchange kinetics as given by [Suresh et al. 2004]. This partially Cs^+ loaded membrane is immediately placed in a DB21C7-DMF

solution so that the motion of Cs^+ ions is arrested by DB21C7 in DMF medium. The amount of crown ether in the DMF solution was in a stoichiometric ratio of 1:1 to the total ion exchange sites in the membrane. The annealing of the crown ether loaded membrane was done by the method described in section 4.2. As calculated from gravimetric measurement, the value of n_{CR} / n_{IES} (n_{IES} = no. of ion exchange site in the membrane) in the Cs-H-Naf-CR membrane was found to be 0.32.

The distribution of Cs^+ ion along the thickness of this membrane was studied by EDS and ToFSIMS methods. The EDS analysis was carried out using a Cam Scan made spectrometric unit (model no 3100) with 20 kV voltage and 150 μA beam current. The scanning was done along the thickness of the membrane in 20 steps (each step covered 10 μm length). At each step, data was acquired for 1 minute. For comparison purpose, this analysis was also carried out for Cs-Naf-CR_h ($N=0.8$, uniform Cs^+ ion distribution throughout the membrane thickness).

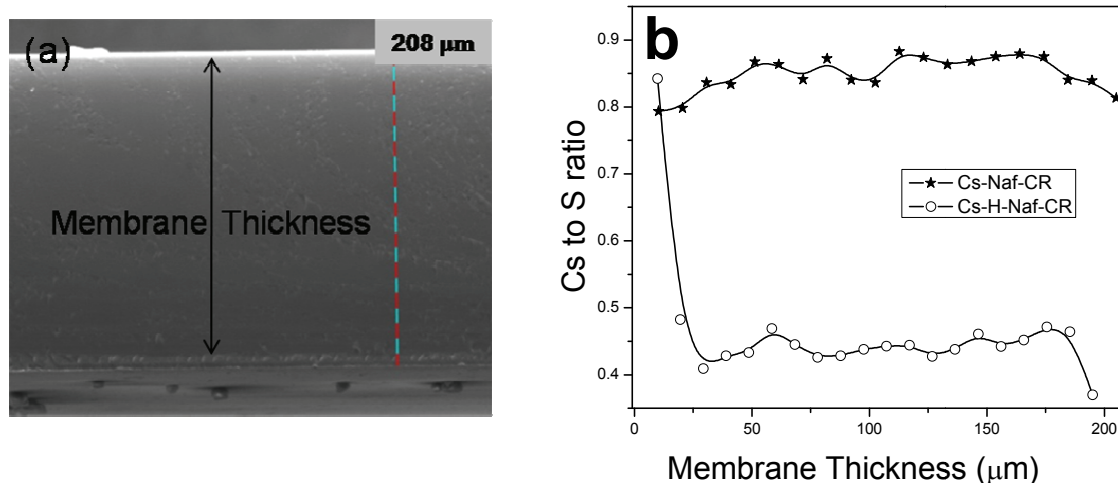


Figure 4.8: (a) Microscopic image of the cross section of Cs-Naf-CR_h ($N = 0.8$) along which EDS analysis has been carried out. (b) Atom % ratio of Cs to S (as obtained from EDS analysis) in Cs-Naf-CR_h ($N = 0.8$) and Cs-H-Naf-CR.

Figure 4.8 (a) shows the cross sectional view of the Cs-Naf-CR2 membrane ($N = 0.8$) under scanning electron microscope. The number of steps that has been taken to cover the full thickness of the membrane for EDS analysis is also marked in the image. The Cs to S (each S atom corresponds to one ion exchange site in the membrane) atom % ratio (as obtained from EDS analysis) in Cs-Naf-CR_h ($N = 0.8$) and Cs-H-Naf-CR are shown in figure 4.8 (b). The constant Cs to S atom % ratio in Cs-Naf-CR_h indicates homogeneous distribution of Cs⁺ throughout the membrane thickness. The sharp fall in Cs/S ratio in Cs-H-Naf-CR in the first few micron (25 μm) indicates that Cs⁺ is loaded only in the initial $\sim 25\mu\text{m}$ thickness. The EDS analysis shows that Cs⁺ is confined only within 25 μm from the surface.

ToFSIMS data was acquired with 30 KeV Au⁺ ion source as the primary beam, using a TRIFT V time of flight instrument, manufactured by ULVAC-Physical Electronics, Mn, USA. The Cs⁺ distribution along the membrane (Cs-H-Naf-CR) thickness as obtained from ToFSIMS analysis is shown in figure 4.9. The first part of the figure (4.9a) shows the variation of Cs⁺ counts at two different locations along the length. The similar nature of the Cs⁺ distribution in both the locations indicates uniform distribution of this cation along the length of the membrane. The second part of the figure (4.9b) shows the overlay spectrum of Cs⁺ ion (green coloured) distribution over total ion (red coloured) along the thickness of Cs-H-Naf-CR. The presence of Cs⁺ only in the initial 25 μm of the membrane thickness is again obvious from both this figure.

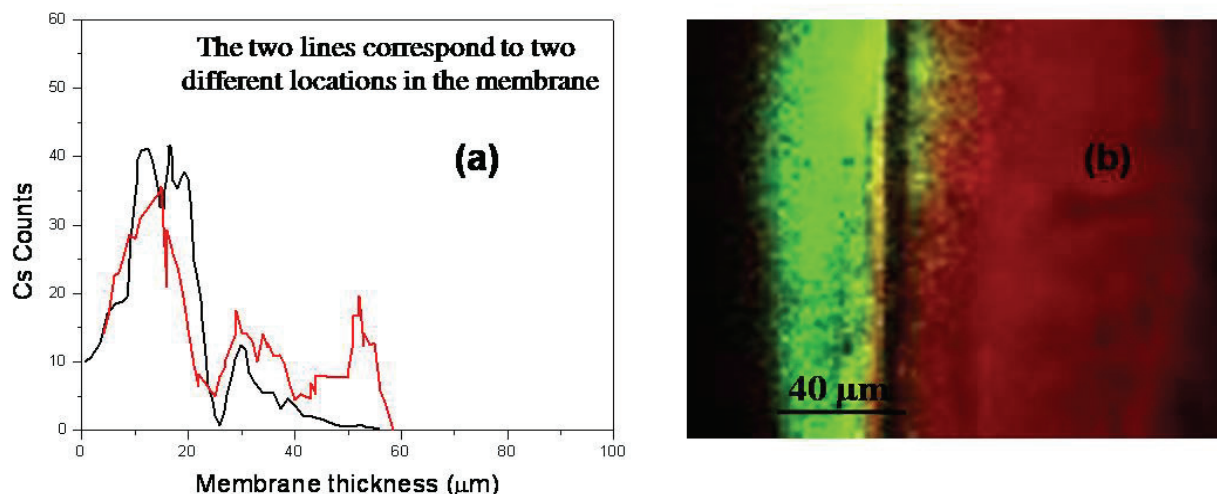


Figure 4.9: ToFSIMS spectra showing (a) Variation of Cs^+ counts and (b) Overlay of Cs^+ ion (green) distribution over total ion (red) along the thickness of Cs-H-Naf-CR membrane.

4.3.1.3. Self diffusion and ion exchange measurement in Cs-Naf- CR_h

The Cs^+ self diffusion measurements in the partially crown ether loaded Cs-Naf- CR_h membranes were carried out at room temperature following the standard radiotracer method as described in chapter 2. For the cases, where complete attainment of equilibrium was not possible, the fractional attainment of equilibrium (F_t) as a function of time (t) was found out indirectly using the following equation

$$F_t = \frac{C_t}{(C_{\text{mem}})_\infty} \quad (4.1)$$

Where, C_t is the radiotracer count in the membrane at time t and $(C_{\text{mem}})_\infty$ is the expected radiotracer count in the membrane at equilibrium.

The amount of radiotracer ion in the membrane at equilibrium ($(C_{\text{mem}})_\infty$) is governed by the ratio of the amount of Cs^+ ion in the membrane to that in the external solution. This quantity is calculated from the following relation

$$(C_{mem})_{\infty} = \frac{I_{mem} C_{sol}}{I_{sol}} \quad (4.2)$$

Where, I_{mem} is the number of available ion exchange sites in the membrane, C_{sol} is the total radioactivity added in the external salt solution and I_{sol} is the mili-equivalence of Cs^{+} in the external solution.

C_{sol} has been obtained by counting 100 μ L of the solution in NaI(Tl) detector connected to a 4k channel analyzer. I_{mem} has been obtained from the dry weight of the membrane sample before incorporation of the crown ether.

For $Na^{+}_{sol} \rightleftharpoons Cs^{+}_{mem}$ ion exchange kinetics measurement, the Cs-Naf-CR_h membrane sample (1 cm X 2 cm) was placed in 30 ml of 0.1 N NaCl solution. The solution was tagged with ^{22}Na radiotracer. The kinetics of exchange between Cs^{+} ion the membrane and Na^{+} ions in the solution was monitored by the same method as described in the previous section. The 511 keV peak of ^{22}Na was monitored. The fractional attainment of equilibrium (F_t) as a function of time (t) was found out indirectly following the same method as described in the previous section.

4.3.1.4. Transport study

In order to study the selective transport of Cs^{+} over Na^{+} (using Cs-Naf/ Cs-Naf-CR_h/ Cs-H-Naf-CR membranes), two compartment permeation experiments were carried out at room temperature. During the experiment, electric field (4V) was applied across the membrane using two Pt electrodes. The membrane active surface area was 1.7 cm². A schematic diagram of the experimental arrangement is shown in figure 4.10. In order to achieve volume reduction along with selective transport, the volume ratio of feed to receiver compartment was kept to be 10. A mixture (32 ml) of NaCl and CsCl was used in the feed and deionized water (3.2 ml) spiked with NaOH (0.004 mmol) has been used in the receiver compartment.

Two different mole ratios of CsCl and NaCl (1:1 or 1:4) were used in the feed compartment. The Cs^+ -gated surface of the membrane was exposed to the feed solution which is tagged with ^{22}Na and ^{137}Cs tracer. The solutions in both the compartments were stirred continuously to avoid any film controlled diffusion at the membrane interface. Amount of Na^+ and Cs^+ transferred from the feed to the receiver side were monitored by taking out 200 μL of aliquots from both the compartments at regular time intervals and counting the ^{22}Na and ^{137}Cs activity in HPGe detector. For comparison of the results, one of the transport experiment ($\text{Cs}^+ : \text{Na}^+ = 1:1$ in feed solution) was repeated with Cs-Naf, keeping other conditions unaltered.

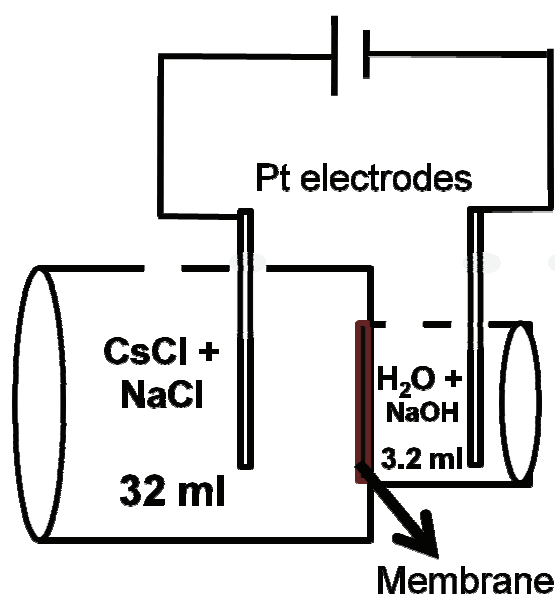


Figure 4.10: Experimental arrangement for transport studies under applied electric field.

Transport experiment was also carried out for the simulated effluent solution of Resorcinol Formaldehyde Polycondensate Resin (Intermediate Level Nuclear Waste treated with RFPR) with the feed composition being 0.1 M NaNO_3 and 3.5×10^{-4} M CsNO_3 in 0.4 M HNO_3 [Banerjee et al. 2014]. During the course of the experiment it was observed that, the crown ether was leaching out from the membrane possibly due to the strong interaction between HNO_3 and DB21C7. The feed solution was thus neutralized with NaOH (pH ~ 7) before the

experiment was carried out. The final feed composition for this simulated waste was 0.5 M NaNO_3 and 3.5×10^{-4} M CsNO_3 .

4.3.2. Results and Discussion

4.3.2. 1. Cs-Naf-CR_h

Four Cs-Naf-CR_h membranes were prepared containing different mole ratio ($N = 0.80, 0.66, 0.36, 0.21$) of DB21C7 with respect to Cs^+ . The $\text{Cs}^+_{\text{sol}} \rightleftharpoons \text{Cs}^+_{\text{mem}}$ isotopic exchange in Cs-Naf-CR_h membrane ($N = 0.8$) is too slow to be observed at room temperature. However, for other Cs-Naf-CR membranes with lower (< 0.8) N , the $\text{Cs}^+_{\text{sol}} \rightleftharpoons \text{Cs}^+_{\text{mem}}$ isotopic exchange takes place at room temperature. The $\text{Cs}^+_{\text{sol}} \rightleftharpoons \text{Cs}^+_{\text{mem}}$ isotopic exchange profiles and the $\text{Na}^+_{\text{sol}} \rightleftharpoons \text{Cs}^+_{\text{mem}}$ ion exchange profiles in these partially DB21C7 loaded Cs-Naf-CR_h membranes are shown in figure 4.11a and 4.11b respectively. The arrows in the figures show the extent of sites available for isotopic/ ion exchange. The results show that, the mobility of Cs^+ in Cs-Naf-CR_h membrane decreases with increase in N and also the fraction of isotopic exchange sites available for $\text{Cs}^+_{\text{sol}} \rightleftharpoons \text{Cs}^+_{\text{mem}}$ exchange decreases. It is also seen from the figures that the $\text{Na}^+_{\text{sol}} \rightleftharpoons \text{Cs}^+_{\text{mem}}$ exchange profiles are faster than the corresponding $\text{Cs}^+_{\text{sol}} \rightleftharpoons \text{Cs}^+_{\text{mem}}$ exchange. However, $\text{Na}^+_{\text{sol}} \rightleftharpoons \text{Cs}^+_{\text{mem}}$ exchange proceeds to the extent that can be expected from the fraction of sites free of crown ether ($1-N$). This shows that there are two different types of Cs^+ ionic sites in these Cs-Naf-CR_h membranes, one associated with crown ether and the other free of crown ether. As seen from the profiles in figure 4.11a, with increasing N , the crown ether associated sites are increasingly difficult for $\text{Cs}^+_{\text{sol}} \rightleftharpoons \text{Cs}^+_{\text{mem}}$ exchange due to change in membrane morphology.

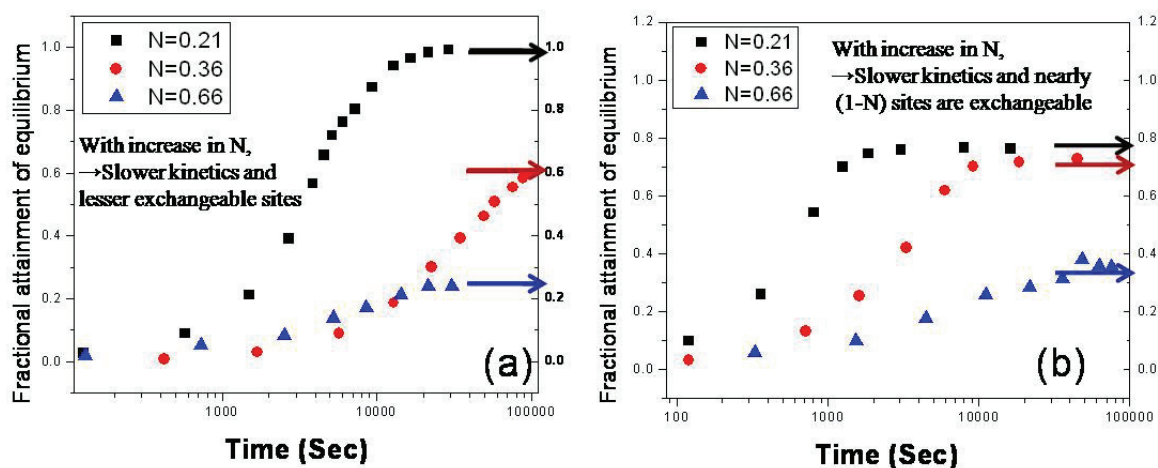


Figure 4.11: Room temperature (a) $\text{Cs}^+_{\text{sol}} \rightleftharpoons \text{Cs}^+_{\text{mem}}$ isotopic exchange profiles and (b) $\text{Na}^+_{\text{sol}} \rightleftharpoons \text{Cs}^+_{\text{mem}}$ ion exchange profiles in Cs-Naf- CR_h membranes with different N . The arrows indicate the fraction of exchangeable sites in the membrane at room temperature.

The time dependent relative cation transport ($\% \text{Cs}^+ / \% \text{Na}^+$) for different membranes [Cs-Naf, Cs-Naf- CR_h ($N=0.36$) and Cs-H-Naf-CR] are shown in table 4.5. The data shown in the table are for the experiments that have been carried out at 4 V with the feed solution having 5 milimoles Cs^+ and 5 milimoles Na^+ . As can be seen from this table, transport selectivity of Cs^+ over Na^+ has not been observed in the two compartment transport experiments for the Cs-Naf and Cs-Naf- CR_h ($N=0.36$) membranes. The absence of selective transport in Cs-Naf- CR_h membranes can be understood on the basis of presence of two types of ion exchange sites in these membranes as explained earlier. The sites free of crown ether provide transport pathways like pure Nafion-117 with lower activation barrier (E_a) and lower selectivity. On the other hand, the diffusion involving crown ether associated ion exchange sites have very high activation barrier (templating effect) for diffusion and high selectivity. These two transport pathways in Cs-Naf- CR_h membrane are represented schematically in figure 4.12a. Since both the ion exchange sites are randomly distributed throughout the membrane,

transport of most of the ions occurs involving the lower activation barrier sites, resulting in transport behavior (no selectivity) similar to that of pure Nafion-117.

Table 4.5: The time dependent relative cation transport ($\% \text{Cs}^+ / \% \text{Na}^+$) for different membranes. The experiments have been carried out at 4 V with the feed solution having 5 milimoles Cs^+ and 5 milimoles Na^+ .

Cs-Naf		Cs-Naf-CR _h (N= 0.36)		Cs-H-Naf-CR	
Time (Minutes)	Relative cation transport ($\% \text{Cs}^+ / \% \text{Na}^+$)	Time (Minutes)	Relative cation transport ($\% \text{Cs}^+ / \% \text{Na}^+$)	Time (Minutes)	Relative cation transport ($\% \text{Cs}^+ / \% \text{Na}^+$)
90	0.91	60	0.87	210	4.08
210	1.12	150	0.99	420	4.49
330	0.87	210	1.05	1380	4.39
450	1.03	360	1.06	1635	4.03
1410	1.05	435	1.03	1860	3.91

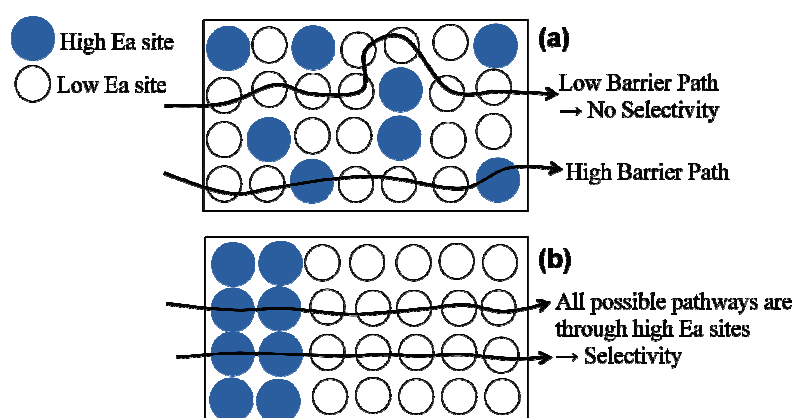


Figure 4.12: Cation transport paths in (a) Uniformly crown ether loaded Cs-Naf-CR_h membrane and (b) Ion gated Cs-H-Naf-CR membrane.

4.3.2. 2. Ion Gated membrane (Cs-H-Naf-CR)

Transport experiments have been carried out with the membrane having one of the surface layers ($\sim 25 \mu\text{m}$) loaded with DB21C7 templated Cs^+ . It is based on the conjecture, that a very thin selective layer, inspite of having high barrier for transport, may allow only Cs^+ to pass through, leading to Cs^+ ion gated membrane.

The results of the experiments carried out using different feed compositions are given in table 4.6. The different experiments carried out are identified with the corresponding experiment numbers in this table. The higher enrichment factor ($\epsilon > 1$) in this table indicates higher selectivity in transport of Cs^+ over Na^+ to the receiver side. The errors shown on the enrichment factors are the corresponding absolute errors on the measured data and have been calculated from the radioactivity counting statistics.

Table 4.6: The details of the two compartment transport experiments carried out at 4V along with corresponding enrichment factor of Cs^+ over Na^+ and Permeability coefficient of Cs^+ .

Experiment No	Feed Composition (milimoles)		Membrane	Enrichment Factor (ϵ)	Permeability Coefficient of Cs^+ (cm/ s)
	Cs^+	Na^+			
1	5	5	Cs-Naf	1.0 ± 0.1	4.2×10^{-5}
2	5	5	Cs-Naf-CR _h (N=0.36)	1.0 ± 0.1	4.7×10^{-5}
3	5	5	Cs-H-Naf-CR	4.5 ± 0.1	2.0×10^{-5}
4	2	8	Cs-H-Naf-CR	4.3 ± 0.1	2.7×10^{-5}
5	0.0084	12	Cs-H-Naf-CR	2.3 ± 0.1	-

The cation transport profiles for different feed compositions are shown in figure 4.13. With Cs^+ form of Nafion-117 membrane (Cs-Naf), after 7 h 24% Cs^+ and 23% Na^+ has been transported to the receiver side without any enrichment ($\epsilon=1.0$). For the experiments with Cs-H-Naf-CR (exp 3 and exp 4), at the same time scale (7 h), the percentage Cs^+/Na^+ transported are 3 / 0.6 and 5.5/ 1.6 respectively, which shows the effect of crown ether on the cationic mobility. The percentages, as shown in figure 4.12, are with respect to the initial amount of cations in the feed side which are available for transport. Along with a volume reduction factor of 10, the observed enrichment factor of Cs^+ over Na^+ for third and fourth experiment are 4.5 ± 0.1 and 4.3 ± 0.1 respectively. The results indicate that, ion gating of the membrane with crown ether has imparted enhanced selectivity over pure Nafion-117 and enhanced transport rate over fully crown ether loaded membrane. It is also to be noted that, in the present set of experiments, as the cation transport is not solely driven by the concentration gradient due to presence of electric field, so more than 50% transport, as seen from figure 4.13 (92% in 3rd experiment), has therefore been observed.

The results of the transport experiment (exp 5) carried out for simulated effluent solution of Resorcinol Formaldehyde Polycondensate Resin (RFPR) [Banerjee et al. 2013] is also shown in table 4.6. It can be seen from the data that here also an enrichment factor of 2.3 ± 0.1 has been observed for Cs^+ over Na^+ . This indicates that the selective transport of Cs^+ in this ion gated membrane is possible inspite of such a high ($\text{Cs}^+:\text{Na}^+= 1:1428$) Na^+ concentration in aqueous solution.

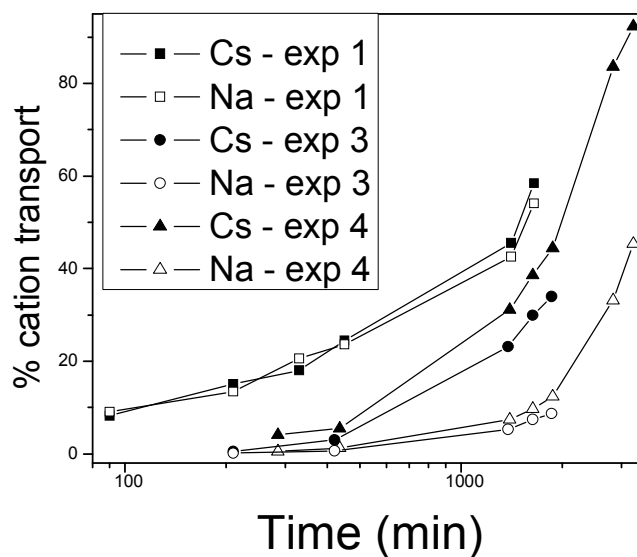


Figure 4.13: Cation (Cs^+ / Na^+) transport profiles under different experimental conditions.

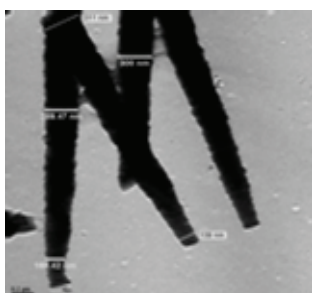
4.4. Conclusion

The mobility of ions (Cs^+ / Na^+) and water is found to reduce drastically in Cs-Naf-CR1/CR2 and Na-Naf-CR1 compared to corresponding cationic form of pure Nafion-117. The temperature dependence of isotopic exchange of Cs^+ and Na^+ ion in Cs-Naf-CR1/CR2 and Na-Naf-CR1 respectively shows that there is a significant increase in the exchange rate with rise in temperature. The activation energies for diffusion of Cs^+ and water in Cs-Naf-CR1 are comparable and are much higher than that in case of pure Nafion. On account of the higher affinity of DB21C7 for Cs^+ than that of DB18C6, the activation barrier for Cs^+ diffusion in Cs-Naf-CR2 is higher than that of Cs-Naf-CR1. This high value of activation barrier is comparable to that of ionic diffusion in ionic crystal lattice. Loading of crown ether in Nafion-117 enhances the hydrophobicity of the membrane matrix, thereby reducing the water uptake in the membranes. The DSC data shows disruption of water clusters in the membrane, and the attendant loss of plasticity, which lowers the SDCs.

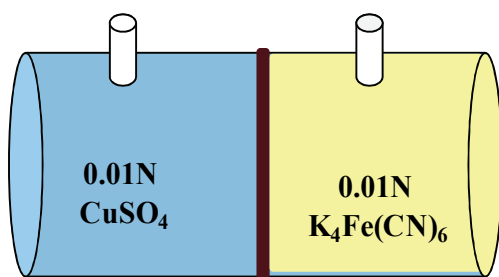
It is also inferred from the results that homogeneous loading of DB21C7 in the bulk of the membrane at different N (<1) enhance the cationic mobility with reduced selectivity. The problem of enhanced selectivity at the cost of mobility has been successfully overcome by confinement of the templating (with crown ether) only at the surface ion exchange sites. In this ion gated membrane, the combined effect of selectivity due to the templating effect of the surface screening layer and the significant mobility of the cation in the bulk under applied electric potential results in selective and quantitative transport of Cs^+ over Na^+ at practical time scale. Further enhancement in transport selectivity is expected with more selective crown ether or calix crown ligand and subsequent tuning of the screening layer thickness.

Chapter 5

Copper Ferrocyanide Loaded Track Etched Membrane: an Effective Cs^+ Removal Medium



**Copper Ferrocyanide
Crystals within the pores
of Track Etched
Membrane**



5.1 Introduction

Irradiation of polycarbonate films with heavy ions and its subsequent chemical etching produces track etched membranes (PTEM) with homogeneously distributed microporous structures. The use of PTEMs for synthesis of different nanostructures is well established. The acid resistant hydrophobic surface of the membrane helps in incorporation of precursor solutions by simple capillary force into the confined spaces without any surface modifications [Suzuki et al. 2010]. The PTEMs acts as a better template than porous anodic alumina membranes for general synthesis of mesoporous metal oxide fibres with various compositions. Suzuki and co-workers as well as Duan and co-workers [Suzuki et al. 2010, Duan et al. 2009] have used these PTEMs as a template for synthesis of copper nanowire arrays. Leo et al [Leo et al. 2007] have reported the synthesis of nanowires or nanotubes of gold by electroless deposition of gold in PTEMs. These membranes have also been used for the synthesis of mesostructured silica and titania rods [Suzuki et al. 2010, Suzuki and Yamauchi 2010]. The possibility of using these different nanostructures embedded PTEMs for selective transport of different metal ions has not been explored yet. Inorganic compounds, which are very selective for a particular metal ion, if grown properly within the pores of the PTEMs, can also be used as an ion selective electrode.

Most of the transition metal (Fe, Ni, Cu, Zn) ferrocyanides are known to be excellent adsorber of Cs^+ , where the adsorption property increases with the ferrocyanides series: $\text{Fe} < \text{Cu} < \text{Zn} < \text{Ni} < \text{Co}$ [Clarke and Wai 1998, Haas 1993, Ismail et al. 1999, Valentini et al. 1972, Pekarek and Vesely 1972]. Though ion exchange mechanism has been proposed for Cs absorption in these compounds, but it is reported that the mechanism is dependent on both the composition and the physical properties of the ferrocyanide solids. It can be a relatively fast ion exchange method or a slower change in chemical structure. In most of the cases,

intermediate rates and mixed mechanisms are often observed [Haas 1993]. It is also reported that copper and cobalt ferrocyanides are resistant to γ -radiation [Pekarek and Vesely 1972].

Practical application of the ferrocyanides for removal of cesium requires suitable chemical and physical stability as well as properties that allow an efficient and very complete separation of solids from the solution [Haas 1993]. Since most of these metal ferrocyanides are available as fine powders, it is difficult to use them for radionuclide separation from aqueous solution by filtration process. Also, low permeability limits their use in column based separation methods [Clarke and Wai 1998]. In order to avoid these associated problems, several attempts have been made to immobilize these compounds on suitable solid supports like, silica granules [Gaur 1996], chelating organic ion exchangers [Clarke and Wai 1998], polyurethane foam [Rao et al. 1999, Rao et al. 2010], cartridge water filter [Hamilton et al. UCRL], polymer chain grafted fibers [Ishihara et al. 2011], nanoscale magnetite substrate [Sheha 2012], mesoporous silica [Sangvanich et al. 2010], latex particles [Avramenko et al. 2011], biopolymer foams [Vincent et al. 2014] etc. Clarke and Wai [Clarke and Wai 1998] have reported 98% removal of cesium from a simulated acid waste solution by immobilizing copper ferrocyanide (KCFCN) on a chelating resin (Chelex - 20). Valsala et al [Valsala et al. 2009(a), Valsala et al. 2009(b)] immobilized cobalt ferrocyanides on organic ion exchangers for removal of ^{137}Cs from low level liquid radioactive waste. Rao et al [Rao et al. 1999, Rao et al. 2010] has applied KCFCN-polyurethane foam for Cs removal from low level radioactive waste. The overall volume reduction factors in this process are reported to be ~ 4000 . Use of such matrices involves filtration of large volume liquid radioactive wastes and generation of voluminous secondary waste. In another attempt Chen et al. [Chen et al. 2013], have reported use of nanoparticle film of copper hexacyanoferrate for electrochemical separation of cesium from waste water. Recently, ion exchange membranes have been used as selective sorbent for preconcentration of different

metal ions from larger volume of solution [Das et al. 2009, Das et al. 2012, Saito et al. 1987]. In this context, immobilization of metal ferrocyanides on some suitable polymeric membrane, like polycarbonate track etched membrane can be a promising alternative radio cesium preconcentration matrix.

With this in view, in the present work, an attempt has been made to grow copper ferrocyanide (CFCN) crystals within the pores of a PTEM and this composite membrane has been used for preconcentration and selective transport of Cs^+ . Among all the metal ferrocyanides, the copper analogus has been chosen as it is reported in literature that the composition of copper ferrocyanide product does not vary with change in mole ratios of the reactants [Haas 1993]. KCFCN is also reported to offer better mechanical characteristics and more radiation stability as compared to others [Haas 1993]. Highest sorption capacities have been reported in literature for copper and zinc ferrocyanides [Haas 1993]. In this chapter, the three different aspects of the work have been described in the following sections i) Synthesis of nanosized copper ferrocyanide crystals within the pores of PTEM and use of this composite membrane for ii) Selective transport of Cs^+ as well as iii) Preconcentration of Cs^+ .

5.2. Synthesis of CFCN loaded PTEM (CFCNm)

In the present work, nanosized CFCN crystals have been synthesized within the pores of PTEM. The characterization of the CFCNm has been carried out using X-ray Diffraction (XRD), Small Angle X-ray Scattering (SAXS), Energy Dispersive X-ray Fluorescence (EDXRF) and Transmission Electron Microscopy (TEM) techniques.

5.2.1. Experimental

The CFCN crystals were grown in the pores of the PTEM by permeation method. For the growth of the crystals, the PTEM was exposed to copper sulphate solution (0.01 M) from one side and potassium ferrocyanide solution (0.01 M) from other side in two compartments

permeation cell without stirring for 4 days under ambient conditions. In order to ensure uniform growth of the crystal within the pores, the solutions in each compartment were replaced on alternate days. After 4 days, the partially loaded membrane was taken out and annealed at 40 °C temperature for 2 h. The annealed membrane was again kept in two compartment cell for further growth of the crystal for 4 days. The details of the characterization techniques are described in chapter 2 of this thesis.

5.2.2. Results and Discussions

The XRD pattern (figure 5.1) of the CFCNm shows the presence of 3 major peaks of $\text{Cu}[\text{Fe}(\text{CN})_6]$ with slight broadening, which indicates presence of nano-sized particles. This has been supported by the SAXS study. Figure 5.2 shows the SAXS profile of the membrane sample displayed on log-log scale. In the high-Q region, $I(Q)$ varies as a power-law Q^{-4} suggesting smooth surfaces for the scattering particles. The data has been fitted to the Debye function [Debye 1957, Emmerling 1995] $I(Q) = I(0)/[1 + (\xi Q)^2]^{-2}$ where, ξ is the correlation length which is proportional to average radius of the particles. From the fitting of SAXS data, the value of average radius for the filler ferrocyanide particles is found to be about 40 nm.

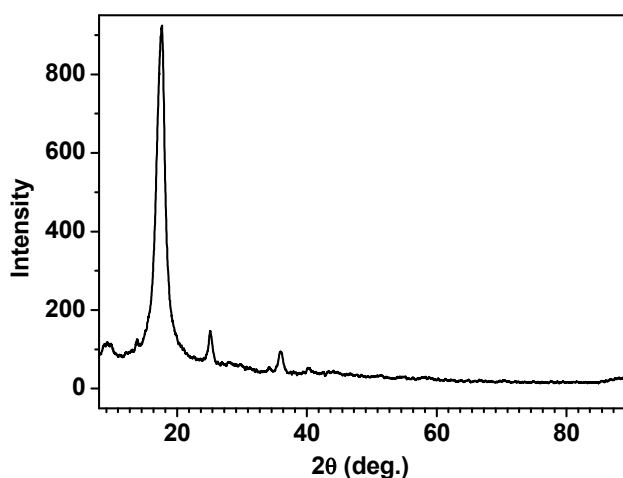


Figure 5.1: XRD pattern of CFCNm.

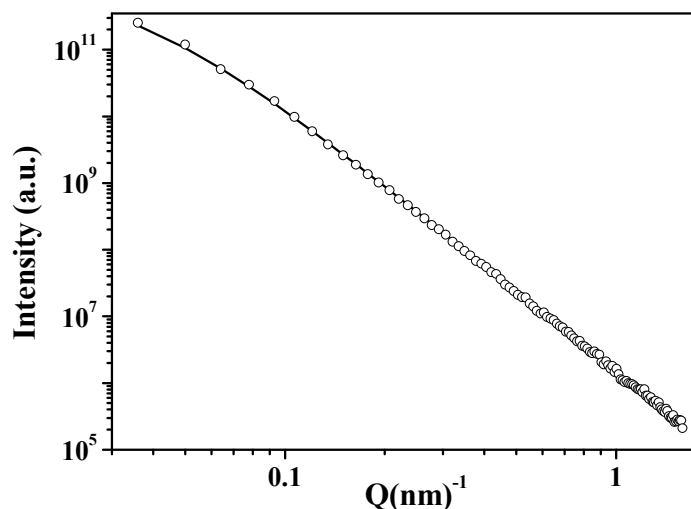


Figure 5.2: SAXS profile of CFCNm. Symbols are observed, line is fit to the data.

Although for the CFCN compound, the XRD pattern show presence of only $\text{Cu}[\text{Fe}(\text{CN})_6]$, the EDXRF data indicates presence of K^+ ion in the membrane, as has been previously reported in literature [Clarke and Wai 1998]. Thus a mixed potassium copper ferrocyanide composition has been assumed, represented as KCFCN in this work. The PTEM loaded with this compound is subsequently referred as KCFCNm in the present work.

The TEM images of the KCFCN loaded membranes are shown in figure 5.3. It can be seen from the figure that the conical shaped pores of the PTEM are almost uniformly filled with KCFCN crystals. The dimension (~ 300 nm dia at surface ~ 140 nm dia inside) of the conical KCFCN rods matched well with the supplier given dimension of pores (~ 200 nm) of the PTEM. These rod like structures as shown in the TEM images are made up of nanosized KCFCN crystals (~ 40 nm) as has been observed from the SAXS analysis.

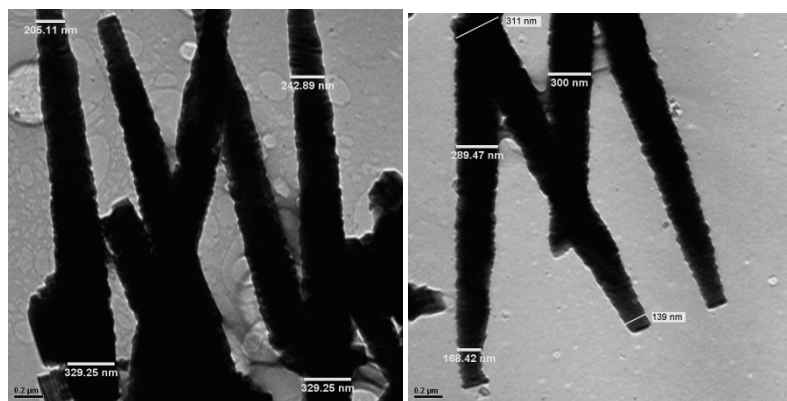


Figure 5.3: Transmission Electron Microscopy images of KCFCN loaded PTM.

5.3. Selective transport of Cs^+

In this work, the composite membrane (KCFCNm) have been used to study the electro-driven selective transport of Cs^+ ions over Na^+ ions, from nitric acid medium. In order to understand the mechanism of cation transport through CFCNm, water transport study has also been carried out and subsequently an attempt has been made to explain the differential transport behavior of Cs^+ over Na^+ . Electrodriven cation transport behavior of a Nafion-CFCNm (Naf-CFCNm) composite system for different relative Cs^+ to Na^+ concentration ratio has also been studied and the results explained.

5.3.1. Experimental

In order to study the selective transport of Cs^+ over Na^+ , two compartment permeation experiments were carried out at room temperature with the feed solution as a mixture of NaNO_3 (1 meq), CsCl (0.05 meq) and HNO_3 (pH=2). The receiver compartment was filled with HNO_3 (pH=2) and the feed solution was tagged with ^{22}Na and ^{137}Cs tracer. The solutions in both the compartments were stirred continuously in order to avoid any film controlled diffusion at the membrane interface. Amount of Na^+ and Cs^+ transferred from feed to receiver

side were monitored by taking out 200 μL of aliquots from both the compartments at regular time intervals and counting the ^{22}Na and ^{137}Cs activity in NaI(Tl) counter for same period of time.

In order to study the effect of applied electric field on the cation transport rate, a potential of 3 V was applied across the membrane using two Pt electrodes, other conditions remaining unchanged. For most of the transport experiments, a Nafion-1135 membrane sample in H^+ form coupled to a KCFCNm was used. A schematic diagram of the experimental arrangement is shown in figure 5.4.

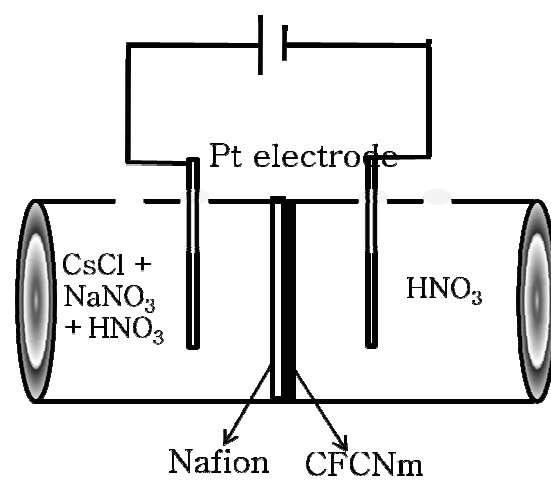


Figure 5.4: Experimental arrangement for transport studies under applied electric field.

In order to study the effect of Cs^+ concentration on the transport properties of the Naf-KCFCNm, experiments with three different ratios (1:20, 1:1 and 10:1) of Cs^+ and Na^+ in feed solution was carried out keeping the HNO_3 concentration ($\text{pH}=2$) fixed in both compartments.

The extent of physical blockage of the pores of the PTEM by KCFCN was studied by water transport measurement using ^3H radiotracer. The transport study was carried out for blank

PTEM and KCFCNm with ^3H labeled water in feed compartment and deionized water in the receiver compartment. The rate of water transport from feed to receiver compartment was monitored by taking out 50 μL of aliquots from both the compartments at regular time intervals and counting ^3H activity by liquid scintillation counting for same period of time. The details of the liquid scintillation counting are given in chapter 2.

The intrinsic selectivity of the KCFCNm was studied by radiotracer absorption method. For this the membrane was kept in a solution containing a mixture of NaNO_3 and CsCl with continuous stirring for ~ 4 h. The solution is tagged with ^{22}Na and ^{137}Cs tracer. The amount of Cs^+ or Na^+ absorbed in the membrane was calculated by measuring the corresponding radiotracer uptake.

5.3.2. Results and Discussions

Table 5.1: Experimental details along with percentage cation transport after ~ 7 h and corresponding enrichment factor of Cs^+ over Na^+ .

Exp No	Potential (V)	Feed Composition	Membrane	% Cation transport after ~ 7 h		ϵ
				Cs^+	Na^+	
1	0	$(\text{Cs}^+ : \text{Na}^+ = 1:20) + \text{HNO}_3(\text{pH}=2)$	KCFCNm	14 ± 0.3	7 ± 0.8	2.1 ± 0.2
2	3	$(\text{Cs}^+ : \text{Na}^+ = 1:20) + \text{HNO}_3(\text{pH}=2)$	KCFCNm	38 ± 0.5	22 ± 1.3	1.8 ± 0.1
3	3	$(\text{Cs}^+ : \text{Na}^+ = 1:20) + \text{HNO}_3(\text{pH}=2)$	Naf-KCFCNm	27 ± 0.2	14 ± 0.2	2.1 ± 0.1
4	3	$(\text{Cs}^+ : \text{Na}^+ = 1:20) + \text{HNO}_3(\text{pH}=2)$	Naf-PTEM	$*15 \pm 0.3$	$*16 \pm 0.5$	-
5	3	$(\text{Cs}^+ : \text{Na}^+ = 1:1) + \text{HNO}_3(\text{pH}=2)$	Naf-KCFCNm	27 ± 0.4	18 ± 0.5	1.6 ± 0.1
6	3	$(\text{Cs}^+ : \text{Na}^+ = 10:1) + \text{HNO}_3(\text{pH}=2)$	Naf-KCFCNm	11 ± 0.3	9 ± 0.4	1.2 ± 0.1

*After ~ 5 h

The cation transport (%) under different experimental conditions and the corresponding observed enrichment factor (ϵ) of Cs^+ over Na^+ in receiver side solution along with the experimental details are given in table 5.1. The different experiments carried out are identified with the corresponding experiment numbers in this table. The errors shown in the table are the corresponding absolute errors on the measured data and are calculated from the radioactivity counting statistics. The comparison of cation transport profiles of KCFCNm under different experimental conditions with HNO_3 (pH=2) in both compartments and 1:20 Cs^+ to Na^+ ratio in feed compartment initially is also shown in figure 5.5. As can be seen from the figure and the table, without any applied potential (exp no. 1), no appreciable cation (Cs^+/Na^+) transport to the receiver compartment is observed for very long time. After ~ 7 h, only $\sim 14\%$ Cs^+ and $\sim 7\%$ Na^+ has been transported to the receiver side with a corresponding enrichment factor of ~ 2.12 . The percentages quoted in table 5.1 are with respect to the initial amount of cations in feed side which are available for transport. On application of electric potential (3 V) across the KCFCNm (exp no. 2), the corresponding percentage cation transport increased. Figure 5.5 shows that, after ~ 7 h, $\sim 38\%$ Cs^+ and $\sim 22\%$ Na^+ has been transported to the receiver side with a corresponding enrichment factor of 1.80. The reason for this increased transport rate has been described in chapter 1.

Figure 5.6 shows the comparison of water transport profiles of PTEM and KCFCNm. It can be seen from this figure that the water transport rate is faster in PTEM as compared to KCFCNm. Slower rate of water transport in the case of KCFCNm indicates physical blocking of the pores of the PTEM by KCFCN. However, the transport of water through this membrane indicates that water channels still exist in the KCFCNm. It can be assumed that the conical shaped rods (as seen in figure 5.3), which are an agglomerate of nanosized KCFCN crystals are porous and allows water to pass through.

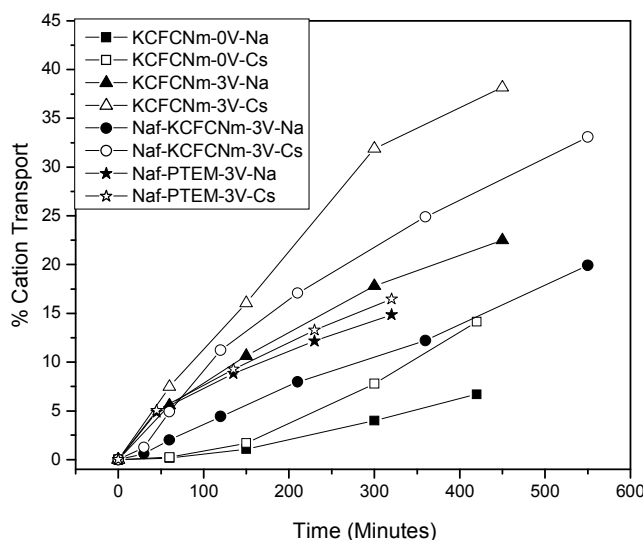


Figure 5.5: Comparison of cation transport profiles under different experimental conditions with HNO_3 ($\text{pH}=2$) in both compartments and 1:20 Cs^+ to Na^+ ratio in feed compartment initially.

In absence of electric field, cation transport from feed to receiver side can occur either by direct salt transport (as NaNO_3 or CsCl) or by ion exchange [M^+ (feed) \rightleftharpoons H^+ (receiver)] process, where f and r refers to feed and receiver compartments respectively. The salt transport can occur only through the water channels within the pores of the membrane and is not expected to give any selectivity in the transport of Cs^+ over Na^+ . Again, simple ion exchange through the water channels in the membrane would not render any selectivity to the process unless KCFCN is involved in the process. Assuming that the transport through solid KCFCN matrix would involve diffusion through ionic crystals, the rate of diffusion will be extremely slow. The radiotracer absorption study has also shown that only Cs^+ is absorbed by the KCFCN crystal. Moreover, the number of miliequivalence (meq) of KCFCN present in the membrane as calculated (0.037 meq) from the difference in dry weight of the membrane before and after loading of the compound was much higher than that (~ 0.02 meq) calculated

from radiotracer (^{137}Cs) absorption. It indicates that only the surface ion exchange sites of the solid (KCFCN) within the pores of the PTEM are available for ion exchange. In the water channels within the membrane, the Cs^+ to Na^+ concentration ratio is higher than that in the feed solution and the corresponding higher rate of Cs^+ (feed) $\rightleftharpoons \text{H}^+$ (receiver) ion exchange gives rise to the observed enrichment in the receiver compartment.

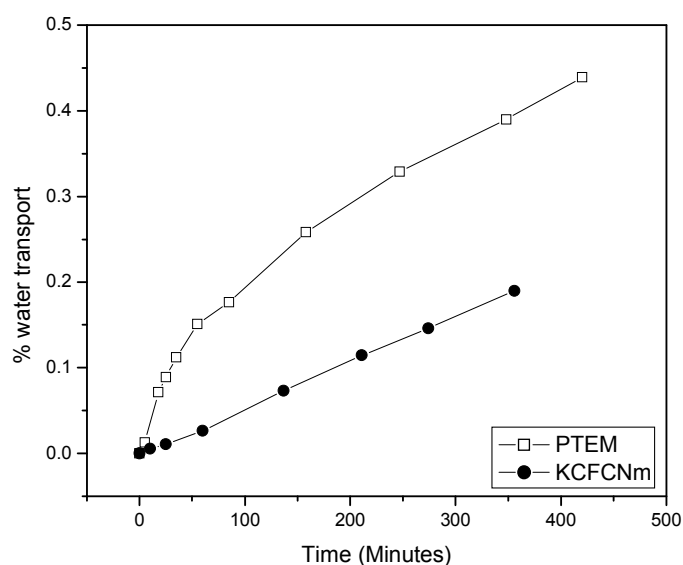


Figure 5.6: Comparison of water transport profiles of blank PTEM and KCFCNm.

On application of electric field, the anion is discharged at the anode and H^+ is discharged at the cathode with the corresponding current carried by the transport of cations from the feed to the receiver compartment. Since this process is not limited by ion exchange, complete cation transport from feed to receiver is possible theoretically. Now this process being current driven, gives enhanced cation transport rate compared to the concentration driven process. In this case also, the higher concentration ratio of Cs^+ to Na^+ inside the membrane aqueous phase as compared to the outside feed solution leads to enriched transport of Cs^+ over Na^+ .

Application of electric field enhanced the membrane degradation due to oxidation of ferrous to ferric in KCFCN crystals as evidenced by a visible color change of the membrane from reddish brown to a yellowish brown [Clarke and Wai 1998] with the progress of electrolysis. Assuming that anions are responsible for early degradation of KCFCN, a cation exchange membrane (Nafion-1135) at the feed side interface was used which will allow only the cations to pass through, preventing the movement of anions. The cation transport profile obtained for Naf-KCFCN (exp no. 3) composite membrane system at 3 V potential, as shown in figure 5.5, indicates an increased percentage cation transport than that with KCFCNm without any applied potential (exp no. 1) but a slower rate than the KCFCNm at 3 V applied potential (exp no. 2). Figure 5.5 shows that, after ~7 h, ~27% Cs^+ and ~14% Na^+ has been transported to the receiver side for this composite system. It can also be seen from table 5.1 that in this case the corresponding observed enrichment factor is 2.04.

When the transport experiment (exp no. 4) was carried out with Naf-PTEM system at 3 V applied potential, as can be seen from figure 5.5, the transport rates of Cs^+ or Na^+ were comparable. Comparing the transport profiles of exp no 3 and 4, it can be seen that, with Naf-KCFCNm, Na^+ transport decreases but Cs^+ transport increases than those with Naf-PTEM. These observations reconfirm what has been proposed earlier. It becomes obvious that KCFCN is playing the main role in enriched transport of Cs^+ from the feed to the receiver compartment. For the experiment with PTEM (in absence of KCFCN), inside the membrane, C_{Cs} and C_{Na} are same resulting in almost same percentage transport rate (no selectivity) of Cs^+ and Na^+ ions.

The cation transport profiles obtained for varying Cs^+ and Na^+ ratio and Naf-KCFCNm at 3 V potential with HNO_3 (pH=2) in both compartment are shown in figure 5.7. The figure indicates that as Cs^+ concentration relative to Na^+ is increased in the feed side, Cs^+ transport decreases significantly. The data in table 5.1 indicates that increase in Cs^+ amount in feed

side also affected the enrichment factor. The ε value decreased from 2.04 to 1.60 to 1.23 as Cs^+ to Na^+ concentration ratio changed from 1:20 to 1:1 to 10:1. This behavior can be explained by the fact that the available ion exchange capacity of the membrane being ~ 0.02 meq, is much less than the amount of Cs^+ to be transported. For this, the Cs^+ flux is limited by the ion exchange capacity of the membrane. As a result, the selective transport of Cs^+ over Na^+ is more and more affected as the amount of Cs^+ in the feed side changes from 0.05 meq to 0.5 meq to 1 meq. This explains the reduced percentage transport rate of Cs^+ with increased Cs^+ amount in feed side. As Na^+ ions are being transported through the available water channels, so the Na^+ transport rate is not affected. It changed from 12% to 17% to 9% as amount of Cs^+ in the feed side changes from 0.05 meq to 0.5 meq to 1 meq.

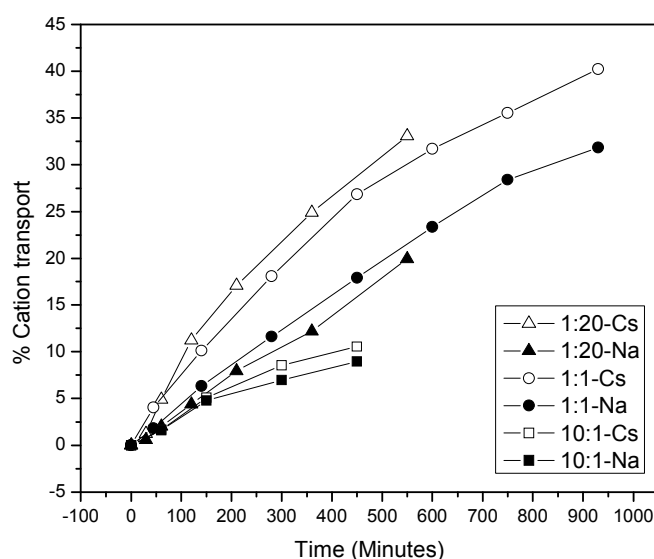


Figure 5.7: Effect of varying Cs^+ conc. on the cation transport profiles for Naf-KCFCNm composite at 3 V potential with HNO_3 (pH=2) in both compartment. # The ratios indicate the ratios of Cs^+ and Na^+ in feed side at the starting of experiment

5.4. Preconcentration of Cs^+

The aim of the present work is to systematically study the KCFCN loaded track etched membrane (KCFCNm) as sorbent for removal of Cs^+ from neutral aqueous solution. The membrane has been characterized for ion exchange capacity and Cs^+ exchange kinetics. The later has been done by the measurement of self-diffusion coefficient of Cs^+ in the KCFCNm. The efficiency of the membrane for ^{137}Cs removal from different volume of solution have also been studied. The composite membrane has been used to remove Cs^+ from a simulated nuclear waste (SNW) solution, whose chemical and radionuclide composition has been found out by Inductively Coupled Plasma-Atomic Emission Spectrometry (ICP-AES) and gamma ray spectrometry. The uptake kinetics and the decontamination from other radionuclides have also been studied. The possibility of using the membrane as effective sorbent for Cs^+ removal from large volume of solution has been discussed.

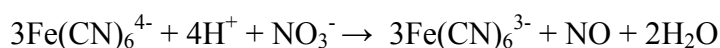
5.4.1. Experimental

5.4.1.1. Measurement of Ion Exchange capacity, SDC and uptake kinetics

The ion exchange capacity and the self diffusion coefficient of Cs^+ in this membrane were measured by standard radiotracer method as described in chapter 2. In order to study the ^{137}Cs removal efficacy, required amount of standardized activity was added to the measured volume of deionised water. A 1 cm X 2 cm KCFCNm piece was dipped into the solution, which was continuously stirred to avoid film controlled diffusion. The ^{137}Cs activity level in the solution was monitored by aliquoting a fixed volume of solution after regular time interval and counting in NaI(Tl) counter. In the case of solution with very low amount of added radioactivity (< 1000 Bq), the membrane sample was counted after regular time interval to avoid long counting time. The measurements were repeated 5 times for 15 ml solutions and twice for 1000 ml solution.

5.4.1.2. Treatment of Simulated Nuclear waste

The waste solution, as obtained, was found to be highly alkaline. It is reported in literature [Haas 1993] that the metal ferrocyanides are chemically stable over a pH range 1 - 12 and is decomposed beyond this pH range. This is due to the chemical reaction [Haas 1993]



Clarke and Wai [Clarke and Wai 1998] observed that all of the immobilized KCFCN is decomposed from the chelating resin in 4 M LiOH solution. The Cs removal efficiency by KCFCN is known to be best in the pH range of 7 to 10 [Haas 1993]. Thus, in the present work, the SNW solution has been neutralized with HNO_3 to pH 6-7. 400 ml of the waste solution has been treated by a 2 cm x 2 cm KCFCNm. The removal of ^{137}Cs by the membrane has been monitored by aliquoting 5 ml solution after regular time interval and counting in HPGe detector. The absolute activity at different gamma ray energies of the waste solution was determined by counting 5 ml of the initial solution in a HPGe detector. The efficiency of the detector at different energy was obtained by counting a standard 5 ml ^{152}Eu source at the same source to detector distance. The SNW was also characterized by atomic emission spectroscopy using Jobin–Yvon Ultima high resolution ICP-AES having practical resolution of 0.005 nm and has a continuous coverage of spectral range 200–800 nm.

5.4.2. Results and discussions

5.4.2.1. Self diffusion and ion exchange capacity

It is reported in literature that the composition of the ferrocyanide solids may influence the rates cesium sorption [Haas 1993] due to the differences in the removal mechanisms. In general, the Cs^+ sorption is rapid for $\text{K}^+ / \text{Na}^+ / \text{H}^+$ containing ferrocyanides as compared to $\text{M}_2\text{Fe}(\text{CN})_6$ [Haas 1993]. Due to the presence of K^+ in the synthesized ferrocyanides, a faster

rate of Cs^+ diffusion in KCFCNm is expected. The self diffusion profile of Cs^+ in KCFCNm, as shown in figure 5.8, supports this. The figure indicates that, within 100 min, 85% exchange of the cation into the membrane takes place. Sheha [Sheha 2012] have reported 80% sorption of Cs onto Zn hexacyanoferrate (II) magnetic nanocomposites within 2 h. Rao et al. [Rao et al. 2010], using copper ferrocyanide loaded composite ion exchange resin, have also reported 85% Cs removal in 200 min. The self diffusion coefficient for Cs^+ ion in this membrane at room temperature, as obtained from a fit of the experimental data as described in chapter 2, is $6.15 \times 10^{-8} \text{ cm}^2/\text{sec}$.

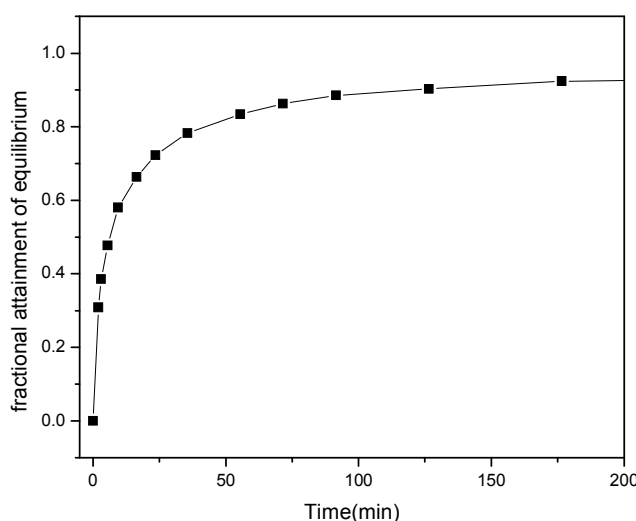


Figure 5.8: Self diffusion profile of Cs^+ in KCFCNm.

Using radiotracer absorption method, the ion exchange capacity of the KCFCNm has been found out to be 1.75 mmol/g. Thus a 1 cm X 2 cm KCFCNm piece can absorb ~15 mCi (specific activity 22 Ci/g) of ^{137}Cs activity. This indicates that only a very small membrane area is required to treat a very large amount of activity. The data given in table 5.2 indicates that this composite membrane has higher ion exchange capacity than most of the other literature reported composite ferrocyanide sorbents. The higher values of Cs^+ exchange capacity as observed by Sheha [Sheha 2012] and Vincent et al. [Vincent et al. 2014] have

been obtained using potassium-zinc hexacyanoferrate and potassium-nickel ferrocyanide respectively.

Table 5.2: Comparison of the different adsorption parameters of KCFCNm with other literature reported ferrocyanide sorbents.

Reference	Log K_d	Ion (Cs^+) exchange capacity (mmol/g)
Present work	5.6	1.75
4	4	1.3
11 ¹	4.4	-
14 ²	3.75	14.7
15 ³	5.04	0.13
16 ⁴	5.6	0.03
17 ⁵	-	1.8
18	4	-
19	3	-
20	4.8	-

¹at 0.1 mM, ²K-Zn-hexacyanoferrate for sample RZ2,
³pH=6.3, ⁴ at <25 g/L NaNO₃, ⁵Ni-K ferrocyanide

5.4.2.2. Removal of ¹³⁷Cs

The percentage ¹³⁷Cs absorption by a 1 cm X 2 cm KCFCNm piece from different volume of water, and the corresponding distribution coefficients (K_d) are given in table 5.3.

The distribution coefficients have been calculated as given by Clarke and Wai [Clarke and Wai 1998].

$$K_d = \frac{\text{activity of } ^{137}\text{Cs sorbed per g of adsorbent}}{\text{activity of residual } ^{137}\text{Cs in solution per mL}}$$

Table 5.3: Dilution effect on the activity removal efficacy of a 1 cm X 2 cm KCFCNm piece with logarithm of the corresponding distribution coefficients (K_d).

^{137}Cs Activity (Bq)	Solution volume (mL)	Contact time (h)	Percentage of ^{137}Cs activity removal	Log K_d
3.8×10^5	15	8	98	$5.3 \pm 0.005\%$
8000	15	8	99	$5.5 \pm 0.1\%$
8000	1000	20	81	$6.0 \pm 0.3\%$
800	1000	20	73	$6.0 \pm 0.8\%$

It is seen from the table that the membrane can efficiently (99 %) remove ^{137}Cs activity (even upto 3.8×10^5 Bq activity) from 15 ml water in 8 h. When the activity is distributed over a large volume, the percentage removal of activity reduces even with higher (~20 h) equilibration time. It is also to be noted that the membrane is able to remove Cs^+ even from a very dilute solution (800 Bq / L). A comparison of the $\log(K_d)$ of KCFCNm, obtained in the present work, with that of other literature reported transition metal ferrocyanide loaded composite sorbents have been given in table 5.2. In the present work, on an average, the value of $\log(K_d)$ has been found to be ~5.6, which is much higher than most of the other literature reported values. Avramenko et al. [Avramenko et al. 2011] have also reported a $\log(K_d)$ value of 5.6 for mixed potassium-copper ferrocyanide. The earlier results have shown negligible uptake of Na^+ in KCFCNm, i.e, the K_d of Na^+ in the membrane is very low. Thus the selectivity of Cs^+ with respect to Na^+ is very high in the composite membrane (KCFCNm).

5.4.2.3. Treatment of Simulated Nuclear waste

The elemental composition of the SNW, as obtained from AES and gamma ray spectroscopy, with corresponding concentration is shown in table 5.4. It is seen from the table that major element in the solution is Na. The radioactive isotopes which are present in the solution at a concentration more than the detection limit of gamma ray spectrometry are ^{137}Cs , ^{125}Sb and ^{106}Ru with corresponding activity concentration of $1.05 \times 10^4 \text{ Bq/L}$, $3.34 \times 10^4 \text{ Bq/L}$ and $2.11 \times 10^4 \text{ Bq/L}$ respectively.

Table 5.4: Elemental composition and corresponding concentration (C_M) of SNW as obtained from ICP-AES. Errors on all the data points are less than 2 %.

Metal ion	Na	Ca	Zn	Cr	Al	Mg	Fe	Cu	Ni	Cd	Co	B	Pb
C_M (mg/L)	19700	8	7	5	3	1.1	0.6	0.4	0.4	<.0.1	<.0.1	<.0.1	<.0.1

The gamma ray spectra of the 5 ml initial SNW solution and the solution after 3 h preconcentration are shown in figure 5.9a. For comparison purpose, both the spectra are normalized to the same counting time. Peaks seen at energies other than that of ^{137}Cs , ^{125}Sb and ^{106}Ru , are due to the background. For better clarity, the zoomed view of the spectra in the energy range 615- 675 keV are shown in figure 5.9b. After 3 h preconcentration, reduction in the peak area of only ^{137}Cs (662 keV) is obvious from this figure, indicating selective uptake of ^{137}Cs in the membrane. Figure 5.9c shows the spectra of the membrane after 3h of preconcentration which shows the peak of ^{137}Cs only, confirming the high degree of selectivity of the membrane.

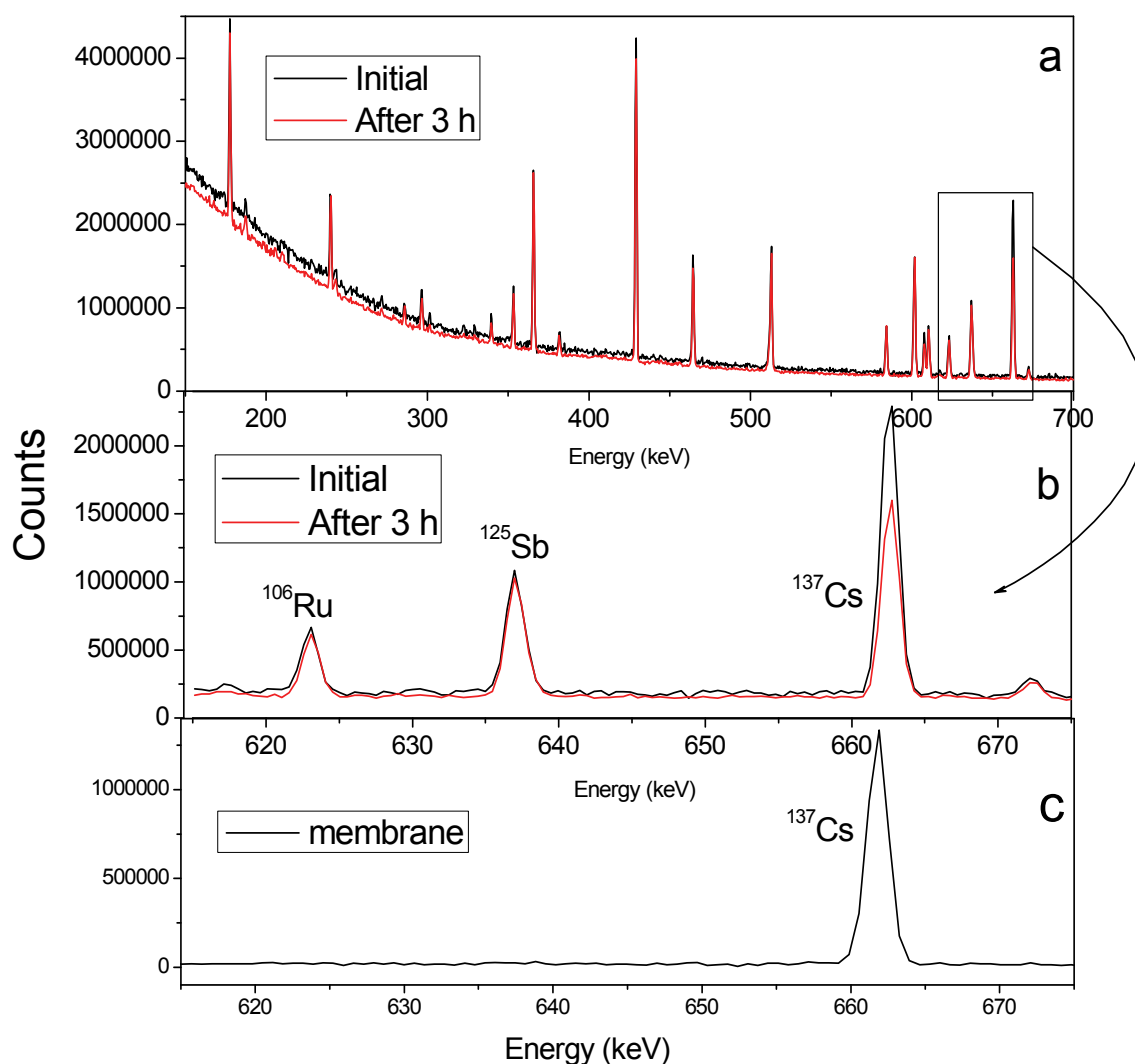


Fig. 5.9: Comparison of the gamma spectra (obtained using HPGe detector) of 5 ml radioactive waste solution, initial and after 3 h membrane pre-concentration (a) Full energy range (b) zoomed view of figure 3a) in the energy range of 615-675 keV. (c) Gamma spectra of KCFCNm after 3 h pre-concentration.

Table 5.5 shows the count rate of different radionuclides in the SNW at different time of equilibration with KCFCNm. It can be seen from the table that, there is continuous decrease in the ^{137}Cs cps with increasing pre-concentration time. There is a 33 % decrease (from 0.3 to 0.2) in the count rate at 662 keV after 3 h pre-concentration. The absorption rate of the ^{137}Cs decreases with increasing time and after 9 h equilibration, the count rate becomes 0.13.

During the process, no significant change in the count rates of ^{125}Sb and ^{106}Ru have been observed. Though the self diffusion profile of Cs^+ in the membrane shows a faster rate of absorption, the actual ^{137}Cs uptake rate from SNW is much slower. Lehto [Lehto and Harjula 1987] reported that the Cs absorption rates by ferrocyanides are much slower for concentrated (high alkali metal) solutions than for dilute solutions. It is also reported in the literature that the presence of large amount of Na in the solution interferes with the Cs ion exchange process with ferrocyanide. As seen in table 5.4, the SNW contains high amount of Na, which might have affected the uptake kinetics.

Table 5.5: Count rates of different nuclides as observed in the 5 ml radioactive waste solution acquired using a HPGe detector.

Energy (keV)	Nuclide	Background Cps	Solution (5 ml) Cps			
			Initial	After 3 h	After 6 h	After 9 h
176.3	^{125}Sb	-	0.2564	0.2522	0.2557	0.2538
238.6	^{232}Th	0.1220	-	-	-	-
352	^{232}Th	0.0731	-	-	-	-
364.5	^{131}I	0.2443	-	-	-	-
427.9	^{125}Sb	-	0.4899	0.4724	0.4704	.4723
463.4	^{125}Sb	-	0.1743	0.1700	0.1711	.1753
511.9	^{106}Ru	0.0574-	0.2371	0.2327	0.2318	0.2368
583.1	^{232}Th	0.0788	-	-	-	-
600.6	^{125}Sb	-	0.2114	0.2074	0.2074	0.2079
621.9	^{106}Ru	-	0.0790	0.0709	0.0706	0.0757
635.9	^{125}Sb	-	0.1376	0.1380	0.1351	0.1340
661.6	^{137}Cs	0.0562	0.3092	0.2023	0.1568	0.1345

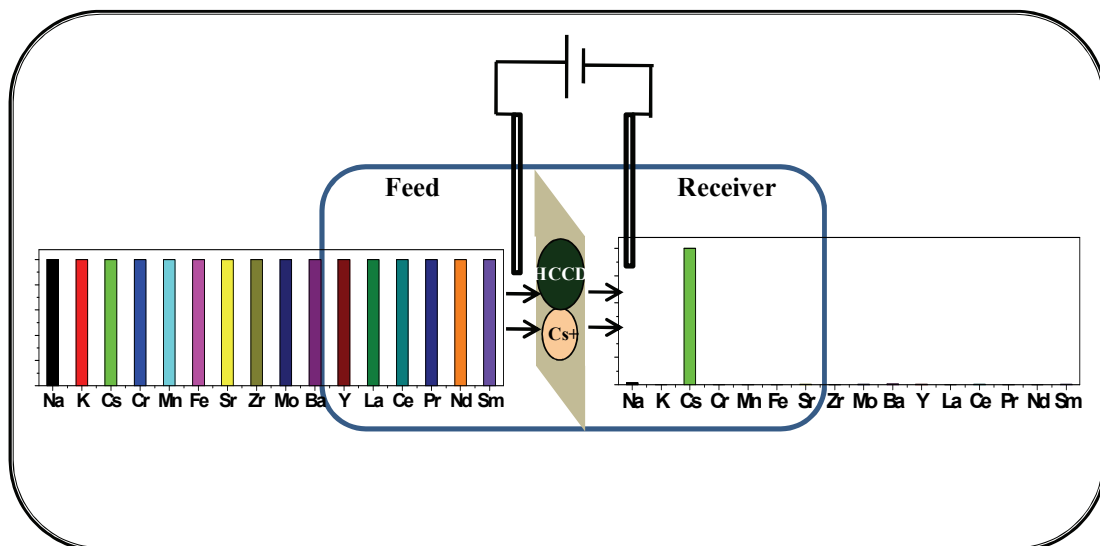
It is seen that the KCFCNm can be used as an efficient adsorbent for removal of radio cesium from the SNW, even in presence of large amount of Na. The advantage of this method lies in the fact that large volume of waste solutions or environmental solutions can be treated using this membrane and the generated low volume secondary waste is very easy to store in terms of disposal.

5.5. Conclusion

Two compartment permeation method using chemical reagents with comparable fluxes appear to be a very good method for synthesis of different inorganic compounds within the pores of PTEM. These different ions selective inorganic nano-structured materials loaded PTEMs can be used for separations of cations under applied electric field. It is to be mentioned that the efficiency of the separation process using this type of systems is limited by the ion exchange capacity and the stability of the compound. KCFCNm absorbs ^{137}Cs efficiently with high selectivity as shown by the equilibration uptake measurement from a SNW. The kinetics of Cs^+ absorption in this membrane is fast in absence of other metal ion but slows down in presence of high Na^+ concentration. For ^{137}Cs removal from radioactive solutions, this method is a promising alternative to commonly used precipitation method or immobilization of copper ferrocyanide in other suitable solid supports. Selective absorption and transport of other metal ions can also be tried with synthesis of suitable compounds.

Chapter 6

Selective transport of Cs^+ using a Polymer Inclusion Membrane of HCCD



6.1. Introduction

Use of different macrocyclic and macromolecular carrier based PIMs [Raut et al. 2012, Mohapatra et al. 2009, Levitskaia et al. 2002, Arena et al. 1998] or SLMs [Raut et al. 2008] for facilitated transport of Cs^+ are well reported in literature. Raut and co-workers [Raut et al. 2012] have studied recovery of Cs from acidic feed solution using calix[4]-bis-2,3-naphtho-crown-6 in PIM, while Mohapatra and co-workers [Mohapatra et al. 2009] have used di-benzo-21-crown-7 and di-tert-butylbenzo-18-crown-6 for selective Cs separation from nuclear waste solution. Arena et al [Arena et al. 1998] have reported selective transport of Cs^+ from high Na^+ background using a calixerene derivative in PIM. The major drawback associated with these ligands is the requirement of anion for charge compensation of the metal ion. Literature reports [Kimura et al. 1983, Sakamoto et al. 1986, Sata et al. 2000, Sata et al. 2001, Nemat-Nasser et al. 2006] are available where the charge compensation of the metal ions has been achieved by incorporating anionic functional groups either in the crown ether or in the polymer backbone of the membrane. As described in chapter 4, in order to make Cs^+ ion selective membranes, cation driven loading of crown ethers within Nafion-117 cation exchange membranes has been done. In this case, however, the Cs^+ selectivity (from crown ether) and anion for charge compensation ($-\text{SO}_3^-$ groups in Nafion) are provided by two different moieties.

CCD^- is one such anion, which itself is highly selective for Cs^+ and the two requirements, viz. charge compensation and selectivity can therefore be fulfilled by this single moiety. HCCD is also reported to display good stability towards radiation [Kyrns 1994]. The solvent extraction of Cs^+ using protonated form of CCD^- (HCCD) as extractant and trifluoromethylphenyl sulfone (FS-13) [Scott Herbst et al. 2008] or nitrobenzene [Murali et al. 2012] as the solvent is well reported in literature. Murali and co-workers [Murali et al. 2012] have studied the efficacy of HCCD for the extraction and recovery of Cs from

simulated high-level waste (SHLW) solutions using 20% nitrobenzene in xylene as the solvent. Scott Herbst and co-workers [Scott Herbst et al. 2008] have studied the solvent extraction of Cs^+ using HCCD in FS-13 and reported that the extraction of Cs by HCCD exclusively involves exchange of proton for cesium by formation of ion-paired CsCCD . Mohapatra et al. [Mohapatra et al. 2010] have reported the selective transport of cesium using HCCD in SLM and have reported a decontamination factor (DF, defined as the ratio of product to impurity in the product divided by that in the feed) of ~ 300 over different transition metal ions. One of the major disadvantage of this study is the requirement of 8-9 M HNO_3 for stripping. Moreover, most of these membrane based studies [Raut et al. 2012, Mohapatra et al. 2009, Levitskaia et al. 2002, Raut et al. 2008, Mohapatra et al. 2010] , except the work of Arena and co-workers [Arena et al. 1998] have not addressed the selective separation of Cs^+ from Na^+ ions from nuclear waste solution.

In general, the ionic carrier facilitated membrane based cation transports requires counter transport of another ion from receiver to feed phase to maintain electrical neutrality. This obviates the need of 8-9 M HNO_3 concentration in the receiver phase, as reported in literature [Mohapatra et al. 2010]. As discussed in chapter 1, it can be avoided if an electric field is applied across the membrane, so that the anion in the feed compartment is oxidized at the anode and the cation moves to the receiver phase without any counter transport. The use of electric field, thus, eliminates the need of adding salt or stripping agent in the receiver side along with the enhancement in the cation transport rate. As described in chapter 4 and chapter 5, the electrodriven Cs^+ transport through inorganic ion exchanger loaded track etched membrane and crown ether modified Nafion membrane has been shown. The DF for Cs^+ over Na^+ in the receiver phase in the two works have been reported to be ~ 2.0 and ~ 4.5 respectively. It is also to be mentioned that electro-driven transport is expected to be more

effective with ionic carriers like HCCD as compared to any other chelating or neutral macrocyclic ligands.

With this in view, in the present work, for the first time, HCCD has been used as a carrier in 2-nitro-phenyl-octyl ether (NPOE) plasticized cellulose tri acetate (CTA) / Poly Vinyl Chloride (PVC) based PIM. The present work describes the electro-driven transport studies of Cs^+ and Na^+ using these membranes, which includes the optimization of the working potential and determination of the current efficiency for the transport process. In view of the different possible compositions of the nuclear waste solutions, experiments have also been carried out for different feed compositions. The suitability of this membrane for selective removal of ^{137}Cs from a simulated nuclear waste solution has been studied. The membrane has been characterized to study its stability. PVC based PIM of HCCD has been used to demonstrate the transport selectivity of Cs^+ from a simulated high level nuclear waste (SHLW) solution containing 3 M HNO_3 . The uniqueness of the method in terms of cation transport rate vis-à-vis selectivity is discussed.

6.2. Experimental

6.2.1. Preparation of membrane

A mixture of 0.08 g cellulose triacetate (CTA), 5 mg HCCD and 0.2 mL NPOE was dissolved in dichloromethane and homogenized by sonication. The solution was poured into a flat petridish and allowed to evaporate at room temperature. The resulting PIM was peeled out by spreading few mL of water on it and subsequently used for the transport studies. The carrier concentration in the membrane matrix is limited by the solubility of HCCD in the plasticizer NPOE. In 0.2 mL NPOE, 5 mg (0.01 mmol) HCCD can be dissolved i.e the weight percentage of the carrier is 1.71. Increase in the amount of the NPOE resulted in over-plasticization of the membrane.

The PVC based membrane was prepared using 0.28 g PVC, 5 mg HCCD and 0.2 mL NPOE. 10 mL tetra hydro furan was used as the solvent for this preparation. Thickness of the membranes was measured using digimatic micrometer (Mitutoyo Corporation, Japan). The thickness of the synthesized CTA and PVC based membrane were 41 μm and 48 μm respectively.

6.2.2. Transport Studies with CTA based PIM

Electrodriven two compartment permeation experiments using CTA based membranes for different feed (32 mL) compositions were carried out. Electric field was applied across the membrane using two Pt electrodes and the current was monitored using a digital multimeter. The active surface area of the membrane was 1.77 cm^2 . Deionized water (3.2 mL) spiked with NaOH (0.004 mmol) was used in the receiver compartment. In order to achieve volume reduction in the receiver compartment, the volume ratio of feed to receiver compartment has been kept at 10. The solutions in both the compartments were stirred continuously to avoid any film controlled diffusion at the membrane interface. The cations (Na^+ / Cs^+) in the feed compartment were tagged with ^{22}Na and ^{137}Cs tracer. The amount of Na^+ and Cs^+ transferred from the feed to the receiver side was monitored by taking out 200 μL of aliquots from both the compartments at regular time intervals and counting the ^{22}Na and ^{137}Cs activity in high purity germanium (HPGe) detector.

In order to optimize the applied electric field, the permeation experiments were carried out at different applied potentials (1 V-7 V). A mixture (32 mL) of 0.0025 M NaCl and 0.0025 M CsCl (tagged with ^{22}Na and ^{137}Cs tracer) was used in the feed compartment. The cation transport was monitored by counting the radiotracers. For the rest of the experiments (at the optimized potential) involving CTA based membranes, described in the work, only feed compositions were varied and all other experimental conditions were kept same (as mentioned in previous section).

In order to study the transport selectivity at different neutral feed compositions, two compartment permeation experiments at the optimized potential were also carried out with varying proportions (1: 1 or 1:25) of Cs^+ and Na^+ in the feed. For these experiments the CsCl concentration (0.0025 M) was kept fixed and the NaCl concentration (0.0025 M / 0.0625 M) has been varied. In order to obtain the transport profiles of the cations (Na^+/Cs^+), they were tagged with their corresponding radiotracers in the feed compartment. Experiments were also carried out at 3V with either 0.0025 M NaCl or 0.0025 M CsCl in the feed compartment (other experimental conditions remaining same) and tagging the cation with respective radiotracers.

Transport experiment with the CTA based PIM was also carried out for a solution having the same Cs^+ to Na^+ ratio as that in the effluent solution (SRELW) of Resorcinol Formaldehyde Polycondensate Resin (Intermediate Level Nuclear Waste treated with RFPR) [Banerjee et al. 2013]. The feed composition was kept as 0.1 M NaNO_3 and 3.5×10^{-4} M CsNO_3 in 0.4 M HNO_3 , while the receiver compartment contained 3.2 mL deionized water spiked with NaOH (0.004 mmol). The transport rates of the cations (Cs^+/Na^+) were monitored by the same method as described in the previous section and the proton transport was monitored by acid-base titration method. In order to obtain the transport profile of salt and HNO_3 , the same experiment was repeated at zero applied potential. The salt transport was monitored by measuring the gamma activity of ^{137}Cs and ^{22}Na in the receiver compartment. The stability of the CTA based membrane was studied using UV-visible spectrophotometry.

6.2.3. Transport Studies with PVC based PIM

The transport selectivity of Cs^+ from a SHLW was studied at optimized potential using HCCD as carrier in a PVC based PIM. The composition of the SHLW, as obtained from inductively coupled plasma- atomic emission spectroscopic (ICP-AES) measurement, is

shown in table 6.1. The metal ions were present in 3 M HNO₃. It can be seen from the table that apart from cesium, the initial feed solution contains high amount of sodium, manganese, potassium and iron. For this study, a two compartment (each of 25 ml) glass cell with the membrane active surface area of 5.3 cm² was used. In this case, the receiver compartment contains 25 ml deionized water spiked with NaOH (0.004 mmol). The transport of the Cs⁺ ion was monitored using radiotracer technique, while the transport of other cations were monitored by atomic emission spectroscopy using Jobin–Yvon Ultima high resolution ICP-AES. The H⁺ transport was monitored by acid-base titration method.

Table 6.1: Elemental composition of the SHLW feed solution used for the transport study.

Element	Conc. (mg/ L)	Element	Conc. (mg/ L)
Cs	220	Mo	62
Na	4620	Ba	23
K	220	Y	60
Cr	112	La	168
Mn	480	Ce	55
Fe	690	Pr	76
Sr	28	Nd	92
Zr	84	Sm	45

6.3. Results and discussion

6.3.1. CTA based PIM for Cs^+ transport from low acidic/ neutral feed solution

The basic principle of electrodriven cation transport is shown in figure 1.10. In presence of Cl^- ion in the feed solution, the anodic reaction involves oxidation of Cl^- ($2\text{Cl}^- \rightarrow \text{Cl}_2 + 2\text{e}^-$) [Strathman 1990], whereas for the experiments with NO_3^- in the feed solution, water is oxidized ($2\text{H}_2\text{O} \rightarrow 4\text{H}^+ + \text{O}_2 + 4\text{e}^-$) at the anode in preference to NO_3^- at a potential greater than 1.48 V.

The Cs^+ transport profiles with the CTA based membrane for a fixed feed composition (0.0025 M NaCl + 0.0025 M CsCl) at different applied potentials are shown in figure 6.1. It can be seen from the figure that at 1 V, Cs^+ transport does not take place. This can be understood from the fact that oxidation of Cl^- at anode is required for the onset of transport process and the standard electrode potential for Cl^- oxidation is 1.36 V. At 2 V, transport of Cs^+ takes place at a very slow rate. The transport profiles at 3 V, 5 V and 7 V indicate that initially there is a continuous increase in the cation transport with increase in potential. However, no significant difference exists at higher percentage (~85 %) of cation transport. It is observed that the DF for Cs^+ over Na^+ is 51 at 3 V, which decreases to 24 at 5V. This indicates that, increase in potential has resulted in loss of selectivity while there is no significant gain in time for ~100% cation transport. Thus, the rest of the experiments were carried out at a working potential of 3 V.

The cation (Cs^+/Na^+) transport profiles (obtained using radiotracer technique) for CTA based PIM at 3 V for different Cs^+ to Na^+ ratio (1:1 or 1:25) in the neutral feed solution are shown in figure 6.2. The selectivity of the membrane for Cs^+ over Na^+ is indicated from the figure, where >90 % Cs^+ is transported within ~14 h, with negligible Na^+ transport (1.8 %) throughout the experiment., resulting in a DF of 51. The figure also shows that, the cation

transport rate is unaffected by the change in feed composition in this range. As shown in table 6.2, the DF for 1:1/ 1:25 $\text{Cs}^+ : \text{Na}^+$ feed compositions are obtained as 51 and 52 respectively.

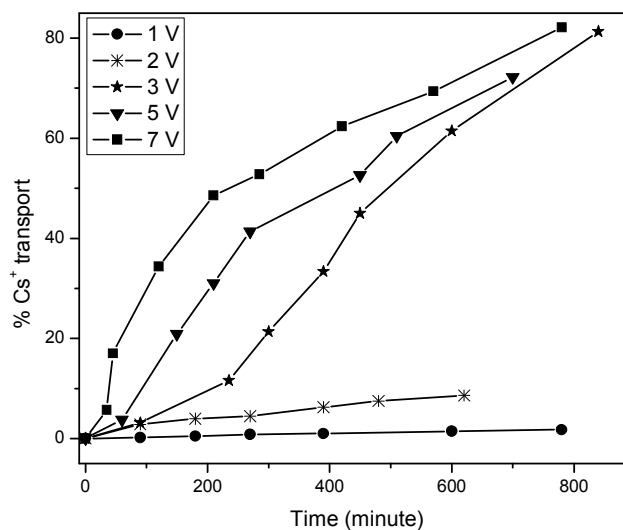


Figure 6.1: Cs^+ transport profiles obtained using CTA based PIM at different applied potential for the same feed composition of 0.0025 M NaCl + 0.0025 M CsCl.

Table 6.2: Decontamination factors (DF) of Cs^+ over Na^+ in electrodriven (3V) transport experiments using PIMs.

No	Base polymer	Feed Composition	DF (at >90% Cs transport)
I	CTA	Cs: Na= 1:1(Neutral)	51
II	CTA	Cs: Na= 1:25 (Neutral)	52
III	CTA	SRELW (0.4 M HNO_3)	410
IV	PVC	SHLW (3M HNO_3)	80

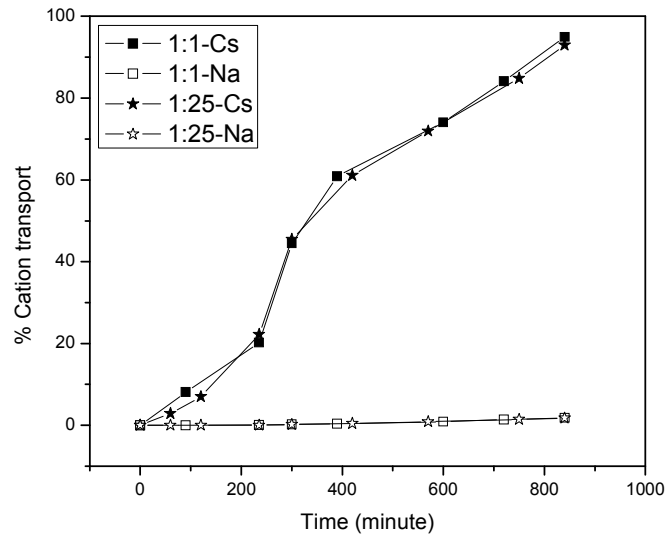


Figure 6.2: Cation (Cs^+ / Na^+) transport profiles obtained using CTA based PIM at 3 V for different Cs^+ to Na^+ ratio in the neutral feed solution. The ratios indicate the Cs^+ : Na^+ ratio in the initial feed solution.

In order to study the possibilities of loss of current due to any unwanted process, the current efficiencies was calculated by measuring the current along with the cation transport at different time intervals. The current profiles, obtained for CTA based PIM at 3 V for different neutral feed compositions are shown in figure 6.3. The current efficiency (I_{eff}) for different feed compositions have been calculated using the following equation and are given in table 6.3.

$$I_{\text{eff}} = \frac{\text{Total current carried by cation}}{\text{Integrated Current}} = \frac{m_c e N_A}{\int_0^t I(t) dt} \quad (6.1)$$

Where, m_c = moles of cation transported, $e=1.6 \times 10^{-19}$ Coulomb and N_A =Avogadro's number.

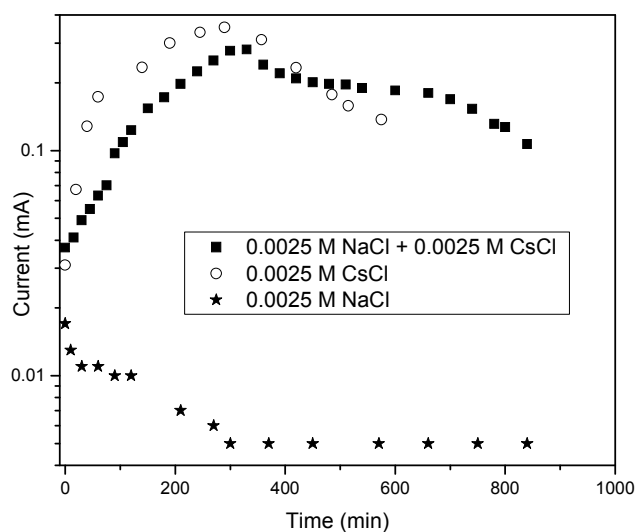


Figure 6.3: Current profiles obtained for CTA based PIM at 3 V for different neutral feed compositions.

As shown in the table, the current efficiency for Cs^+ (0.0025 M CsCl) and Na^+ (0.0025 M NaCl) in the feed compartment is obtained as 95% and 100% respectively. This indicates that cation transport alone can account for the integrated current. The current efficiency for Cs^+ transport from the feed containing 1:1 Cs^+ to Na^+ (0.0025 M NaCl + 0.0025 M CsCl) is obtained as 90%. Of the remaining, 1.8% is accounted for the Na^+ transport.

Table 6.3: Current efficiencies obtained using CTA based PIM at 3 V for different neutral feed compositions.

Feed composition	Current efficiency for cation transport at the end of transport process
0.0025 M NaCl + 0.0025 M CsCl	90%
0.0025 M NaCl	100%
0.0025 M CsCl	95%

The electrodriven selective transport of Cs^+ from SRELW has been attempted using the CTA based PIM of HCCD and the results are summarized in figure 6.4. The gamma spectra (for a fixed counting time) of the initial and final feed solution as well as final receiver solution are shown in figure 6.4 a, b and c, respectively. As seen in figure 6.4c, the quantitative transport of ^{137}Cs as well as the negligible transport of ^{22}Na in the receiver spectra indicates excellent selectivity for Cs^+ over Na^+ . The corresponding DF, as shown in table 6.2, is calculated to be 410.

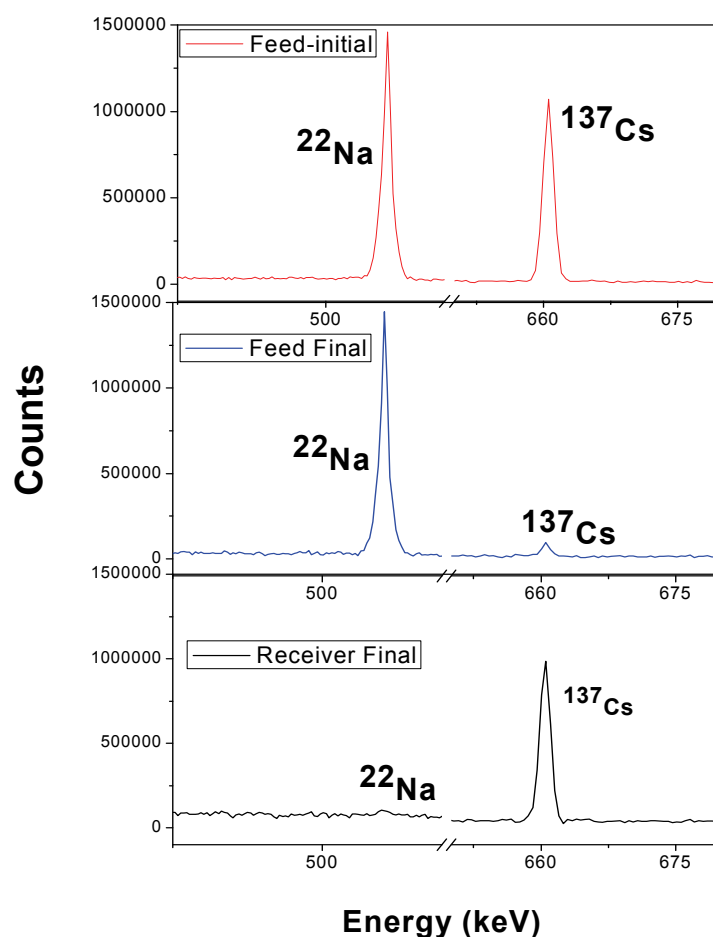


Figure 6.4: Gamma spectra of the initial (SRELW) and final feed solution as well as final receiver (93% Cs transport) solution, showing the selective transport of ^{137}Cs over ^{22}Na through CTA based PIM. The spectra have been normalized for the same counting time.

It is also to be mentioned that, due to presence of large amount of Na^+ as well as H^+ (0.4 M HNO_3), the cation transport rate is very slow i.e. long time (59 h) is required for significant (93 %) Cs^+ transport, which is associated with 2.3 % H^+ transport. This can be explained only if there is a leakage of HNO_3 through the membrane. Otherwise, in case of electrodriven H^+ transport, the pH of the receiver phase would not have decreased as the OH^- generated at the cathode neutralizes the transported H^+ . This is confirmed when the same experiment has been repeated at zero applied potential. In this case, the possible transport is driven by only concentration gradient i. e, HNO_3 is transported (from feed to receiver) as a neutral molecule. The transport profiles of HNO_3 along with that of $\text{CsNO}_3/\text{NaNO}_3$ are shown in figure 6.5. The experimental result indicates that after 59 h, 2.4 % of initial HNO_3 in the feed has been transported to the receiver compartment, whereas no $^{137}\text{Cs} / ^{22}\text{Na}$ radioactivity is observed in the receiver compartment (below the detection limit of gamma spectrometry), i. e, the salt transport remains zero throughout the experiment.

The faster cation transport rate and lower DF in neutral feed solution as compared to that in the SRELW can be explained on the basis of presence of large amount of H^+ in SRELW. In case of SRELW, the feed compartment contains 3.2 mmol of Na^+ ($\text{Cs}^+:\text{Na}^+ = 1:286$) along with 12.8 mmol of H^+ . Proton transport through HCCD-PIM can compete with other cation transport (Cs^+ or Na^+) transport, which leads to slower transport rate of both Cs^+ and Na^+ . Because of the inherent selectivity of the membrane for Cs^+ , in presence of large proton concentration, Na^+ transport is more suppressed as compared to Cs^+ transport through the membrane. This explains the higher DF in the SRELW as compared to that in the case of neutral feed solution.

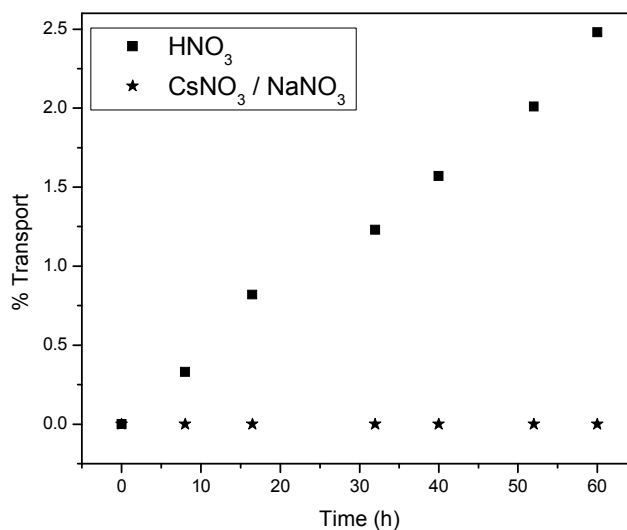


Figure 6.5: Transport profile of HNO₃ and CsNO₃/ NaNO₃ obtained using CTA based PIM at zero applied potential with SRELW in the feed compartment.

From UV-visible calibration of the CTA based PIMs, it is observed that there is a 12% decrease in the carrier concentration of the membrane after 48 h of continuous use. This indicates moderate stability of the CTA based PIM of HCCD and its stability can be further enhanced by grafting.

6.3.2. PVC based PIM for Cs⁺ transport from high level waste solution

Separation of Cs⁺ from SHLW is important from waste management aspect. The SHLW contains a large number of metal ions (table 6.1) in a high HNO₃ (3M) concentration, where CTA based PIM can't be used due to the acid hydrolysis of the CTA matrix. PVC based membrane has thus been prepared for Cs⁺ transport from SHLW. The results obtained for the transport study with SHLW using HCCD as carrier in PVC based PIM are summarized in figure 6.6. The Cs⁺ concentrations in feed and receiver compartments were measured using radiotracer technique, whereas those of the other metal ions were determined using ICP-AES technique. The bar diagrams given in figure 6.6, clearly indicates that, the membrane

exclusively transports Cs^+ from a SHLW solution. The results show that, inspite of presence of large quantity of Na^+ , only 1.2 % of the initial Na^+ is transported to the receiver side at the end of the transport process. The compositions of other elements in the final feed solution remain unaltered as those in the final receiver solution are below 0.1 mg/L. In this case, the DF (as shown in table 6.2) for Cs^+ is calculated to be 80 over Na^+ and in the range of ~500-5000 over other metal ions. Quantitative (>99%) Cs^+ transport takes place in ~42 h. This is accompanied with only 3.3% (of initial feed proton conc.) HNO_3 transport to the receiver phase.

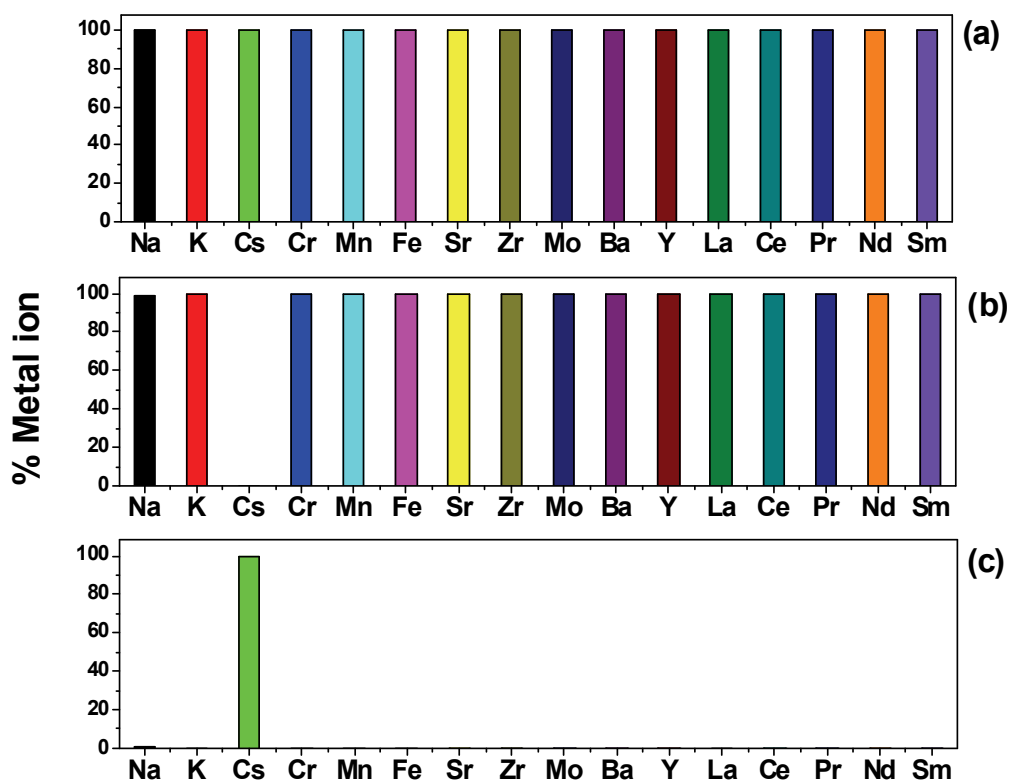


Figure 6.6: Relative concentrations of different metal ions in the (a) initial feed solution (b) final feed solution and (c) final receiver solution for the treatment of SHLW using PVC based PIM.

In general, enhancement in the permeability retaining its selectivity is a challenge for use of ion-exchange membrane in separating ions of similar charge. In our works with Nafion-Crown ether composite membrane, it has been observed that high selectivity is achieved only at the cost of cationic mobility in the membrane. On the other hand, the results described in the present work indicate that HCCD-PIM is a highly Cs^+ selective membrane with which the cation can be transported within reasonable time under electric field. From this aspect, this is indeed a unique approach of separation of Cs^+ from nuclear waste solution.

6.4. Conclusion

The present study, for the first time, demonstrates a novel and cleaner method of Cs^+ -separation of from simulated nuclear waste solution using HCCD as a carrier in PIM. HCCD, being a highly selective ionic carrier for Cs^+ , a very high DF has been obtained in the electro-driven transport study. The work addresses the decontamination of Cs^+ over Na^+ , which is the major challenge in nuclear waste treatment and has not been addressed in any membrane based separation methods. The use of stripping agent (8 M HNO_3), as described in previous literatures, has been avoided by using electric field in the present study. This makes this separation process more safe and environment friendly.

Chapter 7

Summary and Conclusions

Ion exchange membrane (IEM) based separation techniques have considerable commercial and technical impact. As the interaction of the cations in a cation exchange membrane is electrostatic in nature, the mutual separation of ions of same valence is difficult using IEM. One way to increase the metal ion selectivity is to incorporate some ligand within the membrane matrix having high selectivity for the metal ion of interest. However, a general problem with IEM is that, the high selectivity always comes at the cost of cationic mobility in the membrane. In the present work, an attempt has been taken to achieve metal ion selectivity (Cs^+ over Na^+) with significant transport rate using different IEMs like Nafion-117, copper ferrocyanide loaded track etched membrane and polymer inclusion membrane. The novelty of the work is in the use of electrodialysis based transport process instead of the conventional Donnan dialysis based processes. This electromembrane extraction process does not require any counter transport from receiver to feed solution, as in the case of Donnan dialysis based process. The use of electric field, eliminates the need of adding salt or stripping agent in the receiver side. Electric field also helps to enhance the cationic flux in the membrane with subsequent reduction in the transport time.

In the present work, Cs^+ has been chosen as the metal ion of interest, because, it is one of the most abundant fission products present in nuclear waste. It is of major environmental concern because of the long half-life (30 y) and high gamma energy (662 keV) of its radioisotope ^{137}Cs . The conventional methods (solvent extraction, precipitation, ion-exchange resin based methods) of Cs separation have associated drawbacks like requirement of large amount of undesirable solvents and macrocyclic carriers, insufficient selectivity and generation of voluminous secondary nuclear waste. Whereas, the membrane based methods are environmentally benign and require small amount of ligand. Use of different macrocyclic and macromolecular carrier based membranes for facilitated transport of Cs^+ are well reported in literature. The major drawback associated with these ligands is the requirement of

anion for charge compensation of the metal ion. Presence of bulk concentration of Na^+ in the nuclear waste solution is the major challenge in recovery/ removal of Cs^+ . This problem has not been addressed by most of the reported membrane based methods.

The work reported in this thesis has relevance in the $\text{Cs}^+ / \text{Na}^+$ separation using IEM. In the present work, different aspects (effect of mixed cationic environment, activation energy of diffusion) of Cs^+ diffusion as well as selective transport of Cs^+ over Na^+ through different IEM have been studied. Mostly radiotracer based techniques have been used for the measurements of different parameters. Major achievements and conclusions of this work are summarized as follows.

1. The self diffusion coefficient (SDC) of an ion in Nafion-117 membrane is influenced by the ionic composition of the membrane phase, depending upon the path of transport of the two cations within the membrane. Cs^+ with low charge density follows a transport pathway through the aqueous side of the interfacial region, while $\text{Na}^+ / \text{Ba}^{+2}$ moves mainly through the water rich micro phase of the membrane. Hence, in Na-Cs and Cs-Ba systems, the ions follow a mutually independent path and do not influence the SDCs of each other. On the other hand, if the two ions are moving through an overlapping path, then depending upon the electrostatic binding of the cation with the fixed charge group of the membrane, the SDCs will be affected. Thus in Na-Ba and Ag-Ba systems, the SDC of Ba^{+2} decreases continuously as the amount of the other cation increases in the membrane. This ionic composition dependent self diffusion behavior of either cation is ultimately reflected in the specific conductivity of the system. Thus, for Na-Cs system, the specific conductance increases linearly, whereas for Na-Ba system, it increases in a parabolic fashion with increase in Na^+ content in the membrane.

2. The study of temperature dependence of SDCs of Cs^+ and water in dibenzo-18-crown-6 (DB18C6) modified Nafion membrane indicates high activation energy (~ 80 kJ/mole) of diffusion. Such a high value of activation energy indicates that there is no continuous water channel in the composite membrane. Experimental results indicated that, the water uptake of Nafion membrane has reduced significantly on introduction of crown ether in the membrane. This shows that complexation of DB18C6 with Cs^+ ion accompanied by the disruption of the water cluster channel network of Nafion-117 has taken place, thereby reducing the SDCs significantly. The stronger binding of Na^+ (than Cs^+) with DB18C6 is reflected in the slower self-diffusion kinetics of Na^+ (than Cs^+) in the composite membrane matrix. The activation energy of diffusion of Cs^+ in diffusion dibenzo-21-crown-7 (DB21C7) has been obtained as 213 ± 16 KJ/mole, which is much higher than that in DB18C6 loaded Nafion. The result clearly shows much higher affinity of Cs^+ for DB21C7 than DB18C6. The Differential Scanning Calorimetry (DSC) data corroborates our observations already obtained from equilibrium water uptake measurement and self diffusion measurement of cations and water.

In an attempt to make Cs^+ selective membranes, with which Cs^+ can be transported at room temperature, two types of crown ether -Nafion composite membranes have been prepared. In one case, the DB21C7 has been incorporated uniformly in Cs^+ form of Nafion-117 membrane in varying molar ratio with respect to Cs^+ and in the other case, the Cs^+ driven loading of DB21C7 has been confined (ion gating) at one surface of the membrane. The isotopic and the ion exchange studies in the uniformly crown ether loaded membranes has indicated that the decrease in the extent of crown ether loading increases SDC of Cs^+ at the cost of mutual cationic selectivity (Cs^+ over Na^+). This problem has been successfully overcome by confinement of the templating (with crown ether) only at a very small thickness ($25\ \mu\text{m}$) from one of the surfaces of the membrane. At room temperature, under electric field (4V) this ion gated membrane has been found to selectively transport Cs^+ within practical time scale with

an average enrichment factor of 4.5 over Na^+ . When applied for the simulated nuclear waste solution, selective transport of Cs^+ has also been obtained using this gated membrane even in the presence of very high Na^+ concentration in aqueous solution.

3. In another attempt, highly Cs^+ selective copper ferrocyanide nano-crystals have been synthesized within the pores of track etched membrane. Characterization of the composite membrane (KCFCNm) indicates presence of mixed potassium copper ferrocyanide composition, which has been represented as KCFCN in this work. The conical shaped pores of the membrane are almost uniformly filled with the KCFCN crystals and the rod like structures, as has been observed in the TEM images, are made up of nanosized KCFCN crystals (~40 nm).

Under applied electric field, the KCFCNm has been found to selectively transport Cs^+ from acidic feed solution with an average enrichment factor of ~2 over Na^+ . Study of water transport through the membrane indicates that though KCFCN crystals cause physical blocking of the pores of the membrane but some water channels still exist in the KCFCNm. The self diffusion measurement of Cs^+ in the membrane indicates very fast absorption of the cation. Absorption experiments have indicated that the Cs^+ exchange capacity of the membrane as well as the distribution coefficients of Cs^+ in the membrane are much higher than the best reported in literature till date. The ^{137}Cs removal efficacy of the membrane has been found to be affected by the activity dilution and more equilibration time is required when the activity is distributed in larger volume of solution. Application of this composite membrane for removal of Cs^+ from a simulated nuclear waste has indicated exclusive absorption of ^{137}Cs inspite of presence of other radionuclides, though the absorption rate is affected due to their presence. This composite membrane shows promising properties for Cs^+ removal from nuclear waste solution.

4. For the first time, use of the hexachlorinated derivative of cobalt bis (dicarbollide) (HCCD) as a selective carrier for Cs^+ transport through cellulose tri acetate (CTA) / poly vinyl chloride (PVC) based polymer inclusion membrane (PIM) is reported in this work. The electrodriven transport study through this PIM indicated excellent selectivity for Cs^+ over Na^+ . The working potential of the transport system has been optimized as 3 V. Under applied electric field, the CTA based membrane has been found to selectively transport Cs^+ from a neutral feed solution with a decontamination factor (DF) of 51 for Cs^+ over Na^+ . Presence of large concentration of H^+ in the feed solution has been found to slower the cation transport rate and increase the transport selectivity of Cs^+ over Na^+ . Thus, for a simulated nuclear waste solution containing 0.1 M NaNO_3 and 3.5×10^{-4} M CsNO_3 in 0.4 M HNO_3 , a DF of > 400 for Cs^+ over Na^+ has been obtained with a much slower transport rate as compared to neutral feed solution. In order to study transport selectively of Cs^+ from a simulated high level nuclear waste (SHLW) in 3 M HNO_3 , a PVC based membrane, which has higher stability in high acidic medium, has been used. This membrane selectively transported Cs^+ with a decontamination factor of 80 over Na^+ and >500 over other metal ions present in the SHLW. The results indicate that HCCD-PIM, inspite of its high selectivity for Cs^+ , allows the cation to be transported within reasonable time under electric field.

In conclusion, the present study, demonstrates a novel and cleaner method of Cs^+ -separation of from simulated nuclear waste solution. The promising results explore the possibility of using this kind of electrodriven membrane transport methods for nuclear waste treatment. However, further extensive studies for different type of waste solutions need to be pursued to establish it as a standard method.

Bibliography

A

- Alcaraz, A.; Holdik, H.; Ruffing, T.; Ramirez, P.; Mafe, S. *J. Mem. Sci.* **1998**, *150*, 43.
- Almeida, S. H.; Kawano, Y. *J. Therm. Anal. Calorim.* **1999**, *58*, 569.
- Arena, G.; Contino, A.; Magri, A.; Sciotto, D.; Lamb, J. D.; Supramol. Chem. **1998**, *10*, 5.
- Arnaud-Neu, F.; Schwing-Weill, M. J.; Ziat, K.; Cremin, S.; Harris, S. J.; McKerverey, M. A. *New J. Chem.* **1991**, *15*, 33.
- Arnikar H.J., *Isotopes in the Atomic Age*, Wiley, New York, **1989**.
- Avramenko, V.; Bratskaya, S.; Zheleznov, V.; Sheveleva, I.; Voitenko, O.; Sergienko, V. *J. Haz. Mat.* **2011**, *186*, 1343.

B

- Baker, R.W. *Membrane technology and applications*, 2nd edition, John Wiley and sons, **2004**.
- Bakker, E.; Bühlmann, P.; Pretsch, E. *Chem. Rev.* **1997**, *97*, 3083.
- Banerjee, D.; Rao, M. A.; Wattal, P. K.; *Sep. Sci. Technol.* **2013**, *48*, 133.
- Bayley, H.; Martin, C. R. *Chem. Rev.*, **2000**, *100*, 2575.
- Benavente, J.; Can˜as, A.; Ariza, M. J.; Lozano, A. E.; Abajo, J. *Solid State Ionics*, **2001**, *145*, 53.
- Bhattacharya, A.; Goswami, A. J. *Phys. Chem. B*, **2009**, *113*, 12958.
- Bieth C. and SAIF Group, *Nucl. Tracks Rad. Meas.* **1991**, *19*, 875.
- Blasius, E.; Nilles, K.H. *Radiochim. Acta.*, **1984**, *35*, 173.
- Blasius, E.; Nilles, K.H. *Radiochim. Acta*, **1984**, *36*, 207.
- Bonner, O. D.; Smith, L. L. *J. Phys. Chem.* **1957**, *61*, 326.
- Bontha, R.; Pintauro, P. N. *Chem. Eng. Sci.*, **1994**, *49*, 3835.
- Bouzek, K.; Moravcová, S.; Samec, A.; Schauer, J.; *J. Electrochem. Soc.* **2003**, *150*, E329.
- Brown, E. *Introduction to Thermal Analysis*, Kluwer Academic Publishers, Dordrecht, **2001**.

Buck, R. P. *Electroanalytical Chemistry of Membranes, CRC Reviews in Analytical Chemistry*. **1976**.

Buhlmann, P. ; Pretsch, E. ; Bakker, E. *Chem. Rev.* **1998**, 98, 1593.

C

Canas, A.; Ariza, M. J.; Benavente, J. *J. Membr. Sci.* **2001**, 183, 135.

Cerjan-Stefanovic, S.; Blanus, M.; Kastelan-Macan, M. *Fresenius' Z. Anal. Chem.* **1984**, 319, 304.

Charewicz, W. A.; Bartsch, R. A. *Anal. Chem.* **1982**, 54, 2300.

Chaudhury, S.; Agarwal, C.; Pandey, A. K.; Aher, V. T.; Panicker, L.; Ramagiri, S. V.; Bellare J. R.; Goswami, A. *J. Membr. Sci.* **2011**, 382, 262.

Chen, R.; Tanaka, H.; Kawamoto, T.; Asai, M.; Fukushima, C.; Kurihara, M.; Ishizaki, M.; Watanabe, M.; Arisaka, M.; Nankawa, T. *ACS Appl. Mater. Interfaces*, **2013**, 5, 12984.

Cheung, H.M.; Raj, W. R. P. *Membranes, Porous (Synthesized from Microemulsions), Polymeric Materials Encyclopedia*, edited by J.C. Salamone, *CRC Press Inc., Boca Raton, Florida*, **1996**, p. 4083.

Choi, B. G.; Park, H. S.; Im, H. S.; Kim, Y. J.; Hong, W. H. *J. Membr. Sci.* **2008**, 324, 102.

Choppin, G. R.; Rydberg, J.; Liljenzin, J. O.; *Radiochemistry and Nuclear Chemistry*, 2nd Edition Oxford, Pergamon press, **1995**.

Clarke, T. D.; Wai, C. M. *Anal. Chem.* **1998**, 70, 3708.

Cohen, M. H.; Turnbull, D. *J. Chem. Phys.* **1959**, 31, 1164.

Coster, H.G.L.; Chilcott, T.C.; Coster, A.C.F. *Bioelectrochem. Bioenerg.* **1996**, 40, 79.

Crank, J. *The mathematics of diffusion*, **1964**, Oxford Univ. Press.

Crank, J.; Park, G.S. *Diffusion in Polymer*; Chapter 1, Academic Press, London. **1968**.

D

Das, S.; Pandey, A. K.; Vasudevan, T.; Athawale, A. A.; Manchanda, V. K. *Ind. Eng. Chem. Res.* **2009**, *48*, 6789.

Das, S.; Pandey, A. K.; Athawale, A. A.; Natrajan, V.; Manchanda, V. K. *Desalination and water treatment*, **2012**, *38*, 114.

Dietz, M. L.; Horwitz, E. P.; Jensen, M. P.; Rhoads, S.; Bartsch, R. A.; Palka, A.; Krzykewski, J.; Nam, J. *Solv. Extr. Ion Exch.* **1996**, *14*, 357.

Dobler, M. *Ionophores and their structures*, Wiley, New York, **1981**.

Dotson, R. L.; Woodard, K. E. In *Perfluorinated Ionomer Membranes*;

Duan, J. L.; Cornelius, T. W.; Liu, J.; Karim, S.; Yao, H. J.; Picht, O.; Rauber, M.; Muller, S. Neumann, R. *J. Phys. Chem. C*, **2009**, *113*, 13583.

E

Ehmann, W. D.; Vance, D. E., *Radiochemistry and Nuclear Methods of Analysis*, John Wiley & sons, New York, **1991**.

Eisenberg, A.; Yeager, H. L. Eds. *Perfluorinated Ionomer Membranes*; ACS Symposium Series 180; American Chemical Society: Washington, DC, **1982**; p 41.

Elliott, J. A.; Wu, D.; Paddison, S. J.; Moore, R. B. *Soft Matter*. **2011**, *7*, 6820.

F

Fischer B. E., R. Spohr, *Rev. Mod. Phys.* **1983**, *55*, 907.

Fiskum, S. K.; Arm, S. T.; Steele, M. J.; Thorson, M. R.; *Solv. Extr. Ion Exch.* **2008**, *26*, 435.

Fortunato, R.; Branco, L.C.; Afonso, C.A.M; Benavente, J.; Crespo, J. G. *J. Membr. Sci.* **2006**, *270*, 42.

G

- Gaur, S. *J. Chromatogr. A.* **1996**, 733, 57.
- Gavach, C.; Pamboutzoglou, G.; Nedyalkov, M.; Pourcelly, G. *J. Membr. Sci.* **1989**, 45, 37.
- Gebel, G.; Moore, R.B. *Macromolecules* **2000**, 33, 4850.
- Gerow, I. H.; Davis, M.W. *Sep. Sci. Technol.*, **1979**, 14, 395.
- Gerow, I. H.; Smith, J. E.; Davis, M. W. *Sep. Sci. Technol.* **1981**, 16, 519.
- Gokel, G. W.; Leevy, W. M.; Weber, M. E.; *Chem. Rev.* **2004**, 104, 2723.
- Gong, X.; Bandis, A.; Tao, A.; Meresi, G.; Wang, Y.; Inglefield, P.T.; Jones, A. A.; Wen W.-Y.; *Polymer*, **2001**, 42, 6485.
- Goswami, A.; Acharya, A.; Pandey, A. K.; *J. Phys. Chem. B*, **2001**, 105, 9196.
- Gribov, E. N.; Krivobokov, I. M.; Parkhomchuk, E. V.; Okunev, A. G.; Spoto, G.; Parmon, V. N. *Russ. J. Electrochem.* **2009**, 45, 199.
- Guinier, A.; Fournet, G. *Small Angle Scattering of X-Rays*. Wiley, New York, **1955**.

H

- Haas, P. A. *Sep. Sci. Technol.* **1993**, 28, 2479.
- Hamilton, T.; Martinelli, R.; Kehl, S.; Brunk, J.; Lawrence Livermore National Laboratory, UCRL-ABS-217452.
- Hankins, M. G.; Kim, Y. D.; Bartsch, R. A. *J. Am. Chem. Soc.* **1993**, 115, 3370.
- Hassan, N. M.; Adu-Wusu, K.; Marra, J. C. *J. Radioanal. Nuc. Chem.* **2004**, 262, 579.
- Haverlock, T. J.; Sachleben, R. A.; Bonnesen, P.V.; Moyer, B.A. *J. Incl. Phenom.* **2000**, 36, 21.
- Hawthorne, M. F.; Dunks, G. B. *U.S. Patent no.5,698,169*, dated Dec.16, **1997**.
- He, Z.; Mansfield, F. *Energy Environ. Sci.* **2009**, 2, 215.
- Heitner-Wirguin, C. *J. Membr. Sci.* **1996**, 120, 1.

Helffferich F., Ion exchange, McGraw-Hill Book Company, New York, **1962**.

Hirofumi, M.; Miyoshi, H.; Yamagami, M.; Chubachi, M.; Kataoka, T. *J. Chem Eng. Data* **1994**, 39, 595.

Holder, J.V. *Radiochim. Acta*, **1978**, 25, 171.

Hornak Joseph P., *The basics of NMR*, (**1998**) (<http://www.cis.rit.edu/htbooks/nmr>)

Hsu, W. Y.; Gierke, T. D. *Macromolecules* **1982**, 15, 101.

Hsu, W. Y.; Gierke, T. D. *J. Membr. Sci.* **1983**, 13, 307.

I

Ishihara, R.; Fujiwara, K.; Harayama, T.; Okamura, Y.; Uchiyama, S.; Sugiyama, M.; Someya, T.; Amakai, W.; Umino, S.; Ono, T.; Nide, A.; Hirayama, Y.; Baba, T.; Kojima, T.; Umeno, D.; Saito, K.; Asai, S.; Suso, T. *J. Nuc. Sci. Technol.* **2011**, 48, 1281.

Ismail, I. M.; El-Sourougy, M. R.; Abdel Moneim, N.; Aly, H. F. *J. Radioanal. Nuc. Chem.* **1999**, 240, 59.

Izatt, S. R.; Hawkins, R.T.; Christensen, J. J.; Izatt, R.M. *J. Am. Chem. Soc.* **1985**, 107, 63.

J

Jayakody, J. R. P.; Stallworth, P. E.; Mananga, E. S.; Farrington-Zapata, J.; Greenbaum, S. G. *J. Phys. Chem. B*, **2004**, 108, 4260.

Jenkins, R. *Methods and Practices in X-ray Powder Diffraction*, JCPDS, International Centre for Diffraction Data, Swarthmore, **1986**.

Jonscher, A. K. *Dielectric Relaxation in Solid*, Chelsea Dielectric Press, London, **1983**.

K

Karavanova, Yu. A.; Yaroslavtsev, A. B. *Inorganic Materials*, **2010**, 46, 789.

Katsura, S.; Ito, Y.; Takeda, Y. *Inorganica Chimica Acta*. **2004**, 357, 541.

Kaushik, C. P.; Shah, J. G. Challenges in development of matrices for vitrification of high level radioactive waste, BARC News letter, May-June **2000**.

Kimura, K.; Sakamoto, H.; Yoshinaga, M.; Shono, T. *J. Chem Soc., Chem. Commun.* **1983**, 17, 978.

Klug, H. P.; Alexander, L. E. *X-Ray Diffraction Procedures: For Polycrystalline and Amorphous Materials*, Wiley-Interscience, New York, **1974**.

Knoll, M. Ruska, E. *Zeitschrift Fur Physik*, **1932**, 78, 318.

Kuban, P.; Slampova, A.; Bocek, P. *Electrophoresis*, **2010**, 31, 768.

Kusoglu, A.; Modestino, M. A.; Hexemer, A.; Segalman, R. A.; Weber, A.Z. *ACS Macro Lett.* **2012**, 1, 33.

Kyrs, M. *J. Radioanal. Nucl. Chem. Letters*, **1994**, 187, 185.

L

L'Annunziata Michael F., *Handbook of Radioactivity Analysis*, 2nd Edition, Academic Press, California, **2003**.

Langford, J. I.; Daniel, L. *Reports on Progress in Physics*, **1996**, 59, 131.

Lee, E. M.; Thomas, R. K.; Burgess, A. N.; Barnes, D. J.; Soper, A. K.; Rennie, A. R. *Macromolecules*, **1992**, 25, 3106.

Lehto, J.; Harjula, R. *Solv. Extr. Ion Exch.* **1987**, 5, 343.

Leo, M. D.; Pereira, F. C.; Moretto, L. M.; Scopece, P.; Polizzi, S.; Ugo, P. *Chem. Mater.*, **2007**, 19, 5955.

Levitskaia, T. G.; Lamb, J. D.; Fox, K.L.; Moyer, B. A. *Radiochim. Acta*, **2002**, 90, 43.

Lopez, M.; Kipling, B.; Yeager, H. L. *Anal. Chem.*, **1977**, *49*, 629.

Lueck, H.B.; Matthes, H.; Gemende, B.; Heinrich, B.; Pfestorf, W.; Seidel, W.; Turuc, S. *Nucl. Instrum. Methods B*, **1990**, *50*, 395.

M

Maeda, Y.; Tsuyumoto, M.; Karakane, H.; Tsugaya, H. *Polym. J.* **1991**, *23*, 501.

Marcus, Y.; Kertes, A. S. Ion exchange and solvent extraction of metal complexes, Wiley-Interscience, New York, **1969**.

Mauritz, K. A.; Moore, R. B. *Chem. Rev.* **2004**, *104*, 4535.

McDonald, J. R. Impedance Spectroscopy, Wiley, New York, **1987**.

McLean, R. S.; Doyle, M.; Saner, B. B. *Macromolecules*, **2000**, *33*, 6541.

Millet, P. *J. Membr. Sci.* **1990**, *50*, 325.

Miller, J.E.; Brown, N.E. *Development and Properties of Crystalline Silicotitanate (CST) Ion Exchangers for Radioactive Waste Applications*, SAND97-0771, April, **1997**.

Mimura, H.; Akiba, K.; *In the proceedings of WM'02 Conference*, Tucson, AZ, February 24-28, **2002**, pp. 3.

Mohapatra, P. K.; Bhattacharyya, A.; Manchanda, V. K. *J. Haz. Mat.*, **2010**, *181*, 679.

Mohapatra, P.K.; Lakshmi, D.S.; Bhattacharyya, A.; Manchanda, V. K. *J. Haz. Mat.* **2009**, *169*, 472.

Morales-Cid, G.; Cardenas, S.; Simonet, B. M.; Valcarcel, M. *Tr. Anal. Chem.* **2010**, *29*, 158.

Moyer, B. A.; Deng, Y.; Sun, Y.; Sachleben, R. A.; Batra, A. K.; Robinson, R. B. *Solv. Extr. Ion Exch.* **1997**, *15*, 791.

Murali, M. S.; Raut, D. R.; Prabhu, D. R.; Mohapatra, P. K.; Tomar, B. S.; Manchanda, V. K. *J. Radioanal Nucl Chem.* **2012**, *291*, 611.

Muraviev, D.; Gonzalo, A.; Valiente, M. *Anal. Chem.* **1995**, *67*, 3028.

Muslinkina, L.; Pretsch, E. *Electroanalysis*, **2004**, *16*, 1569.

N

Nemat-Nasser, S.; Zamani, S.; Tor, Y.; *J. Appl. Phys.* **2006**, *99*, 104902.

Ngheim, L. D.; Mornane, P.; Potter, I. D.; Perera, J. M.; Cattrall, R.W.; Kolev, S. D.; *J. Membr. Sci.*, **2006**, *281*, 7.

Ng, P. K.; Snyder, D. D. *J. Membr. Sci.* **1983**, *13*, 327.

Nwal Amang, D.; Alexandrova, S.; Sghaetzel, P. *Electrochimica Acta*, **2003**, *48*, 2563.

O

Okada, T.; Moller-Holst, S.; Gorseth, O.; Kjelstrup, S.; *J. Electroanal. Chem.* **1998**, *442*, 137.

Okada, T.; Satou, H.; Okuno, M.; Yuasa, M. *J. Phys. Chem. B*, **2002**, *106*, 1267.

Orth, R. J.; Brooks, K. P.; Kurath, D. E. *Review and Assessment of Technologies for the Separation of Cesium from Acidic Media*, September 1994, Prepared for the U.S. Department of Energy under Contract DE-AC06-76IUO 1830, **1994**..

P

Park, J. S.; Chilcott, T. C.; Coster, H. G. L.; Moon, S. H. *J. Membr. Sci.*, **2005**, *246*, 137.

Paul, D.; Peinemann, K. V. *Membranes (OveMew)*, Polymeric Materials Encyclopedia, edited by J.C. Salamone, CRC Press, Florida, **1996**..

Pedersen-Bjergaard, S.; Rasmussen, K. E. *Trends Anal. Chem.* **2008**, *27*, 934.

Pekarek, V.; Vesely, V. *Talanta*, **1972**, *19*, 1245.

Pintauro, P. N.; Tandon, R.; Chao, L.; Xu, W.; Evilla, R. *J. Phys. Chem.* **1995**, *99*, 12915.

Pourcelly, G.; Oikonomou, A.; Gavach, C.; Hurwitz, H. D. *J. Electroanal. Chem.* **1990**, 287, 43.

Pourcelly, G.; Sistat P.; Chapotot A.; Gavach, C.; Nikonenko V., *J. Membr. Sci.*, **1996**, 110, 69.

Pretsch, E.; Bühlmann, P.; Bakker, E. *Chem. Rev.*, **1998**, 98, 1593.

R

Ramonovsky, V. N. Management of accumulated high level waste at the Mayak production Association in the Russian Federation, in issues and Trends in Radioactive waste management, Proc. International conference, IAEA, Vienna, **2003**.

Rao, K. L. N.; Shukla, J. P.; Venkataramani, B. *J. Radioanal. Nucl. Chem.* **1995**, 189, 107.

Rao, S. V. S.; Lal, K. B.; Narasimhan, S. V.; Ahmed, J. *J. Radioanal. Nuc. Chem.*, 1999, 240, 269.

Rao, S. V. S.; Lekshmi, R.; Mani, A. G. S.; Sinha, P. K. *J. Radioanal. Nucl. Chem.*, **2010**, 283, 379.

Raut, D.R.; Mohapatra, P.K.; Ansari, S.A.; Sarkar, A.; Manchanda, V. K. *Desalination*, **2008**, 232, 262.

Raut, D. R.; Kandwal, P.; Rebello, G.; Mohapatra, P. K.; *J. Membr. Sci*, **2012**, 17, 407.

Reiss, H.; Bassignana, I. C. *J. Membr. Sci.* **1982**, 11, 219.

Robertson, M. A. F. Ph.D. Thesis, Department of Chemistry, University of Calgary, **1994**.

Robertson, M. A. F.; Yeager, H. L. *Macromolecules*, **1996**, 29, 5166.

Robinson, R. A.; Stokes, R. H. *Electrolyte Solutions*, 2nd ed., Butterworths, London, **1965**.

Rollet, A.-L.; Simonin, J.-P.; Turq, P. *Phys. Chem. Chem. Phys.*, **2000**, 2, 1029.

Rollet, A.-L.; Diat, O.; Gebel, G. *J. Phys. Chem. B*, **2002**, 106, 3033.

- Rollet, A.-L.; Blachot, J.-F.; Delville, A.; Diat, O.; Guillermo, A.; Porion, P.; Rubatat, L.; Gebel, G. *Eur. Phys. J.* **2003**, 12, S131-S134.
- Rollet, A. L.; Diat, O.; Gebel, G. *J. Phys. Chem. B*, **2004**, 108, 1130.
- Rubatat, L.; Rollet, A. L.; Gebel, G.; Diat, O. *Macromolecules*, **2002**, 35, 4050.
- Rubatat, L.; Gebel, G.; Diat, O. *Macromolecules*, **2004**, 37, 7772.

S

- Sadat, R.; Ross, A.; Leveziel, H. Food irradiation: A global scenario, in *proceedings of International Conference on Applications of Radioisotopes and Radiation in Industrial Development (ICARID-94)*, February, **1994**.
- Saito, K.; Hori, T.; Furusaki, S.; Sugo, T.; Okamoto, J. *Ind. Eng. Chem. Res.* **1987**, 26, 1977.
- Saito, M.; Hayamimizu, K.; and Okada, T. *J. Phys. Chem. B*, **2005**, 109, 3112.
- Sakamoto, H.; Kimura, K.; Shono, T. *Eur. Polym. J.* **1986**, 22, 97.
- Samanta, S. K.; Theyyunni, T. K.; Misra, B. M.; *J. Nuc. Sci. Tech.* **1995**, 32, 425.
- Samec, Z.; Troja'nek, A.; Samcova', E. *J. Phys. Chem.* **1994**, 98, 6352.
- Samec, Z.; Troja'nek, A.; Langmaier, J.; Samcova', E. *J. Electrochem. Soc.* **1997**, 144, 4236.
- Sangvanich, T.; Sukwarotwat, V.; Wiacek, R. J.; Grudzien, R. M.; Fryxell, G. E.; Addleman, R. S.; Timchalk, C.; Yantasee, W.; *J. Haz. Mat.* **2010**, 182, 225.
- Sarkar, S.; Sengupta, A. K.; Prakash, P. *Environ. Sci. Technol.* **2010**, 44, 1161.
- Sata, T.; Tanimoto, M.; Kawamura, K.; Matsusaki, K.; *Colloid. Polym. Sci.* **2000**, 278, 57.
- Sata, T.; Kawamura, K.; Higa, M.; Matsusaki, K.; *J. Membr. Sci.* **2001**, 183, 201.
- Sata, T. Ion-Exchange membranes-preparation, characterization, modification and application; Royal Society of Chemistry: London, **2004**.
- Schaetzel, P.; Auclair, B. *Electochim. Acta*, **1993**, 38, 329.
- Schaetzel, P.; Favre, E.; Auclair, B.; Nguyen, Q. T. *Electrochim. Acta*, **1997**, 42, 2475.

- Scherer, G. G. *Ber. Bunsen-Ges. Phys. Chem.* **1990**, 94, 1008.
- Schmidt-Rohr, K.; Chen, Q. *Nature Mater.* **2008**, 7, 75.
- Schulz, W.W.; Bray, L.A. *Sep. Sci. Technol.*, **1987**, 22, 191.
- Scott Herbst, R.; Peterman, D. R.; Tillotson, R. D.; Delmau, L. H. *Solv. Extr. Ion Exch.* **2008**, 26, 163.
- Sebesta, F.; John, J.; Motl, A. *Phase II report on the evaluation of polyacrylonitrile (PAN) as a binding polymer for absorbers used to treat liquid radioactive wastes SAND96-1088*, **1996**.
- See, H. H.; Hauser, P. C. *Anal. Chem.* **2011**, 83, 7507.
- Selvey, C.; Reiss, H. *J. Membr. Sci.* **1985**, 23, 11.
- Sen, U.; Çelik, Ü.; Ata, A.; Bozkurt, A.; *Int. J. Hydrogen Energy*, **2008**, 33, 2808.
- Sheha, R. R. *J. Colloid and Interface Sci.* **2012**, 388, 21.
- Shim, J. H.; Koo, I. G.; Lee, W. M.; *Electrochim. Acta*, **2005**, 50, 2385.
- Singh, S. P. N. *U. S. DOE Report SD-RE-PCP-011*, Rockwell Hanford Operations, Richland, WA, **1983**.
- Skoog, D. A.; West, D. M. *Principles of instrumental analysis*, Saunders College, Philadelphia, **1980**.
- Sodaye, S. *Studies on physico-chemical properties of functional polymer systems and their applications*, Ph. D. thesis, University of Mumbai, **2007**.
- Sodaye, S.; Agarwal, C.; Goswami, A. *J. Membr. Sci.* **2008**, 314, 221.
- Sodaye, S.; Pandey, A. K.; A. Goswami *J. Phys. Chem. B*, **2009**, 113, 12482.
- Sokolov, N. V.; Grodzinsky, D. M.; Sorochinsky, B.V. *How does low dose chronic irradiation under the condition of 10-km Chernobyl exclusion zone influence on processes of seed aging. In: Proceeding of International Conference, Fifteen Years after the Chornobyl Accident: Lessons Learned*", 18-20 April, Kiev, Ukraine. Kiev, Ukraine; **2001**, pp. 117.
- Starkweather, Jr, H.W. *Macromolecules* **1982**, 15, 320-323.

Stefanithis, I. D.; Mauritz, K. A. *Macromolecules* **1990**, *23*, 2397.

Strathmann, H. Synthetic Membranes and Their Preparation: Handbook of Industrial Membrane Technology, edited by M.C. Porter, Noyes Publications, New Jersey, **1990**.

Suarez, P. A. Z.; Dullius, J. E. L.; Einloft, S.; Sousa, R. F. D. Dupont, J. *Polyhedron*, **1996**, *15*, 1217.

Subrahmanian, V.; Lakshminarayanaiah, N. *J. Phys. Chem.* **1968**, *72*, 4314.

Suresh, G.; Scindia, Y. M.; Pandey, A. K.; Goswami, A. *J. Phys. Chem. B*, **2004**, *108*, 4104.

Suzuki, N.; Kimura, T.; Yamauchi, Y.; *J. Mat. Chem.* **2010**, *20*, 5294.

Suzuki, N.; Yamauchi, Y. *J. Nanomaterials*, **2010**, 2010.

T

Takeoka, S.; Sakai, H.; Tsuchida, E. *Chem. Lett.* **1990**, *19*, 1539.

Talanova, G. G.; Elkarim, N. S. A.; Hanes, Jr. R. E.; Hwang, H. S.; Rogers, R. D.; Bartsch, R. A. *Anal. Chem.* **1999**, *71*, 672.

Tandon, R.; Pintauro, P. N. *J. Membr. Sci.* **1997**, *136*, 207.

Torma, F.; Kádár, M.; Tóth, K.; Tatár, E. *Anal. Chim. Acta*, **2008**, *619*, 173.

Tsushima, S.; Teranishi, K.; Hirai, S. *Energy*, **2005**, *30*, 235.

V

Valentini, M. T. G.; Meloni, S.; Maxia, V.; *J. Inorg. Nucl. Chem.* **1972**, *34*, 1427.

(a) Valsala, T. P.; Joseph, A.; Shah, J. G.; Raj, K.; Venugopal, V.; *J. Nuc. Mat.* **2009**, *384*, 146.

(b) Valsala, T.P.; Roy, S. C.; Shah, J. G.; Gabriela, J.; Raj, K.; Venugopal, V.; *J. Hazardous Mat.* **2009**, *166*, 1148.

Verbrugge, M. W.; Hill, R. F. *J. Electrochem. Soc.*, **1990**, *137*, 893.

Verbrugge, M.W.; Scheneider, E.W.; Conell, R. S.; Hill, R. F.; *J. Electrochem. Soc.* **1992**, *139*, 3421.

Vincent, C.; Hertz, A.; Vincent, T.; Barre, Y.; Guibal, E.; *Chemical Engineering Journal*, **2014**, *236*, 202.

W

Walker, D. D. *Cesium Sorption/Desorption Experiments with IONSIV IE-911 in Radioactive Waste*, WSRC-TR-2000-00362, December, **2000**.

Walkowiak, W.; Kang, S.; Stewart, I. L.; Ndip, G.; Bartsch, R. A.; *Anal. Chem.* **1990**, *62*, 2022.

Williams, D. B.; Carter, C. B. *Transmission Electron Microscopy: A Textbook for Materials Science*, Springer Limited, New York, **2009**.

Wipff, G.; Lauterbach, M. *Supramol. Chem.* **1995**, *6*, 187.

X

Xia, Z.; Badr, I. H. A.; Plummer, S. L.; Cullen, L.; Bachas, L. G. *Anal. Sci.* **1998**, *14*, 169.

Xue, T.; Trent, J. S.; Osseo-Asare, K. *J. Membr. Sci.* **1989**, *45*, 261.

Y

Yasuda, Y.; Lamaze, C. E.; Ikenberry, L. D. *Macromol. Chem.* **1968**, *118*, 19.

Yasuda, H.; Lamaze, C.E.; Peterlin, *J. Polym. Sci., Part A*, **1971**, *29*, 1117.

Yeager, H. L.; Kipling, B. *J. Phys. Chem.*, **1979**, *83*, 1836.

Yeager, H. L.; Kipling, B.; Datson, R. L. *J. Electrochem. Soc.*, **1980**, *127*, 303.

Yeager, H. L.; Steck, A. *J. Electrochem. Soc.*, **1981**, *128*, 1880.

Yeager, H. L. **(a)** Transport properties of perfluorosulfonate polymer membranes, in Perfluorinated Ionomer membrane, **(b)** Cation exchange selectivity of a perfluorosulfonate membrane, A. Eisenberg and H.L. Yeager (Eds.), *ACS sym. Ser.* **1982**, 180, American Chemical Society, Washington DC.

Z

Zagorodni, A. A.; Muraviev, D. N.; Muhammed, M. *Sep. Sci. Technol.* **1997**, 32, 413.

Zahran, E. M.; Gavalas, V.; Valiente, M.; Bachas, L. G. *Anal. Chem.* **2010**, 82, 3622.

Zawodzinski, Jr. T.A.; Neeman, M.; Sillerud, L.O.; Gottesfeld, S. *J. Phys. Chem.*, **1991**, 95, 6040.

Zhao, Q.; Majsztrik, P.; Benziger, J. *J. Phys. Chem. B*, **2011**, 115, 2717.